

Development of a Continuous Flow Interface for Stacking in Capillary Electrophoresis

By

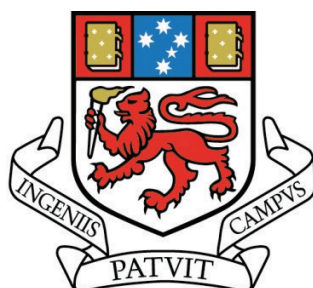
Daniel Gstoettenmayr

Dipl. -Ing. BSc. Bc. Technical Chemistry

Submitted in fulfilment of the requirements for the degree

of

Doctor of Philosophy



**UNIVERSITY
OF TASMANIA**
School of Physical Sciences

December, 2015

DECLARATION OF ORIGINALITY

“This thesis contains no material which has been accepted for a degree or diploma by the University or any other institution, except by way of background information and duly acknowledged in the thesis, and to the best of my knowledge and belief no material previously published or written by another person except where due acknowledgement is made in the text of the thesis, nor does the thesis contain any material that infringes copyright.”

Daniel Gstoettenmayr

AUTHORITY OF ACCESS

The publishers of the papers in this thesis (comprising Chapter 2) hold the copyright for that content and access to the material should be sought from the respective journals. The remaining non published content of the thesis may be made available for loan and limited copying and communication in accordance with the Copyright Act 1968.

Daniel Gstoettenmayr

STATEMENT REGARDING PUBLISHED WORK CONTAINED IN THE THESIS

“The publishers of the papers comprising Chapter 2 hold the copyright for that content, and access to the material should be sought from the respective journals. The remaining non published content of the thesis may be made available for loan and limited copying and communication in accordance with the Copyright Act 1968.”



Daniel Gstoettenmayr

University of Tasmania

December 2015

ACKNOWLEDGEMENTS

I would like to thank the following people for their help during the last few years in my PhD work.

My supervisor Dr Michael C. Breadmore for his keen supervision, patience, advice, encouragements and for helping me to become a better scientist during the whole work of my PhD. Thank you Michael for giving me the chance to work with you and learn from you.

My Supervisor Dr. Joselito P. Quirino for his assistance, patience, guidance and close supervision during the countless hours of working in the laboratory. Thank you Lito for giving me an insight into your ways of working and teaching me how to break big scientific problems down into small ones.

My colleagues Adam Gaudry, Petr Smejkal, Aliaa Shallan, Mohammad Talebi, Philip Zakaria, Emer Duffy, Anton Peristy, Tom Kazarian, Esme Candish, Chris Desire, Aminreza Khodabandeh for their guiding comments and advice.

My uncle Alois for his understanding and advice during the many hours of discussions about chemistry and physics related topics.

All members at the Australian centre for research on separation science for making ACROSS an exceptionally empowering workplace.

The central science laboratory staff members at UTAS Mr. Paul Waller, Mr. John Davis and Mr. Chris Young for their help.

My beloved family members; my brother Dominik, my mother Notburga, my uncles Robert and Alois, my grandparents Johanna and Alois and my father Wolfgang for being my family.

My partner Jemma for her love and support and for being so empathic and understanding at all times.

STATEMENT OF CO-AUTHORSHIP

The following people and institutions contributed to the publication of work undertaken as part of this thesis:

Author details and their roles:

Paper 1, Gstoettenmayr, D.; Quirino, J. P.; Ivory, F. C.; Breadmore, M.; **Stacking in a continuous sample flow interface in capillary electrophoresis**, Journal of Chromatography A, DOI: 10.1016/j.chroma.2015.06.040

This paper comprises the majority of Chapter 2:

Daniel Gstoettenmayr was the primary author (70%) and conducted all the experiments, analysed data and wrote the manuscript. The co-authors contributed a total of 30% to the published work. Michael Breadmore, Joselito Quirino and Cornelius F. Ivory contributed to ideas, formalisation and development. Joselito Quirino offered experimental assistance. All co-authors assisted with refinement and presentation.

We the undersigned agree with the above stated “proportion of work undertaken” for the above submitted manuscripts contributing to this thesis:

Prof. Michael Breadmore

Supervisor

School of Physical Sciences

University of Tasmania

Date:

9/12/2015

for

Prof. John Dickey

Head of School

School of Physical Sciences

University of Tasmania

11/12/15

Acting HoS

List of publications and presentations

Parts of research works described in this thesis have been or will be reported in the following publications and presentations:

1. Gstoettenmayr, D.; Quirino, J. P.; Ivory, F. C.; Breadmore, M.; **Stacking in a continuous sample flow interface in capillary electrophoresis**, Journal of Chromatography A, Article in press, DOI: 10.1016/j.chroma.2015.06.040
(Chapter 2)
2. Gstoettenmayr, D.; Quirino, J. P.; Breadmore, M.; **Comparison of different Field Enhanced Sample Injection Techniques in Capillary Electrophoresis**; 11th Asia Pacific International Symposium on Microscale Separations and Analysis (APCE), Hobart, Australia, 27-30 November 2011.
3. Gstoettenmayr, D.; Quirino, J. P.; Breadmore, M.; **Development of a novel ultrasensitive capillary electrophoresis-mass spectrometry system for the analysis of environmental pollutants**; 20th Research & Development Topics Conference, Geelong, Australia, 11-14 December 2012.
4. Gstoettenmayr, D.; Quirino, J. P.; Breadmore, M.; **Development of a Flowing Sample Interface for Stacking in Capillary Electrophoresis**; 13th Asia Pacific Symposium on Microscale Separation and Analysis (APCE), Jeju, Korea (south), 3-6 November 2013.
5. Gstoettenmayr, D.; Quirino, J. P.; Breadmore, M.; **Development of a Flowing Sample Interface for Stacking in Capillary Electrophoresis**; 40th International Symposium on High Performance Liquid-Phase Separations and Related Techniques (HPLC 2013), Hobart, Australia, 18-21 November 2013.

6. Gstoettenmayr, D.; Quirino, J. P.; Breadmore, M.; **Development of a Flowing Sample Interface for Stacking in Capillary Electrophoresis**; 20th Research & Development Topics Conference in Analytical and Environmental Chemistry, Canberra, Australia, 11-13 December 2013.
7. Gstoettenmayr, D.; Quirino, J. P.; Breadmore, M.; **Development of a Flowing Sample Interface for Stacking in Capillary Electrophoresis**; 5th Australian and New Zealand Micro/Nanofluidics Symposium (ANZMNF), Hobart, Australia, 14-16 April 2014.
8. Gstoettenmayr, D.; Quirino, J. P.; Breadmore, M.; **Development of a Flowing Sample Interface for Stacking in Capillary Electrophoresis**; 30th International Symposium on Chromatography (ISC 2014), Salzburg, Austria, 14-18 September 2014.
9. Gstoettenmayr, D.; Quirino, J. P.; Breadmore, M.; **Development of a Flowing Sample Interface for Stacking in Capillary Electrophoresis**; 22nd Annual RACI Research & Development Topics Conference, Adelaide, Australia, 13-15 December 2014.

LIST OF ABBREVIATIONS

CE	Capillary electrophoresis
CEC	Capillary electrochromatography
CFD	Computational fluid dynamics
CGE	Capillary gel electrophoresis
CIEF	Capillary isoelectric focusing
CITP	Capillary isotachopheresis
CZE	Capillary zone electrophoresis
EKI	Electrokinetic injection
EOF	Electroosmotic flow
FASI	Field amplified sample injection
FASS	Field amplified sample stacking
i.d.	Inner diameter
ITP	Isotachopheresis
LIF	Laser induced fluorescence
LOD	Limit of detection
LVSS	Large volume sample stacking
MS	Mass spectrometry
MEKC	Micellar electrokinetic chromatography
Pt	Platinum
RSD	Relative standard deviation
SDS	Sodium dodecyl sulfate
UV	Ultra violet

ABSTRACT

The main purpose of the present work was to develop and optimize a continuous flow interface to improve the poor concentration detection limits of capillary electrophoresis which are one of its main limitations. The question was how the flow rate, applied voltage, interface and capillary dimensions and conductivities of background electrolyte and sample solution affect the electrokinetic sample injection in a continuous sample flow interface. Optimizing these parameters has the potential to perform near quantitative injection from large sample volumes in a short time. This can lead to the improvement of a variety of existing techniques that aim at lowering the concentration detection limits of CE.

The injection voltage and flow rate have been optimized and their effect on the injected sample amount has been investigated using a tee connector in a commercial capillary electrophoresis instrument. The effect of sample injection from both flowing and static sample volumes was investigated. Using a tee connector interface with flowing sample injection, four times more analyte could be injected into the capillary than in a static system. Theoretical simulations along with experiments were performed to investigate the effect of flow rate and injection voltage on the injected sample. The results confirmed that more analyte could be injected into the capillary in a flowing sample interface due to depletion of the ions from the flowing stream indicating near quantitative injection of all of the ions. Significant enhancement in the proportion of sample ions that are injected when injecting from a flowing sample stream has been demonstrated and this work is the only to compare electrokinetic injection of the same sample volume, under the same conditions with the only difference being whether the sample stream was flowing or static.

After having established the influence of the flow rate and injection voltage on the injected sample amount a mathematical model of the continuous sample flow interface was

developed. The aim was to investigate the influence of the interface dimensions on the depletion flow rate, which is the maximum flow rate at a given voltage at which > 90% of all sample ions are being injected. Besides this the influence of the capillary dimensions and the conductivity ratio of the sample and background electrolyte on the depletion flow rate were investigated. The mathematical model proposed that the total applied voltage, the electrophoretic sample mobility and the conductivity ratio between the liquid in the interface and the capillary should be as high as practically possible to give high depletion flow rates. The conductivity ratio and the electrophoretic sample mobility are determined by the chosen stacking method and analyte of interest in an experimental setup. High currents pose a practical limitation to the total voltage that can be applied. The results proposed further that there is an optimum interface diameter and length at which the depletion flow rate reaches a maximum. It should be noted that the depletion flow rate changed only around 5% when changing the interface length within a range of 2 to 20 mm and the interface diameter within 450 to 2750 μm . The mathematical model revealed that the depletion flow rate increases exponentially with the capillary inner diameter. Therefore the capillary inner diameter should be as big as practically possible. Out of all investigated variables a reduced capillary length showed the biggest improvements in depletion flow rate. The limitation when using a short separation capillary would be that the voltage needs to be reduced accordingly to avoid high currents.

To study the predictions of the mathematical model experiments were performed. First the effect of the interface inner diameter on the depletion flow rate was investigated. The mathematical model predicted a less than 4 % change in depletion flow rate when increasing the interface diameter from 500 to 1500 μm . A 500, 1000 and 1500 μm inner diameter sample flow interface was constructed and integrated into a homemade CE system. A fluorescence microscope was used to observe the injection of a fluorescent dye in the

transparent interface. During the injection process a plug of incoming sample replaced the BGE in the interface. It was found that the majority of BGE had to be replaced by the sample in order for the injection to reach stable conditions. In the 1000 μm inner diameter interface the depletion flow rate was found to be 0.08 $\mu\text{L/s}$. In the 1500 μm interface the main challenge was the formation of electrolysis bubbles around the electrode which prevented the determination of a depletion flow rate. In the 500 μm interface bubbles formed not only around the electrode but throughout the interface channel. This limited the number of injections that could be performed and no depletion flow rate could be determined. Bubble formation was attributed to overheating of the sample solution since the 500 μm channel is four times smaller in volume compared to the 1000 μm inner diameter interface. The formation of bubbles from electrolysis and overheating progressed with ongoing injection time in all interfaces used. Thus an injection approach was required that reached stable stacking conditions within a shorter timeframe. To achieve this sample was placed inside the interface from the start of the injection while the capillary was filled with BGE. This was expected to allow stable conditions from the start of the injection. Unexpectedly this approach caused the stacked sample zone to be move towards the capillary outlet within 10 sec of injection and did not allow the determination of a depletion flow rate either. A different BGE was chosen which was expected to stabilize the stacked sample zone at the capillary entrance during injection. This in contrast led to the formation of a stacked sample zone outside the capillary entrance and did not allow finding the depletion flow rate. For prospective future work fine tuning of the BGE parameters is therefore required. This would allow the formation of a stacked sample zone before bubble formation and to find the depletion flow rate in the 500 and 1500 μm inner diameter interface.

The mathematical model is a simplification that did not take into account the parabolic flow profile of the liquid flowing through the interface and the exact electric field line

distribution in the interface. A simulation model was developed to get better guidelines on how to choose the interface inner diameter for maximizing the depletion flow rate. The simulation model proposed that the depletion flow rate increases with bigger interface inner diameters. This result stands in contrast to the mathematical model which predicts a decrease in depletion flow rate with bigger interface diameters. It was found that the concentrations in the simulation model are not regulated by the Kohlrausch function. In contrast the concentration changes in the mathematical model were assumed to follow Kohlrausch's regulating function. This difference was found to be the cause for the differences in the predictions of the two models. A closer look at the simulation model revealed that stacking of ions occurred without the presence of a conductivity difference between the liquid in the capillary and the liquid in the interface. A combination of hydrodynamic flow of liquid into the capillary that counteracts the electrophoretic movement of ions out of the capillary entrance was found to be the cause for stacking without a conductivity difference. These findings were experimentally confirmed when stacking of a fluorescent dye in the absence of a conductivity difference was achieved. Therefore it can be assumed that the simulation model predictions are correct. Thus it is anticipated that with bigger interface diameters higher depletion flow rates can be achieved which can enhance the sensitivity of CE equipment when used with a continuous flow interface. The increase of depletion flow rate with interface inner diameter will have to be investigated in future work. This is a promising new direction and presents great potential for the sensitivity enhancement by electrokinetic injection from a flowing sample stream.

TABLE OF CONTENTS

Declaration.....	ii
Authority of access.....	ii
Statement regarding published work contained in the thesis.....	iii
Acknowledgement.....	iv
Statement of co-authorship.....	v
List of publications and presentations.....	vi
List of Abbreviations.....	viii
Abstract.....	ix
Table of contents.....	xiii

Chapter 1 INTRODUCTION AN LITERATURE REVIEW

1.1 INTRODUCTION.....	1
1.2 THE FAMILY OF CE MODES.....	2
1.3 CAPILLARY ELECTROPHORESIS.....	2
1.3.1 THEORY OF ELECTROMIGRATION.....	6
1.4 PRECONCENTRATION IN CE.....	9
1.5 CHEMICAL ANALYSIS.....	9
1.5.1 STACKING.....	11
1.5.1.1 FIELD INDUCED CHANGES IN VELOCITY.....	11
1.5.1.1.1 FIELD AMPLIFIED SAMPLE STACKING.....	13
1.5.1.1.2 FIELD AMPLIFIED SAMPLE INJECTION.....	15
1.5.1.1.3 LARGE VOLUME SAMPLE STACKING.....	18
1.5.2 SWEEPING.....	21
1.5.3 LIMITATIONS.....	23
1.6 CONTINUOUS FLOW INTERFACES.....	25
1.7 PROJECT AIMS.....	30
1.8 REFERENCES.....	32

Chapter 2 STACKING IN A CONTINUOUS SAMPLE FLOW INTERFACE IN CAPILLARY ELECTROPHORESIS

2.1	INTRODUCTION.....	40
2.2	EXPERIMENTAL SECTION	41
2.2.1	REAGENTS	41
2.2.2	INSTRUMENTATION	42
2.2.3	CONTINUOUS SAMPLE FLOW INTERFACE.....	42
2.2.4	PREVENTION OF PRESSURE INJECTION.....	45
2.2.5	ELECTROPHORETIC PROCEDURES.....	47
2.2.6	COMPUTER SIMULATION	49
2.3	RESULTS AND DISCUSSION.....	50
2.3.1	COMPARISON OF THE STATIC VIAL AND CONTINUOUS SAMPLE FLOW INTERFACE PERFORMANCE	50
2.3.2	COMPUTATIONAL FLUID DYNAMICS (CFD) SIMULATIONS OF THE INJECTION FROM A FLOWING SAMPLE.....	57
2.3.3	EXPERIMENTAL VALIDATION OF THE SIMULATION RESULTS	62
2.4	CONCLUSIONS.....	65
2.5	REFERENCES.....	66

Chapter 3 MATHEMATICAL MODEL AND EXPERIMENTS

3.1	INTRODUCTION.....	67
3.2	DEVELOPMENT OF THE MATHEMATICAL MODEL	68
3.2.1	DEFINITIONS AND DIMENSIONS	68
3.2.2	ELECTROKINETIC AND HYDRODYNAMIC FORCES FOR ELECTROKINETIC INJECTION FROM A FLOWING SAMPLE STREAM.....	69
3.2.2.1	APPARENT VELOCITY OF THE SAMPLE ION.....	72
3.2.2.2	DERIVATION OF THE INJECTION VOLTAGE	75
3.2.2.3	DEPLETION FLOW RATE FOR COMPLETE SAMPLE INJECTION	79
3.2.3	SENSITIVITY ANALYSIS OF THE DEPLETION FLOW RATE	81
3.2.3.1	INFLUENCE OF INTERFACE DIAMETER	82
3.2.3.2	EFFECT OF TOTAL APPLIED VOLTAGE AND SAMPLE MOBILITY	85
3.2.3.3	INFLUENCE OF CONDUCTIVITY RATIO.....	85
3.2.3.4	INFLUENCE OF INTERFACE LENGTH	86
3.2.3.5	INFLUENCE OF CAPILLARY DIMENSIONS.....	89

3.2.3.6	GUIDELINES FOR INTERFACE DESIGN FROM THE MATHEMATICAL MODEL.....	92
3.3	EXPERIMENTAL VALIDATION OF THE MATHEMATICAL MODEL.....	94
3.3.1	EXPERIMENTAL	94
3.3.1.1	MATERIALS AND INSTRUMENTATION	94
3.3.1.2	HOMEMADE CE SYSTEM	95
3.3.1.3	DETERMINATION OF INJECTED SAMPLE PROPORTION	101
3.3.1.4	ELECTROPHORETIC PROCEDURES.....	103
3.3.1.5	HYDROGEL PREPARATION.....	104
3.3.2	RESULTS AND DISCUSSION.....	104
3.3.2.1	FLOW STUDIES	104
3.3.2.1.1	PREVENTION OF SAMPLE MATRIX INJECTION USING A HYDROGEL.....	105
3.3.2.1.2	PREVENTION OF SAMPLE MATRIX INJECTION BY ADJUSTING LIQUID LEVELS.....	105
3.3.2.1.3	EFFECT OF FLOW RATE ON SAMPLE MATRIX INJECTION.....	109
3.3.2.2	LINEARITY	111
3.3.3	DEPLETION FLOW RATE IN THE 1000 μm DIAMETER INTERFACE.....	114
3.3.3.1	INJECTION OF A FLUORESCENT DYE	114
3.3.3.2	INJECTION AS A FUNCTION OF TIME	116
3.3.3.3	PROPORTION OF INJECTED SAMPLE AMOUNT.....	119
3.3.3.4	DEPLETION FLOW RATE DETERMINATION.....	121
3.3.4	DEPLETION FLOW RATE IN A 1500 μm DIAMETER INTERFACE.....	126
3.3.5	DEPLETION FLOW RATE IN A 500 μm DIAMETER INTERFACE.....	130
3.3.6	AVOIDING BUBBLE FORMATION.....	133
3.3.6.1	INJECTION WITH A SAMPLE FILLED INTERFACE AS STARTING CONDITION	133
3.3.6.2	INJECTION WITH A HEPES-KOH BUFFER	136
3.4	CONCLUSIONS.....	138
3.5	REFERENCES.....	141

Chapter 4 COMPUTATIONAL FLUID DYNAMICS MODEL OF THE CONTINUOUS FLOW INTERFACE

4.1 INTRODUCTION..... 142

4.2 COMPUTATIONAL FLUID DYNAMICS MODEL 143

4.3 RESULTS AND DISCUSSION..... 147

 4.3.1 DEPLETION FLOW RATE f_{10} FOR 2.5 mm INTERFACE DIAMETER..... 147

 4.3.1.1 INJECTED SAMPLE PROPORTION 147

 4.3.1.2 DEPLETION FLOW RATE f_{10} 150

 4.3.2 MAXIMIZING THE DEPLETION FLOW RATE f_{10} 154

 4.3.3 COMPARISON OF THE SIMUALTION MODEL WITH THE MATHEMATICAL MODEL 158

 4.3.3.1 COMPARISON OF THE INJECTION VOLTAGES 160

 4.3.3.2 CONDUCTIVITY COMPARISON 162

4.4 CONCLUSIONS..... 170

4.5 REFERENCES..... 172

Chapter 5 GENERAL CONCLUSIONS AND FUTURE DIRECTIONS

5.1 GENERAL CONCLUSIONS..... 173

5.2 FUTURE DIRECTIONS..... 177

Chapter 1

INTRODUCTION AND LITERATURE REVIEW

1.1 INTRODUCTION

One of the earliest contributions to electrophoresis might have been made by Tiselius [1,2] in 1937. He introduced moving boundary electrophoresis and used it to monitor the movement of protein molecules in an electric field. Earlier on Michael Faraday summarized his findings by the law of electrolysis. Further Helmholtz, Hittorf and Kohlrausch extensively studied the migration of small inorganic ions under the influence of an electric field [3]. Supporting media such as starch, paper, gels and other stabilizers which contained the buffer solution were used which is summarized beautifully in an excellent review by Righetti [4]. There are numerous more great inventors who contributed to the field and made efforts to overcome the limitations due to band broadening and instrumentation.

Originally electrophoresis was described in free solution carried out in capillaries. Hjerten was the first to describe the use of a high electric field using 2450 V for separation in his machine which employed glass tubes of 3mm i.d. [5]. A further reduction in i.d. was achieved by Mikkers *et al.* who employed Teflon capillaries of 200 μm i.d. using currents of around 30 μA [6,7]. This further reduced convective problems. Jorgensen and Lukas employed open tubular glass capillaries with an i.d. of 75 μm using up to 30 kV in which they performed capillary zone electrophoresis [8]. This was the first demonstration of the power of CE

showing that capillaries with i.d.'s smaller than 100 μm can result in highly efficient electrophoretic separations. Further advantages of Jorgensen and Lukas's system were the use of on-line detection and the successful dissipation of heat due to small i.d. while still functioning successfully at high voltages.

Then in the 1980s, commercial instruments were developed to allow for a temperature controlled environment which makes it possible to use different modes of CE and opens up a variety of new possibilities on how to use this versatile separation method.

1.2 THE FAMILY OF CE MODES

The collectively named "capillary electrophoresis" modes comprise capillary zone electrophoresis (CZE), often referred to as free solution capillary electrophoresis, micellar electrokinetic chromatography (MEKC), capillary isoelectric focusing (CIEF), capillary gel electrophoresis (CGE), capillary electrochromatography (CEC), and capillary isotachopheresis (CITP).

CZE is the simplest and most widely used mode of CE. The CZE system can be manipulated to become other modes of CE such as MEKC by adding surfactants, CGE by adding gel forming agents and CEC by adding packed chromatographic particles or monolithic polymer substrates.

1.3 CAPILLARY ELECTROPHORESIS

The migration of charged species under the influence of an electric field is referred to as electrophoresis. The migration can be carried out in free solution, in a capillary or a non-convective surrounding [9]. Due to the differing migration velocities the analyte ions are

separated in the electric field. The basic instrumental set-up of a CE system is illustrated in Figure 1.1. The separation of the analyte ions takes place inside a thin fused silica capillary (25-100 μm i.d.). Depending on the analyte ion to be investigated, the inner surface of the capillary may be coated or uncoated. This coating influences the magnitude and the direction of the electroosmotic flow (EOF). In the case of an uncoated fused silica capillary the silanol groups on the inner surface of the capillary lead to the formation of a cathodic EOF, depending on their degree of dissociation. Both ends of the capillary, which is entirely filled with the background electrolyte (BGE), are placed into the BGE vials. A potential difference of up to 30 kV is applied from end to end of the capillary. Due to this an electric field is established which induces an electric current. Sample injection (a few nL) can be done by removing the buffer reservoir at the inlet and placing the inlet of the capillary into the sample vial. The sample is introduced into the capillary either by a height difference of the inlet and outlet vials, by applying pressure to the inlet vial, by applying vacuum at the outlet vial, or by electrokinetic injection which uses an electric field.

Ions have different mobilities if their charge to effective hydrodynamic radius in solution ratios are different. If the analytes are not exactly physically identical the resulting mobilities can also be different. They migrate through the capillary at different velocities and if the resolving power of the used instrumentation is big enough this leads to analyte separation. Consequently, sample ions are separated according to their relative migration through the capillary. The net migration velocity of a sample ion is equal to the vector sum of its electrophoretic velocity plus the electroosmotic velocity of the solution. The electroosmotic flow (EOF) is equal for all analytes. Depending on degree of dissociation and on the inner surface of the capillary wall the EOF can vary in size and direction.

There are various methods for the detection of the analyte ions. Ultraviolet (UV) absorbance detectors or laser induced fluorescence (LIF) detectors are used very frequently. In the case of UV detectors a light beam is used to measure the absorbance of the sample ions as they pass by the detection window. In a LIF detector an excitation beam induces fluorescence in the sample and the emission of the sample is measured. These detectors allow an on-line detection of the samples.

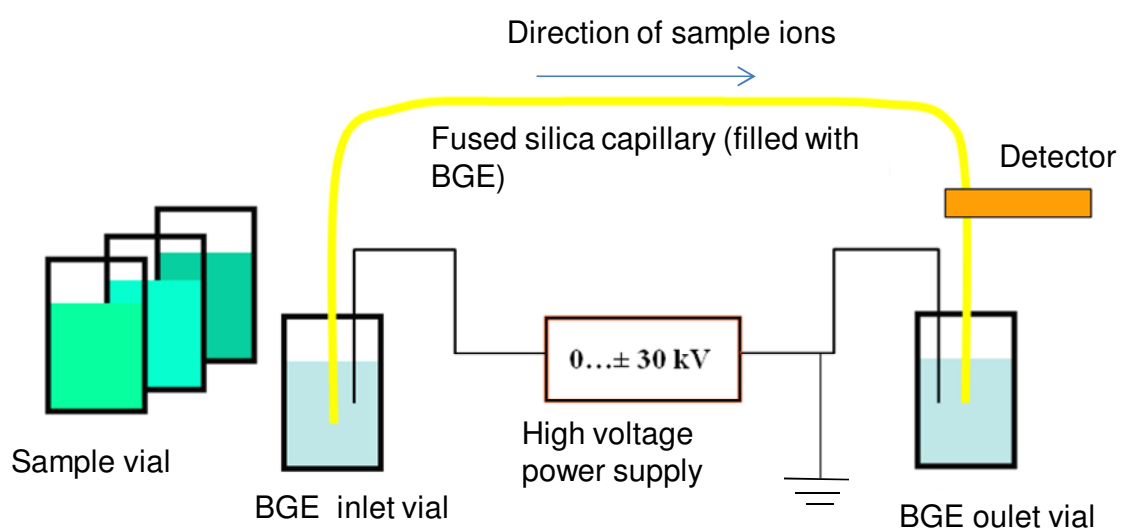


Figure 1.1 Instrumental set-up of a CE system

1.3.1 THEORY OF ELECTROMIGRATION

When a charged component is placed into an electric field it is accelerated by the electric force F_e which is proportional to the electric field strength.

$$F_e = \frac{z \cdot F \cdot E}{N_A}$$

F_e	electric force
z	charge number
F	Faraday constant
N_A	Avogadro constant
E	electric field strength

The friction force F_d , which is determined by Stoke's law counterbalances the electric force.

$$F_f = 6 \cdot \pi \cdot \eta \cdot r \cdot u_{ep}$$

F_f	friction force
η	dynamic viscosity
r	Stoke's radius
u_{ep}	electrophoretic migration velocity

At equilibrium the electric force and the friction force are equal in size.

$$F_e = F_f$$

Transforming this equation yields:

$$u_{ep} = \frac{z \cdot F \cdot E}{N_A \cdot 6 \cdot \pi \cdot \eta \cdot r} = \frac{z \cdot e \cdot E}{6 \cdot \pi \cdot \eta \cdot r}$$

Since $\mu_{ep} = \frac{u_{ep}}{E}$ the electrophoretic mobility μ_{ep} can be calculated by the following formula:

$$\mu_{ep} = \frac{u_{ep}}{E} = \frac{z \cdot e}{6 \cdot \pi \cdot \eta \cdot r}$$

u_{ep} electrophoretic migration velocity
 μ_{ep} electrophoretic mobility
 e elemental charge

Depending on the inner capillary wall surface a certain EOF, which is superimposed on the electrophoretic migration, will arise. Electroosmosis causes the bulk flow of the entire BGE and depends on the electric field strength. The surface charge on the inner capillary wall leads to the formation of an EOF. In the case of a fused silica capillary the negatively charged surface is caused by deprotonated silanol groups. The BGE cations balance the negative surface charge and thereby form a mobile layer of opposite charge (Figure 1.2).

Upon application of an electric field, a flow of the entire mobile layer towards the cathode is created. The Helmholtz equation describes the EOF. Its quantity can be measured by measuring the migration velocity of a detectable neutral substance, which is called an EOF marker. The net velocity u_{app} is the vectorial sum of u_{ep} and u_{eo} (Figure 1.3) and describes the separation of the ions in the analyte sample solution.

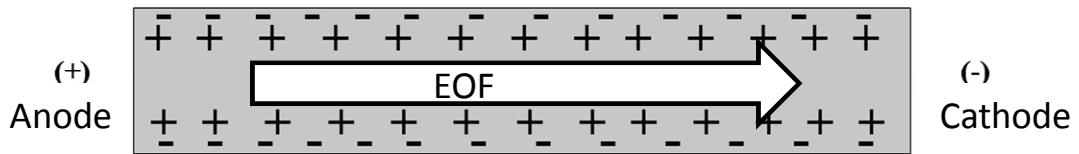


Figure 1.2 Formation of the EOF in a CE system.

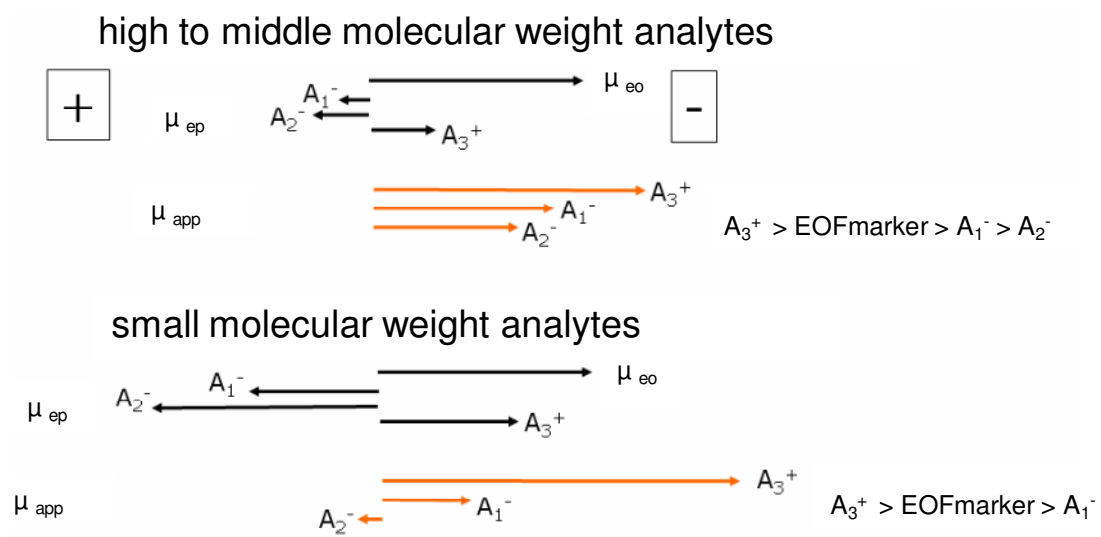


Figure 1.3. Apparent mobility as the vector sum of u_{eo} and u_{ep}

1.4 CHEMICAL ANALYSIS

A chemical analysis can comprise sampling, sample pretreatment in the field, laboratory treatment, laboratory assay, calculations, and results presentation. The initial step of the analysis is sampling in which a representative portion of a bulk material is removed. Immediately after collection it may be necessary to pretreat the sample chemically or physically at the sampling site. The sample then arrives at the laboratory which is commonly termed the laboratory sample. The laboratory sample usually needs to be further reduced in quantity and might need to be processed further by a set of operations in which it is converted to the test sample. It may be necessary to remove or mask interferences, or isolate the intended analyte from its sample matrix to obtain the test sample. In many analytical procedures the analyte needs to be converted chemically to another form to make its measurement possible. If the concentration of the analyte prior to performing the assay does not fall within the range of the analytical method its concentration needs to be adjusted. Once the sample is prepared instrumental methods can be used to perform the laboratory assay. In the last stage calculations are performed and the results are presented in a meaningful manner.

1.5 PRECONCENTRATION IN CAPILLARY ELECTROPHORESIS

CE can be applied to a diverse range of analytes ranging from small inorganic ions to large biomolecules. Thus it is a promising high-resolution separation technique used in many biotechnological and clinical research fields. The main advantages compared to liquid chromatography techniques are its instrumental simplicity, rapid analysis time, minor reagent consumption, and the different modes (see 1.2.) of CE depending on the analytes. It can be used in the studies of proteins [10], pharmaceutical and environmental pollutants [11] and for

DNA analysis [12]. Despite this the main limitation of CE with absorbance detection is its high concentration LOD stemming from a short light-path for absorbance detection and a small sample volume [13]. A number of preconcentration techniques can be used in order to overcome this issue. One way is to perform off-line preconcentration methods which are utilised before sample loading. Another way is to combine the preconcentration step with the separation, which is referred to as on-line preconcentration. Off-line preconcentration methods usually use a large sample volume from which the sample is reconstituted into a smaller volume. Then a small proportion of the preconcentrated sample is injected into the CE system. The major drawbacks of this method in comparison with on-line preconcentration methods are that it is more time consuming and labor intensive and that analyte loss during sample handling and incomplete transfer of sample from the preconcentration device to the CE can appear. Incomplete transfer may stem from incomplete solubility of the analytes as it can appear in liquid-liquid extraction or irreversible adsorption of analytes in solid-phase-extraction. In comparison on-line sample preconcentration merely involves only filtering of the solution.

To perform a chemical analysis using CE with preconcentration the following steps need to be performed. The first step is sampling followed by sample pretreatment in the field. The laboratory treatment stage only involves filtering of the solution. The preconcentration, injection and separation stage are all combined into one step in CE with preconcentration. This makes CE with preconcentration an attractive alternative to CE with offline preconcentration.

1.5.1 STACKING

Most of these strategies are based on a chemical discontinuity that is located inside the capillary around which analytes are concentrated. This concept is commonly called ‘stacking’ or ‘sweeping’ and a range of different discontinuities can be created including conductivity (field amplified sample injection [6-8,14-18], field amplified sample stacking [6,19] and isotachophoretic stacking [20-24]), pH (dynamic pH junction [25]) and micellar effects [26,27] (sweeping [28,29] and micelle collapse [30,31]). A key requirement for all methods is the presence of an electrophoretic velocity component that changes upon entering a boundary and causes a preconcentration.

1.5.1.1 FIELD INDUCED CHANGES IN VELOCITY

The principle of stacking due to field induced changes in velocity are shown in Figure 1.4. A sample ion travels at a certain velocity under a given electric field strength (E). Once the sample ion enters a zone with a lowered E it will slow down and stack into a narrow zone resulting in a stacked sample zone with higher concentration.

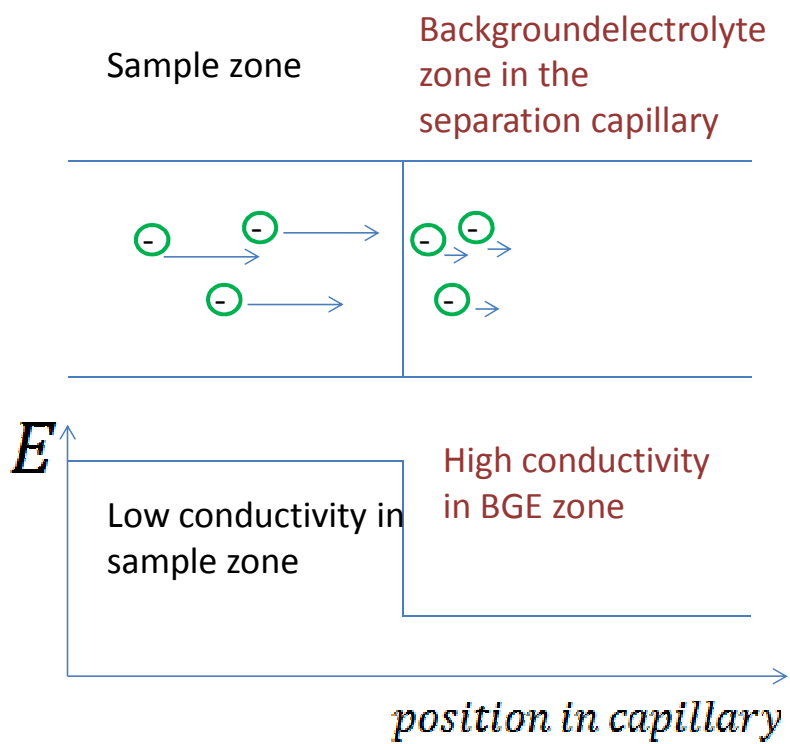


Figure 1.4 Schematic of stacking due to field induced changes in velocity

1.5.1.1.1 FIELD AMPLIFIED SAMPLE STACKING

Field amplified sample stacking (FASS) is the easiest and most common sample stacking technique. It is also known as the normal stacking mode (NSM). A low conductivity sample plug is injected hydrodynamically. The conductivity of the sample plug is at least ten times lower than that of the background electrolyte (BGE). Upon application of voltage the electric field strength in the sample zone is higher than that in the BGE. The ions in the sample zone travel at a certain speed under the given electric field. Once they enter the BGE zone with lower electric field strength they slow down at the boundary and stack into a zone of higher concentration. The concentration enhancement or sensitivity enhancement for a sample ion is determined by its ratio of the velocities in the sample zone and the BGE zone. The sensitivity enhancements that can be achieved by the normal stacking mode are usually around 10 to 20 times compared to injection from a sample zone that has the same conductivity as the BGE.

There are two major drawbacks to this stacking approach. The first one is that the sample should be prepared in a low conductivity matrix to provide the necessary conductivity difference between sample zone and BGE. Thus, its applicability is limited to low conductivity samples. In general this can be achieved by preparing the sample in water [32] or diluted buffer. The use of organic solvents has shown to have beneficial effects on FASS besides lowering the sample zone conductivity [33]. Another limitation of FASS is the maximum length of the hydrodynamically injected sample plug. It is limited to about 5% of the capillary volume. Exceeding this limit will result in band broadening due to the mismatch of the local electroosmotic velocities in the BGE and the sample zone. The pressure differential created by this difference leads to a flow inside the capillary that will broaden the stacked sample zone.

Because of its simplicity and ease of use FASS can be used in combination with many different types of detection methods such as fast-scan cyclic voltammetry detection [34], contactless conductivity detection [35], as well as many types of BGEs at high or low pH [36] that may contain chiral selectors or organic solvents. Another advantage is that it can be combined with other on-line preconcentration techniques such as sweeping and reversed field stacking [37]. Due to its ease of use it can be coupled with off-line preconcentration techniques such as Soxhlet extraction [38] or subcritical water extraction [39]. For example, Chen *et al.* [40] developed a rapid high-throughput magnetic solid phase extraction (MSPE) method coupled with capillary zone electrophoresis for the determination of illegal drugs. They used FASS to further enhance the sensitivity of this method. A 30 mM phosphate buffer solution at pH 2.0 containing 15% v/v ACN was used. Under optimized conditions the sensitivity was increased about tenfold compared to injection and separation without stacking. A home-made MSPE array was used that has potential to treat 96 samples simultaneously.

1.5.1.1.2 FIELD AMPLIFIED SAMPLE INJECTION

While in FASS the sample is introduced hydrodynamically, it is introduced by electrokinetic injection in field amplified sample injection (FASI). When performing electrokinetic injection two situations, depending on the direction of the electroosmotic flow (EOF), can arise. Under co-EOF conditions (the EOF is oriented in the same direction as the sample ions movement) the sample will be injected by the electroosmotic flow as well as by its own electrophoretic movement. In this case more sample ions are injected than at a FASS injection of the same sample zone length. Under counter EOF conditions (the EOF is oriented in the opposite direction of the sample ions) the sample matrix will be pumped into the capillary but the sample ions migrate towards the inlet. Under these conditions less sample ions will be injected when comparing it to FASS. The direction and magnitude of the EOF is therefore an important factor to consider when performing FASI. There are also two major drawbacks to FASI. Firstly this approach is restricted to low conductivity samples since the stacking effect relies on the differences in electric field strength. The other disadvantage arises from the fact that during FASI the sample matrix is introduced into the capillary by EOF (in a co-EOF injection). Once approximately 5% of the capillary volume is filled with sample matrix the peaks begin to become broader for the same reason as discussed in section 1.5.1.1.1. Another important fact about FASI is that the sample ions will be injected to a different extent based on their differences in mobility. While the mobility based injection and the discrimination effect resulting from it may seem a disadvantage, FASI can give up to 1000 fold increase in sensitivity. A way to improve reproducibility is to inject a short water-plug prior to sample injection. This approach prevents analytes from being lost from the inlet and it can enhance the sensitivity of the stacking method.

If the EOF is suppressed completely the physical volume that enters the capillary will be reduced and therefore allows longer injection times. Hou *et al.* [41] described an interesting study where they suppressed the EOF to simultaneously stack cationic and anionic compounds in a single run by two-end field amplified sample injection. Firstly the capillary was filled entirely with a high conductivity buffer and then a water plug was injected into each end of the capillary. This created two high-field strength zones at both ends of the capillary upon application of voltage. This approach allowed simultaneous stacking of anions and cations. The sample cations and anions were detected by a common detector which was placed in the capillary center. They used model cationic (matrine and oxymatrine) and anionic (5-sulfosalicylic acid) compounds to optimize the separation. Limits of detection of 20 ng/L for the cationic and 60 ng/L for the anionic model compounds were determined, respectively. When comparing this approach with non-stacking conditions sensitivity enhancement factors of 1003-, 1330- and 1380 could be obtained for the model cationic (matrine and oxymatrine) and anionic (5-sulfosalicylic acid) compounds, respectively.

Due to its simplicity FASI is compatible with many different detection systems such as contactless conductivity detection [42] [43] and electrochemiluminescence detection [44]. It can also be combined with offline preconcentration techniques such as magnetic solid phase extraction [45], polymer monolith microextraction [46], liquid-liquid extraction [47], solid phase extraction [48], solvent-bar microextraction [49], as well as dispersive liquid-liquid microextraction [50]. Another advantage when using FASI is that it can be combined with online preconcentration techniques such as sweeping [51] or MEKC [52]. In a recent study by Hai *et al.* [53] FASI was combined with in-capillary derivatization for the determination of selenomethionine and selenomethionine selenoxide. The derivatizing agent phthalic anhydride

was first introduced into the capillary hydrodynamically. The derivatization itself was done by simply injecting the sample solution electrokinetically. This allowed preconcentration of the analytes. The sample solvent was 2 mM borate solution. As BGE they chose a borate buffer which was suitable for the derivatization and the separation. Sensitivity enhancement of about 800-fold could be achieved when comparing it to direct CE-UV detection without derivatization or stacking in the same setup.

An example for the versatility of FASI is that it is applicable to a range of buffer types at low [54,55] or high pH [56], to buffer systems with chiral selectors [57] as well as to ionic liquid electrolyte systems [58]. FASI has a wide range of applicability and can be used in combination with other CE methods. In a study by Wei *et al.* [59] it was combined with monolith microextraction in an octadecyl phosphonic acid-modified zirconia-coated CEC column for the analysis of antidepressants in human plasma and urine. Further FASI has been used for the separation of multiplex polymerase chain reaction products in non-gel sieving capillary electrophoresis [60]. FASI is an almost universal stacking method that can be applied under a number of different conditions.

1.5.1.1.3 LARGE VOLUME SAMPLE STACKING

FASS and FASI are both limited by the physical volume of sample that can be injected into the separation capillary. Volumes larger than 5% cause a loss in efficiency due to the EOF mismatch as explained in section 1.5.1.1.1. Large volume sample stacking (LVSS) allows larger volumes of sample to be injected by removing the sample matrix continuously while the analytes stack at the sample/BGE boundary. The sample matrix is removed from the capillary by the EOF. Before the samples exit the capillary inlet the matrix removal is stopped and the separation begins. There are different approaches to perform the transition between the removal step and the separation start. The transition can be done by polarity switching or by chemical variation of the EOF.

When performing LVSS with polarity switching a reversed polarity is applied after hydrodynamic sample injection causing the sample matrix to be removed by the EOF. Before the stacked analyte zone exits the capillary the polarity is reversed and the separation starts. To ensure that no sample is lost the transition is controlled by monitoring the current. Once the current reaches 95-99% of the final current – the current when the capillary is entirely filled with BGE – the polarity is switched and the separation starts. LVSS with polarity switching was recently employed for the online concentration and analysis of flavonoids in *Brassica oleracea* (broccoli) [61], the determination of natural polyphenols in plant extracts [62], trace determination of sulfonylurea herbicides in water and grape samples [63], the analysis of haloacetic acids in water [64], the sensitive determination of barbiturates in biological matrix [65] and for the characterization and inhibition studies of the nucleoside-metabolizing enzymes purine nucleoside phosphorylase and adenosine deaminase present in membrane preparations of human 1539 melanoma cells [66]. In the last study only 10 fold sensitivity enhancements could be achieved when compared with CE without stacking. The

authors state that this represents the highest sensitivity for nucleoside and nucleobase analysis using CE with UV detection reported so far.

In the case of LVSS without polarity switching the transition can be performed by reversing or suppressing the EOF. When performing the transition by reversing the EOF a dynamic EOF reversal agent in the BGE is used. Upon application of voltage the BGE enters the capillary from the detector side, since the bulk EOF points towards the capillary inlet. The EOF in the sample zone points towards the inlet while the EOF in the BGE zone has opposite direction. Once the sample matrix gets shorter and shorter the EOF in the sample zone and the EOF in the BGE zone reach a point where they counterbalance each other and the apparent EOF becomes zero. This is the point where the matrix removal stops and the separation starts. The advantage of LVSS without polarity switching is that the transition is controlled chemically and not manually which is instrumentally simpler and allows better control over analyte loss from the capillary inlet. The downside is that its success depends on the control and reproducibility of the EOF.

Another approach to perform LVSS without polarity switching is to suppress the EOF by using a high pH sample matrix in combination with a low pH BGE. When voltage is applied the bulk EOF causes the BGE to enter the capillary from the detection end. Once the matrix gets removed the average EOF is determined by the low EOF in the BGE and the transition starts. The bulk solution travels slower towards the inlet than the sample ions towards the detector. This approach is commonly termed LVSS using an EOF pump (LVSEP). In a complex approach that combines different CE-techniques, Wang *et al.* [67] developed a highly sensitive method for enantioseparation of fenoprofen and amino acid derivatives with vancomycin as the chiral selector using LVSEP. They used the partial filling method, LVSEP,

as well as anion-selective exhaustive injection (LVSEP-ASEI) to increase the sensitivity of the method. Enantioseparation of racemic fenoprofen and six 9-fluorenylmethyl chloroformate (FMOC)-amino acid derivatives (at the concentration level of ng/mL) with the background electrolyte composed of 100mmol/L Tris-H₃PO₄ (pH 6.0) and 2 mmol/L vancomycin was performed. The capillary was coated with poly(dimethylacrylamide) solution to depress the EOF which is required to perform LVSEP-ASEI. By coating the capillary they could further minimize the adsorption of the chiral selector to the capillary wall. Under the optimized conditions, they could achieve a 1000-fold enhancement in detection sensitivity compared with the normal injection. In the field of chiral analysis another study by Kawai *et al.* [68] investigated the effects of the addition of cyclodextrin (CD) into the BGE on the LVSEP preconcentration of ibuprofen in urine which was desalted with a C 18 solid-phase extraction column. This study is good example for the versatility of LVSEP and its applicability to many separation modes. Further LVSEP has been recently used for the analysis of oligosaccharides [69] and in combination with partial filling affinity capillary electrophoresis (PFACE) for profiling of glycoprotein-derived oligosaccharides [70]. In microchips Kawai *et al.* [71] used LVSEP for the determination of natural polyphenols in plant extracts and could achieve sensitivity enhancement of up to 2200-2900-fold compared to conventional microchip CE analysis.

Due to the simplicity of LVSS it can be combined with offline preconcentration methods such as phase transfer membrane supported liquid-liquid-liquid microextraction [72] and dispersive solid-phase extraction [73]. LVSS can also be used together with other CE techniques as presented in a study undertaken by Al-Ghobashy *et al.* [74]. They employed on-line micellar sample stacking for the determination of protein concentration of

biopharmaceuticals. Protein samples were denatured using SDS and then injected into polyethylene oxide (PEO) - filled capillaries. The protein-SDS molecules stacked at the interface between the sample plug and the PEO plug. SDS further enhanced the sensitivity due to micelle formation in which the protein-SDS molecules partitioned. A useful tool for the determination of melamine and its derivatives in liquid milk products has been developed by Jin *et al.*[75]. The three different stacking approaches LVSS, sweeping and selective-exhaustive injection sweeping have been successfully combined to enhance the sensitivity of the method. In order to detect all four analytes simultaneously LVSS-sweeping was used. To further enhance the sensitivity of the method selective-exhaustive injection-sweeping of the anions and cations was performed separately. Limits of detection of 10 ng/L for melamine and ammeline, 50 ng/L for cyanuric acid as well as 20 ng/L for ammelide could be achieved by combining the different stacking approaches. A more recent study employed microemulsion electrokinetic capillary chromatography coupled with on-line LVSS for the analysis of plant hormones [76].

1.5.2 SWEEPING

By using a pseudostationary phase in CE non-charged analytes can be separated and investigated. SDS was used as a pseudostationary phase in micellar electrokinetic chromatography (MEKC) which was originally developed by Terabe *et al.* [77,78].

Quirino and Terabe initially developed sweeping in order to increase the concentration detection sensitivity for charged and neutral analytes in MEKC when the sample and BGE have the same conductivity [27,79]. Sample was first injected without the pseudostationary phase. Upon application of voltage the micelles from the BGE pass through the sample zone

and sweep the analytes into a narrow band much like a broom picking up dust from the floor. The chromatographic retention factor k describes the enrichment of the analytes. k is a measure for the analyte-micelle interaction. Since sweeping can be applied to neutral and charged analyte molecules and to high conductivity it is a universal concentration method.

A further enhancement can be achieved when sweeping is combined with stacking. This can be achieved by having a sample that has a lower conductivity than the BGE. Besides sweeping of the analytes due to the moving micelle front, stacking increases the sample zone concentration further [79]. Using a combination of sweeping with SDS micelles and stacking can give enrichment factors from 31 to 300. It has been successfully employed for the determination of analytes in human serum/plasma, bacterial growth medium, urine, and medicinal products [80-85].

With equal conductivity between sample and BGE the analyte focusing is solely determined by the retention factor k of the micelles. This approach can be used for neutral analytes with SDS micelles [86-89] as well as charged analytes and anionic sulphated- β -cyclodextrin as the pseudostationary phase [90]. This approach allowed 25 – 2500-fold increase in sensitivity compared to normal MEKC. It could be successfully applied to the analysis of steroids in urine, herbicides in cereal, vegetable and water samples.

A new method was developed by Rabanes *et al.* It was employed for the determination of charged alprenolol enantiomers. The sample solution contained a high content of organic solvent [90]. The pseudostationary phase used was sulfated- β -cyclodextrin. Due to the presence of the organic solvent the analyte has only a weak interaction with the pseudostationary phase in the sample solution. The analytes are electrokinetically injected from the sample solution and move in the opposite direction of the pseudostationary phase.

Once the analytes enter the aqueous BGE zone they get swept by the pseudostationary phase. In the conventional sweeping mechanism the analyte gets focused when the pseudostationary phase front moves through the sample zone. The enhancement factor was greater than two orders of magnitude when introducing the sample electrokinetically for the chiral separation of alprenolol enantiomers in standard solutions.

1.5.3 LIMITATIONS

Sample stacking methods can be used with sample injected either hydrodynamically or electrokinetically. Sensitivity enhancements with hydrodynamic injection are limited by the volume of the capillary – it is impossible to inject more than one capillary volume. Therefore much greater sensitivity enhancements can be achieved with electrokinetic injection (EKI) as it is not limited by the volume of the capillary. Sensitivity enhancements of $10^4 - 10^6$ have been demonstrated, although with these enhancements sample depletion is observed [91,92]. Sample depletion limits the sensitivity enhancement that can be achieved.

One way to overcome the limitations associated with sample depletion would be to increase the sample volume that is available for injection in a static sample vial. By optimizing the spatial relation between the capillary inlet and the electrode setup more of the sample volume can be made available for injection. Hirokawa *et al.* explored this issue [93] and found that only analytes in an effective potential field, which is essentially the volume of sample between the electrode and the capillary tip, could be introduced into the capillary while analytes outside the field are not injected. This suggests a localized injection zone in which the ions are depleted. The analyte ions from outside this region only enter the field

region by diffusion. Therefore long injection times may be required to inject a large fraction of ions from the total sample volume.

This led them to develop circular Pt-electrodes placed at the very top of the sample such that a 3D electric field is created that covers almost the entire sample volume [94]. Utilizing a different electrode design greatly improved the transport of ions to the capillary tip, introducing about 70 % of analyte amount existing in 230 μL of sample volume within 450 s into the capillary.

Another way to overcome the limitations associated with sample depletion would be to replenish the sample volume that is being available for injection continuously. Hirokawa's [94] group achieved replenishing of the sample stream by stirring the sample solution. They increased the sample volume from typical 500 μL to 17 mL using a ring electrode for injection. An improvement in sensitivity of 100 000 was obtained compared to a conventional hydrodynamic injection. Despite this the drawback when stirring the sample is that the sample depletes with injection time and the injection gets less efficient with ongoing injection time.

In order to overcome the drawbacks of localized depletion the effective potential area needs to be replenished with undepleted sample during the injection by injecting from a flowing sample stream. Supplying an undepleted stream of sample during the injection can in theory lead to more sample injection in a shorter time period.

1.6 CONTINUOUS FLOW INTERFACES

In a conventional CE setup the capillary entrance is placed in a sample vial and sample is injected. Then the sample vial is replaced by a vial containing BGE and the separation is started by applying voltage between the capillary ends. A continuous flow interface is used instead of separate vials containing sample and BGE. The capillary entrance is placed in a continuous stream of liquid. First the continuous flow interface is flushed with sample and injection is performed. Then the continuous flow interface is changed to BGE and voltage is applied between the capillary ends to start separation. The construction of such an interface is critical and the underlying principles will be discussed here in detail. Several aspects have to be considered when constructing a continuous flow interface for CE.

- The first one is that the BGE as well as the sample solution are continuously flushed through the interface. This may overcome the problems that originate from decomposition due to electrolysis of the BGE or the sample solution. In conventional CE systems the sample vials need to be replaced frequently otherwise migration time drifts as well as baseline irregularities may be observed. When the solutions are continuously replenished electrolysis will not affect the separation performance.
- Another difference is that in a conventional CE setup the voltage needs to be interrupted when performing an injection. Also the vials need to be moved physically in between. In a flow interface-CE system there is no need to move the vial or to interrupt the voltage for injection purposes. Further the reproducibility should be improved when no moving parts are involved.

- The polarity of the electrodes plays an important role. The grounding electrode should preferably be placed in the interface itself. If the high voltage is connected to the interface special measures have to be taken to isolate the high voltage from the rest of the interface channels such as the waste outlet and the pump that replenishes the interface. Otherwise uncontrolled currents may appear and influence the precision of the whole setup.
- Any hydrodynamic flow into the CE capillary should be avoided. Therefore the inner diameter of the waste channel should be maximized. The inlet and the outlet of the CE capillary have to be kept at the same level otherwise hydrostatic pressure will occur and cause hydrodynamic flow inside the capillary.
- Each type of interface requires individual optimization of parameters such as flow rate, length of injection and applied voltage. In practice the optimum set of parameters may be quite narrow. The optimization of these parameters is crucial when setting up a flow injection-CE interface and it is not trivial [96].

The first report of using flowing interfaces for CE were Kuban *et al.* [97] who developed a flow-through channel and Fang *et al.*[98] who developed a flow-through reservoir. They basically consist of a flow through channel into which the electrode and the CE capillary inlet are inserted. The first interface (Figure 1.5 a) consists of a poly(methyl methacrylate) (PMMA) block into which a horizontal flow-through channel is drilled as well as two vertical channels into which the electrode and the CE capillary are inserted. The capillary as well as the electrode are aligned in a way that they reach the center of the flow-through channel. In the interface in Figure 1.5 b an Eppendorf pipette tip (P) forms a conical flow through channel

which is placed in a supporting vial (R). The electrode (E) is simply inserted into the supporting vial and the CE capillary (C) is placed into the center of the conical pipette tip. The capillary inlet of the CE capillary is positioned as close as possible to the narrow end of the conical tip (2 mm distance between CE capillary inlet and the narrow end of the pipette tip). In both cases the interface is continuously replenished by means of a peristaltic pump. The electrode in the interface, which is usually a Pt wire, is connected to the ground of the CE instrument. The CE capillary is electrically connected to the high voltage of the CE via a second Pt electrode that is placed in the capillary outlet vial.

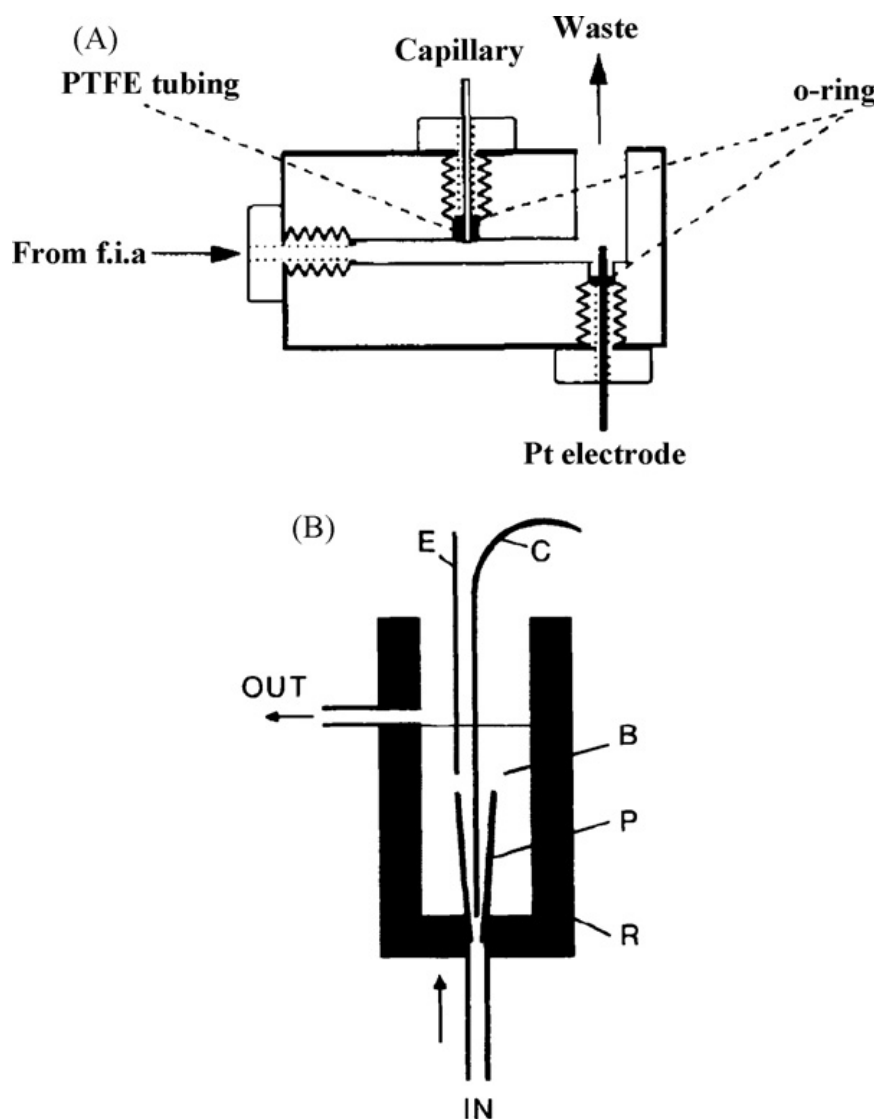


Figure 1.5 A schematic diagram of the two original on-line flow injection-CE interfaces developed by Kuban *et al.* (A) and Fang *et al.* (B). R, plastic reservoir body; P, platinum electrode; C, capillary column; OUT, waste solution outlet; IN, inlet; P, conical pipette tip; B, buffer electrolyte solution (with sample waste).

Different interface designs have since been used, e.g., an H-channel structure [99], a modified flow through chamber interface [100], various interfaces using tubular electrodes [101-104], and an interface using an on-column polymer-embedded graphite inlet electrode [105].

Using these types of interfaces, there have been three reports on the examination of FASI. Kuldvee *et al.* [106] demonstrated that a short FASI (10 s at 8 kV) from a flowing sample stream afforded a 100 fold increase in sensitivity when compared to FASI from a static sample (2.5 s at 18 kV). It should be noted, however, that this static sample was in the custom-interface and the actual volume that was sampled was considerably smaller than is typically used with a conventional CE. The static sample was also considerably smaller than the volume sampled while flowing. Also, the electrokinetic injection time could not be extended due to the hydrodynamic introduction of sample matrix which reduced the field strength at the capillary tip during injection. Liu *et al.* [107] used FASI (15 s at 7.5 kV) in combination with sweeping MEKC and obtained a sensitivity enhancement of 64-86 compared to non-stacking conditions. The system was not systematically studied. Kuban *et al.* [108] were able to perform a longer FASI (6 min at 2 kV) by eliminating the pressure-induced flow through the capillary, and this resulted in a 2000-fold enhancement compared to a typical hydrodynamic injection. They used a homebuilt CE system as well as a homemade interface and no comparison was made to FASI in a static sample to establish whether there was any improvement from having a flowing sample during injection.

1.7 PROJECT AIMS

From the results in the existing literature it is evident that CE in combination with flow injection interfaces provides the possibility for on-line monitoring. It has also been demonstrated that flow interfaces can be combined with stacking methods which allow for a reasonable enhancement in sensitivity. Despite this there have been no systematic studies looking at changing the individual parameters of a flow interface and how it affects the amount of injected sample.

The first aspect that has not been well studied in the existing literature is how the injection voltage and flow rate affect the injected sample amount. Besides this there is no study that directly compares the injection of a static vial to the injection from a flowing sample stream under the same conditions. Another aspect is that there are no comprehensive studies of continuous flow interfaces that investigate how the interface and capillary dimensions, the conductivity ratio between sample and back ground electrolyte (BGE) affect the injection.

Therefore the general aim of this work is to understand the effect that the individual parameters of a continuous flow interface have on the injected sample amount and to ultimately enhance the sensitivity of existing stacking methods using a continuous flow interface.

The specific aims of the project are to:

1. Show that a continuous flow interface has the potential to be more sensitive than an injection from a static vial. This is discussed in chapter 2 where the injection from the continuous flow interface with an injection from a static vial under the same conditions is compared.

2. Develop a computational fluid dynamics model that allows to investigate the effect of the injection voltage and flow rate on the injected sample amount which is addressed in chapter 2.
3. Verify the results proposed by the simulations experimentally and find the optimum combination of injection voltage and flow rate for maximum sensitivity enhancement. This is presented in chapter 2.
4. Develop a set of guidelines on the choice of parameters when developing a continuous sample flow interface to achieve the maximum flow rate for complete sample injection. This is achieved by developing a simplified mathematical model in chapter 3.
5. Verify the predictions of the mathematical model experimentally. This is discussed in chapter 3 where interfaces with different dimensions were built and the effect of interface dimensions on the maximum flow rate for complete sample injection is investigated and compared to the mathematical model.
6. Refine the guidelines and rules for interface design proposed by the mathematical model. This is addressed in chapter 4 where a more accurate computational fluid dynamics model is developed.
7. Summarize the findings from the mathematical model, the simulation model and the experiments into a final set of guidelines for the design of a continuous flow interface that allows complete sample injection at the highest flow rate possible. This can be found in the final chapter 5.

1.8 REFERENCES

- [1] A. Tiselius, *Biochem. J.* 31 (1937) 1464.
- [2] A. Tiselius, *Biochem. J.* 31 (1937) 313.
- [3] P. Camilleri, *Capillary Electrophoresis: Theory and Practice* (1993).
- [4] P.G. Righetti, *J. Chromatogr. A* 1079 (2005) 24.
- [5] S. Hjertén, *Chromatogr. Rev.* 9 (1967) 122.
- [6] F.E.P. Mikkers, F.M. Everaerts, T.P.E.M. Verheggen, *J. Chromatogr. A* 169 (1979) 11.
- [7] F.E.P. Mikkers, F.M. Everaerts, T.P.E.M. Verheggen, *J. Chromatogr. A* 169 (1979) 1.
- [8] J.W. Jorgenson, K.D. Lukacs, *Anal. Chem.* 53 (1981) 1298.
- [9] W.G. Kuhr, *Anal. Chem.* 62 (1990) 403.
- [10] V. Dolník, K.M. Hutterer, *Electrophoresis* 22 (2001) 4163.
- [11] Y.S. Fung, H.S. Tung, *Electrophoresis* 20 (1999) 1832.
- [12] C. Heller, *Electrophoresis* 22 (2001) 629.
- [13] M.C. Breadmore, *J. Chromatogr. A* 1221 (2012) 42.
- [14] R.L. Chien, D.S. Burgi, *J. Chromatogr.* 559 (1991) 141.
- [15] J.P. Quirino, S. Terabe, *Anal. Chem.* 70 (1998) 1893.
- [16] R.L. Chien, J.C. Helmer, *Anal. Chem.* 63 (1991) 1354.

- [17] D.S. Burgi, R.L. Chien, *Anal. Chem.* 63 (1991) 2042.
- [18] R.L. Chien, *Anal. Chem.* 63 (1991) 2866.
- [19] R.L. Chien, D.S. Burgi, *Anal. Chem.* 64 (1992) 489A.
- [20] Z.K. Shihabi, *Electrophoresis* 23 (2002) 2394.
- [21] F. Foret, E. Szoko, B.L. Karger, *Electrophoresis* 14 (1993) 417.
- [22] S. Auriola, I. Jääskeläinen, M. Regina, A. Urtti, *Anal. Chem.* 68 (1996) 3907.
- [23] L. Krivankova, P. Gebauer, W. Thormann, R.A. Mosher, P. Bocek, *J. Chromatogr.* 638 (1993) 119.
- [24] T. Hirokawa, H. Okamoto, B. Gaš, *Electrophoresis* 24 (2003) 498.
- [25] P. Britz-McKibbin, G.M. Bebault, D.D.Y. Chen, *Anal. Chem.* 72 (2000) 1729.
- [26] S. Terabe, K. Otsuka, K. Ichikawa, A. Tsuchiya, T. Ando, *Anal. Chem.* 56 (1984) 111.
- [27] J.P. Quirino, S. Terabe, *Science* 282 (1998) 465.
- [28] J.P. Quirino, J.B. Kim, S. Terabe, *J. Chromatogr. A* 965 (2002) 357.
- [29] J.P. Quirino, S. Terabe, *Anal. Chem.* 71 (1999) 1638.
- [30] J.P. Quirino, P.R. Haddad, *Anal. Chem.* 80 (2008) 6824.
- [31] J.P. Quirino, *J. Chromatogr. A* 1214 (2008) 171.
- [32] X. Wang, E. Masschelein, P. Hespel, E. Adams, A. van Schepdael, *Electrophoresis* 33 (2012) 402.

- [33] H.W. Liao, S.W. Lin, U.I. Wu, C.H. Kuo, *J. Chromatogr. A* 1226 (2012) 48.
- [34] H. Fang, T.L. Vickrey, B.J. Venton, *Anal. Chem.* 83 (2011) 2258.
- [35] F.S. Lopes, O.A. Junior, I.G.R. Gutz, *Electrochem. Commun.* 12 (2010) 1387.
- [36] K. Michalska, G. Pajchel, S. Tyski, *J. Sep. Sci.* 34 (2011) 475.
- [37] Z.F. Wang, S. Cheng, S.L. Ge, H. Wang, Q.J. Wang, P.G. He, Y.Z. Fang, *Anal. Chem.* 84 (2012) 1687.
- [38] H. Dong, B. Gao, W. Wang, L. Fan, Y. Xu, X. Zhang, C. Cao, *Chromatographia* 73 (2011) 609.
- [39] H. Wang, Y. Lu, J. Chen, J. Li, S. Liu, *J. Pharm. Biomed. Anal.* 58 (2012) 146.
- [40] M.L. Chen, L.L. Suo, Q. Gao, Y.Q. Feng, *Electrophoresis* 32 (2011) 2099.
- [41] X. Hou, D. Deng, X. Wu, Y. Lv, J. Zhang, *J. Chromatogr. A* 1217 (2010) 5622.
- [42] H.F. Lau, N.M. Quek, W.S. Law, J.H. Zhao, P.C. Hauser, S.F.Y. Li, *Electrophoresis* 32 (2011) 1190.
- [43] R. Wei, W. Li, L. Yang, Y. Jiang, T. Xie, *Talanta* 83 (2011) 1487.
- [44] Q. Xiang, Y. Gao, B. Han, J. Li, Y. Xu, J. Yin, *Luminescence*.
- [45] X.Z. Hu, M.L. Chen, Q. Gao, Q.W. Yu, Y.Q. Feng, *Talanta* 89 (2012) 335.
- [46] H.B. He, X.X. Lv, Q.W. Yu, Y.Q. Feng, *Talanta* 82 (2010) 1562.

- [47] P.L. Hwang, S.Y. Wei, H.H. Yeh, J.Y. Ko, C.C. Chang, S.H. Chen, *Electrophoresis* 31 (2010) 2778.
- [48] H. Ye, S. Xia, L. Yu, X. Xu, C. Zheng, H. Xu, L. Wang, X. Liu, Z. Cai, G. Chen, *Electrophoresis* 32 (2011) 2823.
- [49] L. Xu, C. Basheer, H.K. Lee, *J. Chromatogr. A* 1217 (2010) 6036.
- [50] A.V. Herrera-Herrera, J. Hernández-Borges, T.M. Borges-Miquel, M.A. Rodríguez-Delgado, *Electrophoresis* 31 (2010) 3457.
- [51] P. Anres, N. Delaunay, J. Vial, P. Gareil, *Electrophoresis* 33 (2012) 1169.
- [52] T.F. Jianga, Z.H. Lva, Y.H. Wanga, M.E. Yueb, J.H. Peng, *J. Anal. Chem.* 65 (2010) 945.
- [53] X. Hai, T. Nauwelaers, R. Busson, E. Adams, J. Hoogmartens, A. Van Schepdael, *Electrophoresis* 31 (2010) 3352.
- [54] J. Li, Y. Jiang, *Biomed. Chromatogr.* 24 (2010) 186.
- [55] A. Zinellu, S. Sotgia, M.F. Usai, G. Pintus, L. Deiana, C. Carru, *Anal. Bioanal. Chem.* 399 (2011) 1815.
- [56] Y. Li, Y. Cui, X. Zhao, B. Jia, Y. Qi, *Zhongguo Zhongyao Zazhi* 36 (2011) 1466.
- [57] J. Li, Y. Bi, L. Wang, F. Sun, Z. Chen, G. Xu, G. Fan, *J. Pharm. Biomed. Anal.* (2012).
- [58] X. Hu, S. Cui, J.Q. Liu, *Chromatographia* 72 (2010) 993.

- [59] F. Wei, J. Fan, M.M. Zheng, Y.Q. Feng, *Electrophoresis* 31 (2010) 714.
- [60] S. Zhang, C. Jiang, L. Jia, *Anal. Biochem.* 408 (2011) 284.
- [61] I.S.L. Lee, M.C. Boyce, M.C. Breadmore, *Food Chem.* 133 (2012) 205.
- [62] J. Honegr, J. Šafra, M. Polášek, M. Pospíšilová, *Chromatographia* 72 (2010) 885.
- [63] C. Quesada-Molina, M. Del Olmo-Iruela, A.M. García-Campaña, *Anal. Bioanal. Chem.* 397 (2010) 2593.
- [64] J.O. Bernad, A. Damascelli, O. Núñez, M.T. Galceran, *Electrophoresis* 32 (2011) 2123.
- [65] L.Y. Fan, T. He, Y.Y. Tang, W. Zhang, C.J. Song, X. Zhao, X.Y. Zhao, C.X. Cao, J. *Forensic Sci.* 57 (2012) 813.
- [66] J. Iqbal, C.E. Müller, *J. Chromatogr. A* 1218 (2011) 4764.
- [67] Z. Wang, C. Liu, J. Kang, *J. Chromatogr. A* 1218 (2011) 1775.
- [68] T. Kawai, H. Koino, K. Sueyoshi, F. Kitagawa, K. Otsuka, *J. Chromatogr. A*.
- [69] T. Kawai, M. Watanabe, K. Sueyoshi, F. Kitagawa, K. Otsuka, *J. Chromatogr. A* 1232 (2012) 52.
- [70] E. Fukushima, Y. Yagi, S. Yamamoto, Y. Nakatani, K. Kakehi, T. Hayakawa, S. Suzuki, *J. Chromatogr. A* (2012).
- [71] T. Kawai, K. Sueyoshi, F. Kitagawa, K. Otsuka, *Anal. Chem.* 82 (2010) 6504.
- [72] P. Li, X. Zhang, B. Hu, *J. Chromatogr. A* 1218 (2011) 9414.

- [73] A.V. Herrera-Herrera, L.M. Ravelo-Pérez, J. Hernández-Borges, M.M. Afonso, J.A. Palenzuela, M.Á. Rodríguez-Delgado, *J. Chromatogr. A* 1218 (2011) 5352.
- [74] M.A. Al-Ghobashy, M.A.K. Williams, G. Laible, D.R.K. Harding, *Chromatographia* 73 (2011) 1145.
- [75] Y. Jin, L. Meng, M. Li, Z. Zhu, *Electrophoresis* 31 (2010) 3913.
- [76] Z. Chen, Z. Lin, L. Zhang, Y. Cai, *Analyst* 137 (2012) 1723.
- [77] S. Terabe, Otsuka, K., Ando, T. , *Anal.Chem.* 57 (1985) 834.
- [78] S. Terabe, Otsuka, K., Ichikawa, K., Tsuchiya, A. Ando, T., *Anal. Chem.* 56 (1984) 111.
- [79] J.P. Quirino, S. Terabe, *HRC J. High Resolut. Chromatogr.* 22 (1999) 367.
- [80] Y. Rang, W. Zhang, Z. Chen, *Analytical Letters* 46 (2013) 2503.
- [81] Y.Y. Lin, C.C. Wang, Y.H. Ho, C.S. Chen, S.M. Wu, *Analytical and Bioanalytical Chemistry* 405 (2013) 259.
- [82] S. Dziomba, P. Kowalski, T. Baogonekczek, *J.Chromatogr. A* 1267 (2012) 224.
- [83] Y.H. Ho, C.C. Wang, Y.T. Hsiao, W.K. Ko, S.M. Wu, *J. Chromatogr. A* 1295 (2013) 136.
- [84] K. Michalska, J. Cielecka-Piontek, G. Pajchel, S. Tyski, *J. Chromatogr. A* 1282 (2013) 153.
- [85] J. Chen, J. Sun, S. Liu, *Analytical Letters* 46 (2013) 887.

- [86] R. Fang, G.H. Chen, L.X. Yi, Y.X. Shao, L. Zhang, Q.H. Cai, J. Xiao, *Food Chemistry* 145 (2014) 41.
- [87] C.C. Wang, S.F. Cheng, H.L. Cheng, Y.L. Chen, *Analytical and Bioanalytical Chemistry* 405 (2013) 1969.
- [88] C.C. Wang, J.L. Chen, Y.L. Chen, H.L. Cheng, S.M. Wu, *Anal. Chim. Acta* 744 (2012) 99.
- [89] M. Hernández-Mesa, C. Cruces-Blanco, A.M. García-Campaña, *J. Sep. Sci.* 36 (2013) 3050.
- [90] H.R. Rabanes, J.P. Quirino, *Electrophoresis* 34 (2013) 1319.
- [91] J.P. Quirino, S. Terabe, *Anal. Chem.* 72 (2000) 1023.
- [92] C.X. Zhang, W. Thormann, *Anal. Chem.* 70 (1998) 540.
- [93] T. Hirokawa, E. Koshimidzu, Z. Xu, *Electrophoresis* 29 (2008) 3786.
- [94] Z. Xu, K. Nakamura, A.R. Timerbaev, T. Hirokawa, *Anal. Chem.* 83 (2011) 398.
- [95] Z. Xu, E. Koshimidzu, T. Hirokawa, *Electrophoresis* 30 (2009) 3534.
- [96] P. Kubáň, B. Karlberg, *Anal. Chim. Acta* 648 (2009) 129.
- [97] P. Kuban, A. Engström, J.C. Olsson, G. Thorsén, R. Tryzell, B. Karlberg, *Anal. Chim. Acta* 337 (1997) 117.
- [98] Z.-L. Fang, Z.-S. Liu, Q. Shen, *Anal. Chim. Acta* 346 (1997) 135.
- [99] L.Y. Fan, H.L. Chen, X.G. Chen, Z.D. Hu, *J. Sep. Sci.* 26 (2003) 1376.

- [100] D.D. Wang, F. Li, X.P. Yan, *J. Chromatogr. A* 1117 (2006) 246.
- [101] G.A. Blanco, Y.H. Nai, E.F. Hilder, R.A. Shellie, G.W. Dicoski, P.R. Haddad, M.C. Breadmore, *Anal. Chem.* 83 (2011) 9068.
- [102] A.A. Alhusban, A.J. Gaudry, M.C. Breadmore, N. Gueven, R.M. Guijt, *J. Chromatogr. A* 1323 (2014) 157.
- [103] N. Teshima, T. Hino, T. Sakai, *Anal. Sci.* 23 (2007) 751.
- [104] B. Santos, B.M. Simonet, B. Lendl, A. Ríos, M. Valcárcel, *J. Chromatogr. A* 1127 (2006) 278.
- [105] J. Samskog, S.K. Bergström, M. Jönsson, O. Klett, M. Wetterhall, K.E. Markides, *Electrophoresis* 24 (2003) 1723.
- [106] R. Kuldvee, M. Kaljurand, *Anal. Chem.* 70 (1998) 3695.
- [107] L. Liu, X. Chen, Z. Hu, *Microchimica Acta* 159 (2007) 125.
- [108] P. Kuban, M. Berg, C. García, B. Karlberg, *J. Chromatogr. A* 912 (2001) 163.

Chapter 2

STACKING IN A CONTINUOUS SAMPLE FLOW INTERFACE IN CAPILLARY ELECTROPHORESIS

2.1 INTRODUCTION

In the chapter which follows, a continuous sample flow interface is described that was constructed using a commercially available Tee connector integrated into a commercial CE to allow direct comparison of the benefit of performing field amplified sample injection (FASI) on a flowing sample. Sample injection was performed electrokinetically, therefore no physical valve was necessary to perform sample injection. The hydrodynamic introduction of sample was minimized by adjusting the liquid levels in the buffer and waste vials allowing injection times of up to 40 min. FASI with sweeping followed by micellar electrokinetic chromatography (FASI-sweep-MEKC) was used to compare sample injection from a static system and a flowing stream. It is demonstrated that by continuously flushing the sample through the interface, the efficiency of FASI is increased, providing enhanced sensitivity. Simulations along with experimental studies were used to study the influence of injection voltage and flow rate, and to establish the conditions in which there is near quantitative injection of the selected analytes. Significant enhancement in the proportion of sample ions that are injected when injecting from a flowing sample stream is demonstrated and this work

is the only to compare electrokinetic injection of the same sample volume, under the same conditions with the only difference being whether the sample stream was flowing or static.

2.2 EXPERIMENTAL SECTION

2.2.1 REAGENTS

All reagents (sodium dodecyl sulphate (SDS), phosphoric acid, sodium hydroxide, HPLC grade acetonitrile) were purchased from Sigma-Aldrich (St. Louis, MO). Stock solutions of 1 M phosphoric acid, 200 mM SDS and 4 M sodium hydroxide were prepared. 1 M phosphoric acid was prepared by mixing an appropriate amount of purified water with phosphoric acid. Other solutions were prepared by dilution of the stock solutions with water. All solutions were filtered through a 0.45 μm filter from MicroScience (Co Durham, UK) prior to use. The background electrolyte (BGE) was 200 mM phosphoric acid with 20% (v/v) acetonitrile, and the sweeping solution was 100 mM phosphoric acid, 100 mM SDS with 20% (v/v) acetonitrile. The ${}_w^s\text{pH}$ (pH measured in acetonitrile/water with electrodes calibrated in water) [1] values of these solutions were adjusted to 2 with 4 M NaOH after the addition of acetonitrile and before final dilution in a volumetric flask. The sample diluent was 0.5 mM phosphoric acid or 200 mM phosphoric acid with 20% (v/v) acetonitrile, ${}_w^s\text{pH}$ 2, for the FASI-sweeping-MEKC and the capillary zone electrophoresis (CZE) experiments, respectively. Alprenolol hydrochloride and propranolol hydrochloride were purchased from Sigma-Aldrich (St. Louis, MO) and were prepared in water (1000 mg/L).

2.2.2 INSTRUMENTATION

Water was purified using a Milli-Q system from Millipore (Bedford, MA). The s_pH was measured using an Activon Model 210 pH meter (New South Wales, Australia). All capillary electrophoresis experiments were conducted on an Agilent 3D-CE instrument (Waldbronn, Germany) equipped with a diode array detector and a fused silica capillary (25 μm and 365 μm inner and outer diameters, respectively) from Polymicro Technologies (Phoenix, AZ). The total length was 50 cm with 20 cm from the inlet end to the detector. Capillary temperature was controlled at 20°C. The lift offset, which determines the distance between the capillary entrance and the tip of the cylindrical electrode which surrounds the capillary, was set to 4 mm.

2.2.3 CONTINUOUS SAMPLE FLOW INTERFACE

The construction of the continuous sample flow interface was similar to that described by Blanco *et al.* [2]. It accommodates a flow through channel so that it can be flushed with liquid in a continuous manner much like a river flowing. The separation capillary entrance is placed in the continuous stream of liquid. To perform sample injection the channel is flushed with sample. While the sample is flowing voltage is applied via a ring electrode that is part of the flow through channel. Since sample is injected electrokinetically no valves are required for injection. To start the separation the sample liquid is flushed out of the interface and replaced by a continuous stream of BGE. For the separation to start voltage is applied between the electrode in the interface and the outlet of the separation capillary. During the separation the BGE is flowing through the interface continuously. A schematic of the flowing sample interface can be seen in Figure 2.1 A. Briefly, a Tee connector (P-727, Upchurch Scientific)

with a 500 μm thru-hole was used to connect the capillary and stainless steel electrode (200 mm of stainless steel tubing, U-145, Upchurch Scientific), which served as the anode during injection and as the cathode during separation. The stainless steel electrode was aligned opposing the sample inlet tube (508 μm inner diameter and 794 μm outer diameter) which consisted of a 22 cm piece of polyether ether ketone (PEEK) tubing (1569, Upchurch Scientific). For the waste outlet, a piece of rubber tubing (1250 μm x 500 μm x 30 cm) was connected to the electrode in the interface. The sample inlet tube was connected to a 30 cm piece of capillary (25 μm ID, 365 μm OD from Polymicro Technologies (Phoenix, AZ)) using a connector (P-643, Upchurch Scientific) which was placed in the inlet vial that contained either the sample solution or the micellar solution. All capillaries and the electrode in the interface were connected using the supplied fittings and ferrules. The entrance of the separation capillary was aligned so that it was 365 μm away from the opposing wall of the Tee connector. The continuous sample flow interface axis between the inlet capillary and the electrode was positioned vertically inside the capillary cassette. The separation capillary coupled to the Tee connector was horizontal. To more accurately regulate the external pressure of the CE instrument, a manual pressure regulator (Norgren, R37G-3GK-FRN) was installed in the external pressure line. This allowed adjustments of pressures from 0.1 to 6 bar \pm 5%, which are below the capabilities of the Agilent CE to be applied at the inlet of the capillary coupled to the sample inlet tube. In order to switch quickly between the full external pressure (6 bar) and the lower external pressure from the manual regulator, the first open-close valve (Onomi, 1/4) was installed parallel to a series connection of the regulator and a second open-close valve.

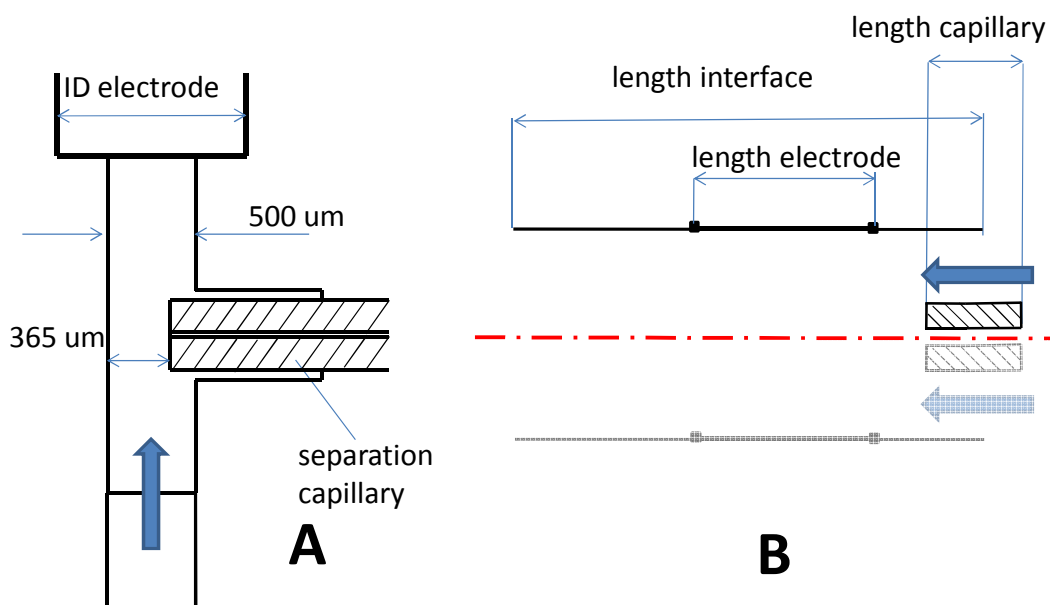


Figure 2.1 Schematic of the continuous sample flow interface used for experiments (A) and simulations (B). In the experimental setup (A) the ID of the electrode was 1150 μm and the separation capillary dimensions were 25 μm ID and 365 μm OD. For the simulations (B) the interface length was 3mm, electrode length 500 μm, capillary ID 50 μm, capillary OD 150 μm and the capillary length was 2mm. The blue arrows indicate the direction of the flow of liquid. The second electrode is at the outlet of the separation capillary. For further explanation, see text.

2.2.4 PREVENTION OF PRESSURE INJECTION

The introduction of sample matrix into the separation capillary needs to be minimized. To prevent hydrodynamic sample matrix introduction the inner diameter of the separation capillary was 25 μm and the channel diameter of the Tee connector was 20 times bigger at 500 μm . The sample can also be introduced by hydrostatic pressure differences between the inlet and outlet of the separation capillary. The hydrostatic pressure difference is affected by the liquid levels of the inlet and outlet vials and the liquid level in the waste vial. Therefore the influence of the liquid level in the waste vial on the length of the injected matrix plug length was studied which is shown in Figure 2.2. It was found to be at a minimum when the waste liquid level is at a height of -7 cm below the liquid levels in the inlet and outlet vials. For all runs in the presented work the waste liquid level was set to -7 cm in order to avoid hydrostatic injection of sample.

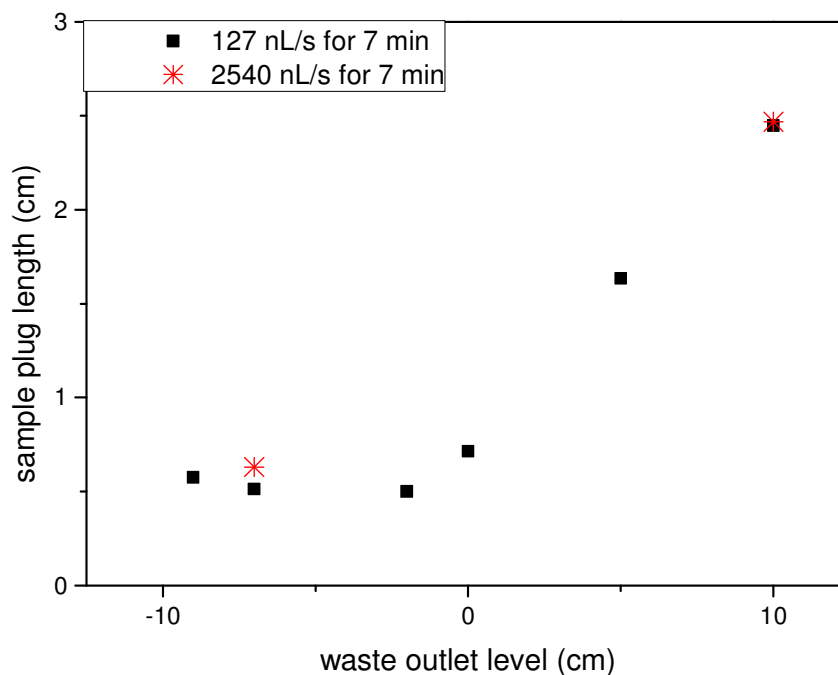


Figure 2.2 Effect of waste outlet level on sample plug length injected into the separation capillary at a low and high flow rate. sample solution, 1000 ng/mL of PNL, APL in 0.5 mM phosphoric acid; BGE, 200 mM phosphate buffer with 20% (v/v) acetonitrile (pH 2.0); capillary 25 μ m I.D. x 50 cm (20 cm to the detector); temperature, 25 $^{\circ}$ C ; detection, UV absorbance at 210 nm; CE instrument, Hewlett-Packard 3D CE, other explanations are in the text

2.2.5 ELECTROPHORETIC PROCEDURES

New capillaries were conditioned by flushing with 1 M sodium hydroxide for 30 min at 1 bar and purified water for 10 min at 1 bar. Before each CE experiment, capillaries were conditioned by flushing with BGE for 3 min at 4 bar. For the FASI-sweep-MEKC from a flowing sample stream, the sample was injected at 5 kV at increasing injection times up to 40 min at sample flow rates of 123 nL/s with the cathode being at the capillary outlet. When doing the flow rate and injection voltage study, injection was performed for 5 min at 123, 387 and 558 nL/s and 5, 10, 15, 20 and 30 kV, respectively. For the FASI-sweep-MEKC runs from a static vial at injection times of up to 40 min, a sample volume of 100 μ L was used. For the FASI-sweep-MEKC runs from a static vial at a fixed time of 40 min a sample volume of 295 μ L was used. In all experiments separations were run at -20 kV with the cathode being in the interface. Detection was performed at 210 nm. Comparison was made with a hydrodynamic injection (50 mbar, 10 s). Other conditions can be found in the text or figures.

FASI-sweep-MEKC with the continuous sample flow interface consisted of the following steps (see Table 2.1 for details): (1) cleaning, (2) conditioning, (3) filling the Tee with sample with full external pressure, (4) switching the external pressure to use the manual pressure regulator, (5) applying voltage for FASI of the analytes under continuous sample flow, (6) switching back to full external pressure, (7) filling the lines and Tee with SDS, and (8) sweeping and separation by MEKC. During the separation the BGE was flushed through the interface using 50 mbar of pressure. The procedure for FASI-sweep-MEKC was similar to the one described by Quirino and Terabe [3]. During FASI, sample ions stack at the boundary between S and BGE due to a discontinuity in electric field strength. After injection, anionic

SDS micelles from the cathodic end enter the capillary sweep the analytes followed by separation by MEKC.

Step Nr.	Procedure
1	Application of 4 bar for 3 min at inlet reservoir (BGE); Application of 4 bar for 3 min at inlet (BGE) and outlet reservoir (BGE)
2	Application of 4 bar for 3 min at outlet reservoir (BGE)
3	Application of 4 bar for 30 s at inlet reservoir (sample)
4	Bypass valve is closed, valve in line with regulator is opened; Application of manually set pressure at inlet reservoir (sample)
5	Application of 5 kV at the interface and application of the manually set pressure for the time of injection at inlet reservoir (sample)
6	Valve in line with regulator is closed, Bypass valve is opened
7	Application of 4 bar for 1 min at inlet reservoir (SDS), outlet reservoir is switched to SDS
8	Application of – 20 kV at the interface

Table 2.1 Steps involved in the EKI-sweep-MEKC procedure with the continuous sample flow interface

2.2.6 COMPUTER SIMULATION

The multiphysics software COMSOL (version 4.3b) was used to simulate the system to explain how the amount of sample injected depends on the flow rate and voltage used during sample injection. Figure 2.1 B shows the basic 2D-axisymmetric geometry of the flow interface used in this simulation. The cylindrical flow interface, which is an open channel at both ends, (length 3 mm and 500 μm ID) surrounds the capillary (150 μm OD and 50 μm ID). The capillary end in the simulation was open to both hydrodynamic flow and electrophoretic flux. The influence of electroosmotic flow was not included in the model. The cylindrical cathodic electrode (length 500 μm) is located on the wall of the flow cell 1 mm upstream from the capillary entrance. The simulated sample in the reservoir was iodate with a mobility set to $50 \times 10^{-9} \text{ m}^2/\text{Vs}$, with an initial concentration of 0.1 mmol/L. The counterion was 0.1 mmol/L sodium (mobility of $55 \times 10^{-9} \text{ m}^2/\text{V}$). The interface and capillary was filled with 1 mmol/L sodium nitrate ($70 \times 10^{-9} \text{ m}^2/\text{V}$) at the start of each simulation. The voltages applied were 100, 250, 500, 1000, 2000, 3000, 4000 and 5000 volts between the anodic end of the capillary end and the electrode. The EOF was assumed to be zero. Time increments were set as 0.1 s from 0 to 0.3 s, 0.05s from 0.3 to 0.5 s, 0.1s from 0.5 to 1 s, 2.5 s from 2.5 to 5 s, 5 s from 5 to 10 s and the simulation was continued for 10 s of injection. All simulations were carried out on a supercomputer (SGI Altix ICE 8200 Cluster) with an 8 GHz clock and required approximately 2-3 days of computation time.

2.3 RESULTS AND DISCUSSION

The primary limitation of FASI from a sample vial in an Agilent CE instrument where the capillary is in line with the symmetry axis of a cylindrical electrode is that only sample ions occurring in an effective potential field (essentially the volume of sample between the cylindrical electrode and the capillary tip) can be injected [4]. One solution is to perform FASI from a continuous sample stream since the proportion of sample ions around the capillary entrance is continuously replenished and this may lead to more efficient injection of ions into the capillary. To examine this idea, a continuous sample flow interface was developed using a commercially available Tee connector with a cylindrical electrode at the sample outlet. This electrode design was inspired by the cylindrical electrode that allowed near quantitative injection of all sample ions in work published by Hirokawa *et al.* [5].

2.3.1 COMPARISON OF THE STATIC VIAL AND CONTINUOUS SAMPLE FLOW INTERFACE PERFORMANCE

In a flowing interface at a fixed sample flow rate, the injection time determines the volume of sample from which the ions are injected and hence should also influence the total mass of analyte ions injected. To verify this, the effect of the injection time on the injected amount of analyte in the flowing sample interface was studied using a mixture of alprenolol (APL) and propranolol (PNL) and compared to injection from a static sample in a conventional vial. The results in Figure 2.3 verify that the peak area (corrected by migration time) increased linearly ($R^2 = 0.9626$) from 0.37 at 5 min to a value of 2.36 at 40 min injection time. A 40 min injection does not seem practical at first but the purpose here is to show that the injected sample amount increases linearly with injection time. This has the potential to enhance the

preconcentration of the sample by simply increasing the injection time. Therefore a 40 min injection might still be justified instead of labor and time intensive offline preconcentration techniques. These results contrast with injections from a static vial (lift offset 4 mm) which are also shown in Figure 2.3. It can be seen from these data that the corrected peak area for PNL initially increases as the injection time is increased until approximately 20 min, after which the peak area does not increase further. This plateau is due to depletion of the analytes in the sample zone around the entrance of the separation capillary and is consistent with the results reported by Hirokawa [4] and others [3]. This shows that with a static sample it is not possible to enhance the sensitivity enhancement by increasing the injection time. With a 40 min injection, the peak area for PNL was 4.3 times larger with the flowing sample than the area from the static system. This suggests that the flowing sample interface can provide further improvements over existing stacking systems. However, with the flowing sample injection a total volume of 295 μL of sample volume was flushed through the interface, while the static system had a volume of 100 μL .

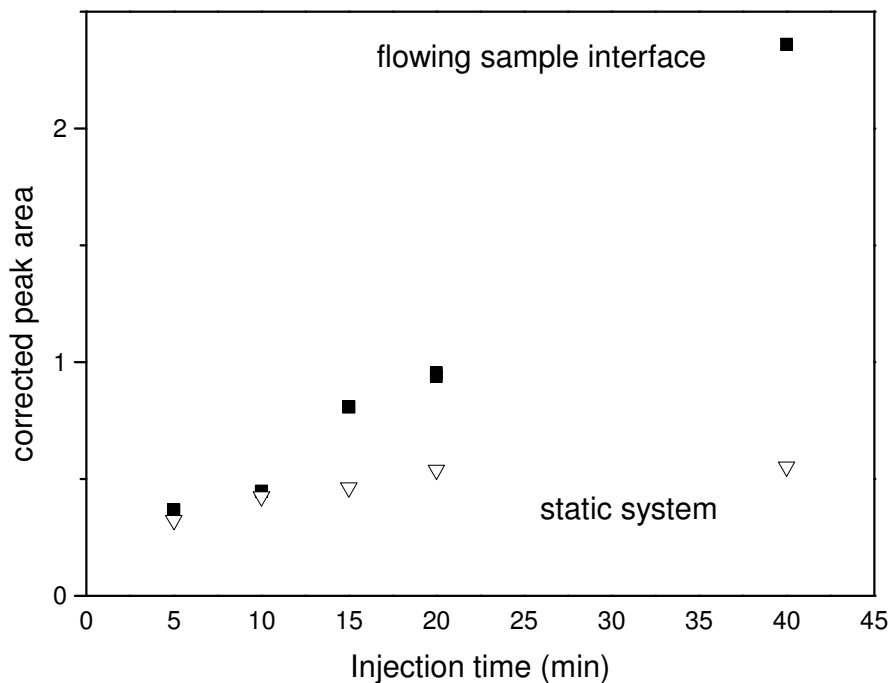


Figure 2.3 Comparison of the effect of injection time on corrected peak area of PNL when injecting from the flowing sample interface and a 100 μL sample volume in a static system. sample solution, 10 ng/mL of PNL, APL in 0.5 mM phosphoric acid; BGE, 200 mM phosphate buffer with 20% (v/v) acetonitrile (pH 2.0); SDS sweeping solution, 100 mM phosphate buffer, 100mM SDS with 20% (v/v) acetonitrile (pH 2.0); voltage injection from a flowing sample interface, 5 kV at a sample flow rate of 123 nL/s; voltage injection from a static system, 5 kV from a sample volume of 100 μL ; separation voltage, 20 kV reversed polarity; capillary 50 μm I.D. x 50 cm (20 cm to the detector); temperature, 25 $^{\circ}\text{C}$; detection, UV absorbance at 210 nm; lift offset, 4mm; CE instrument, Hewlett-Packard 3D CE, other explanations are in the text.

In order to better understand the origin of the improved performance of injecting from a flowing sample, injections from the same sample volume for the same length of time were performed under both flowing and static conditions and these were compared with a standard hydrodynamic injection. The static and hydrodynamic injections were performed using the instrument as it is intended with a commercial CE vial and no flow interface. Using a volume of 295 μL , with a 40 min injection in the static system an equivalent volume of sample (over the same 40 min time) was delivered through the interface using a flow rate of 123 nL/s. Typical separations of hydrodynamic injection, the 40 min static injection and 40 min flowing injection can be seen in Figure 2.4. The hydrodynamic injection was performed without SDS micelles, therefore the peak order is reversed. No separation could be obtained when using MEKC conditions with hydrodynamic injection due to a 50% shorter separation time. The baseline difference before and after the first system peak in the static vial and flowing sample interface is due to the presence of SDS micelles in the BGE when performing sweeping.

The LOD when injecting from the flowing sample is 4.03 times lower for PNL compared to the static vial which clearly indicates that FASI from a continuous flowing sample is more efficient than from a static vial. The LOD was calculated based on peak height and $S/N = 3$. The sensitivity enhancement factor (SEF) for PNL was 23 000 fold better compared to a hydrodynamic injection (see Table 2.2).

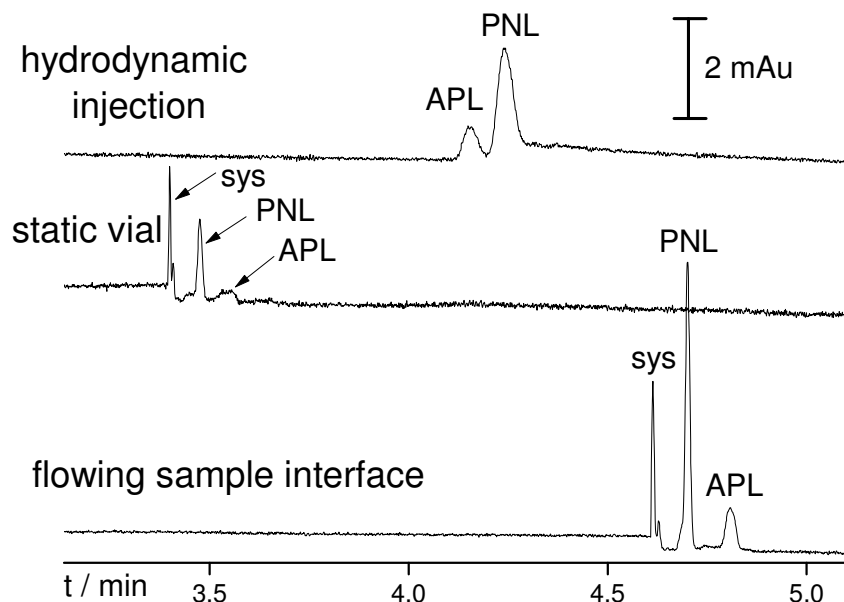


Figure 2.4 Comparison of electropherograms obtained by CZE with hydrodynamic injection, FASI-sweeping-MEKC in the static system, FASI-sweeping-MEKC in the flowing sample interface using a standard mixture of propranolol (PNL) and alprenolol (APL); sample solution, 50 mg/L PNL, APL in BGE (hydrodynamic injection), 10 ng/mL of PNL, APL in 0.5 mM phosphoric acid (flow interface and static vial); voltage (electrokinetic) injection from a static system, 5 kV for 40 min from a sample volume of 295 μ L; voltage injection from a flowing sample interface, 5 kV for 40 min at a sample flow rate of 123 nL/s, which corresponds to a sample volume of 295 μ L; hydrodynamic injection, 50 mbar for 20 s; separation voltage, 20 kV (hydrodynamic injection), 20 kV reversed polarity (static vial and flow interface); detection, 210 nm; BGE, 200 mM phosphate buffer with 20% (v/v) acetonitrile, s_pH 2; SDS sweeping solution, 100 mM phosphate buffer, 100mM SDS with 20% (v/v) acetonitrile (s_pH 2.0) (static vial and flow interface);

Figure 2.4 caption continued. capillary, 50 μm I.D. x 50 cm (20 cm to the detector); Peak assignement, SDS- sweeping front (sys), alprenolol (APL), propanolol (PNL); temperature, 25 $^{\circ}\text{C}$; detection, UV absorbance at 210 nm; CE instrument, Hewlett-Packard ^{3D} CE, other explanations are in the text.

Peak	LOD ^a			SEF ^b	
	flowing sample ^c (ng/mL)	static sytem ^d (ng/mL)	hydrodynamic injection ^e (µg/mL)	flowing sample ^c	static system ^d
PNL	0.32	1.29	7.33	22918	5681
APL	1.67	6.97	23.52	14075	3375

^a LOD was calculated based on peak height and S/N = 3.

^b SEF = LOD from CZE / LOD from flowing sample or static sample injection.

^c flowing sample injection was 40 min at 5kV at a flow rate of 123 nL/s, which corresponds to a sample volume of 295 uL.

^d static sample injection was 40 min at 5kV from a static vial with 295 uL sample volume.

^e CZE injection was 10 s at 50 mbar

Table 2.2 LODs for typical flowing sample, static sample and CZE migrations of PNL and APL. Sensitivity enhancement factor (SEF) in terms of LOD for flowing sample and static system, other conditions see Figure 2.4.

2.3.2 COMPUTATIONAL FLUID DYNAMICS (CFD) SIMULATIONS OF THE INJECTION FROM A FLOWING SAMPLE

It is apparent that the mass of ions injected into the capillary from the flowing stream will be a function of both the flow rate and the applied voltage. To examine the relationship between these variables and injection, CFD simulations were performed using COMSOL. Since a full 3D simulation would not allow for obtaining useful data in a reasonable timeframe, it was necessary to make some assumptions and simplifications to the interface design in the simulation. First, a symmetrical structure was chosen such that the 2D simulations could be performed around a symmetry axis to create a 3D environment. In order to do this, it was necessary to change the orientation of the capillary in the interface. Experimentally, the capillary axis was oriented perpendicular to the sample flow direction (Figure 2.1 A) while, in the simulation, the capillary axis was parallel with the sample flow direction (Figure 2.1 B). The simulated channel surrounding the capillary was open at both ends. The dimensions, flow rates and voltages were as close as possible to those used experimentally, but there are slight differences meaning that the simulations allow only for qualitative comparison and to aid in understanding the trends, rather than in predicting quantitative differences.

The linear velocities of the sample fluid were set to 2.5, 4.25 or 7.5 mm/s, and the injection voltages were 0, 100, 250, 500, 750, 1000, 2000, 3000, 4000 and 5000 V. In all simulations, the interface and capillary were filled with electrolyte (1 mM NaNO₃) and the inflowing solution changes to sample (0.1 mM NaIO₃) at time 0s. Depending on the flow rate, the sample required 0.2 – 0.4 s to reach the capillary inlet. Figure 2.5 shows 2D plots of the change in iodate concentration at a flow rate of 2.5 mm/s and voltages of 100V and 5000 V, at

0, 0.5, and 10 s. From the figure it can be seen that only a small fraction of the iodate enters the capillary when a voltage of 100V is applied, while when 5000 V is used, almost all of the ions are injected. This clearly shows that under certain conditions it is possible to completely inject the sample ions from the flowing sample.

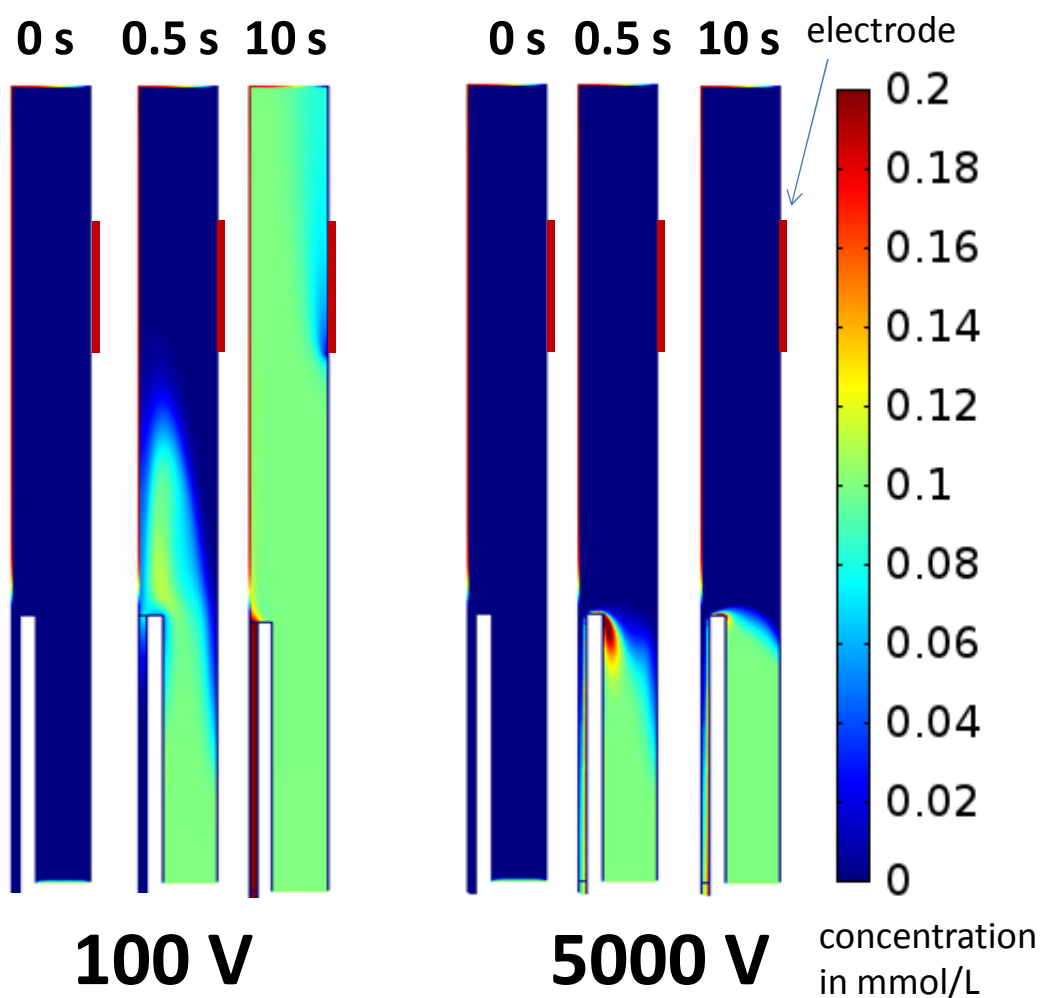


Figure 2.5 Illustration of the sample concentration distribution at 0, 0.5 and 10 sec when injecting at 2.5 mm/s using 100 and 5000 V; sample solution, 0.1 mmol/L of IO_3^- ; capillary 50 μm I.D. The inlet flow enters at the bottom-right, outside the capillary, and leaves at the top of the apparatus. This simulation was carried out in COMSOL version 4.3b using an axisymmetric geometry centered on the lumen axis; other explanations are in the text.

To estimate the amount of ions injected into the capillary in the simulations, the flux of iodate (mobility of $50 \times 10^{-9} \text{ m}^2/\text{Vs}$) entering the capillary was measured at each time point and integrated until a time of 10 s. The total iodate flux at the three different flow rates and 10 different voltages is shown in Figure 2.6. It can be seen at all flow rates that, as the voltage is increased, the amount of iodate injected initially increased in an almost linear manner, but flattened at higher voltages before leveling off. The point at which it levels off is the depletion voltage. Above this voltage, 100% of the iodate is extracted from the flowing sample and injected into the capillary. It can be seen in Figure 2.6 that, at a flow rate of 2.5 mm/s, the depletion voltage is reached at around 3000 V. At higher flow rates higher voltages are required to reach the depletion limit, which can also be seen in Figure 2.6 for flow rates corresponding to 4.25 mm/s and 7.5 mm/s. This means higher flow rates and voltage combinations are required in order to reduce the injection time.

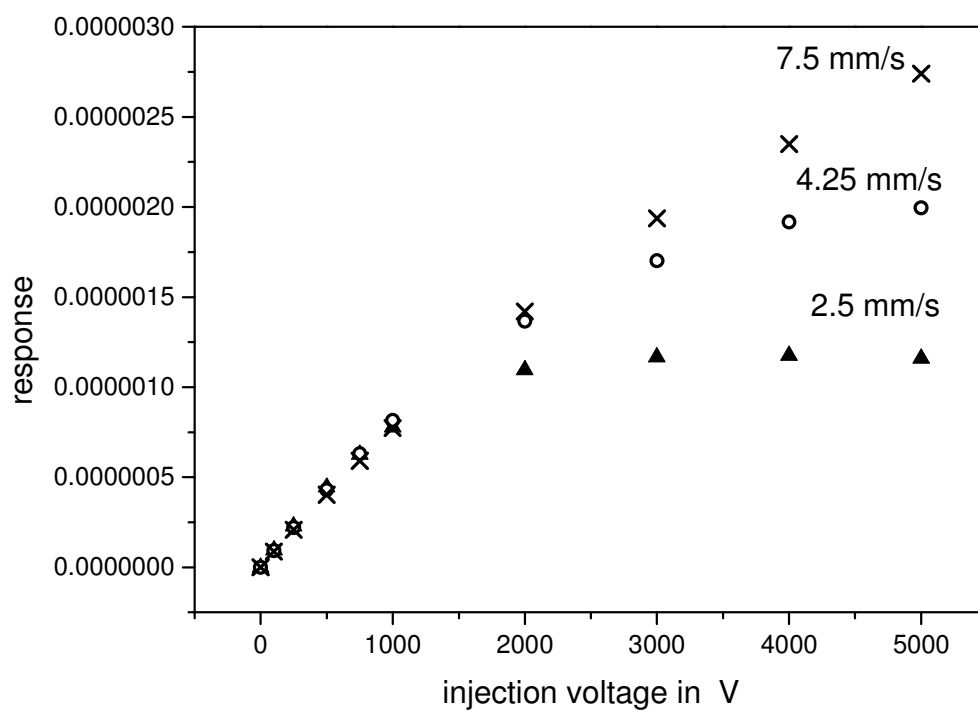


Figure 2.6 Simulation results of the effect of injection voltage and flow rate on injected sample amount when injecting at 0, 100, 250, 500, 750, 1000, 2000, 3000, 4000 and 5000 V and 2.5, 4.25 and 7.5 mm/s; sample solution, 0.1 mmol/L of IO_3^- ; capillary 50 μm I.D.; COMSOL version 4.3b, other explanations are in the text.

2.3.3 EXPERIMENTAL VALIDATION OF THE SIMULATION RESULTS

One of the key findings from the simulation data was that at a defined flow rate there is a voltage – the depletion voltage – above which there is no further increase in ions injected due to depletion of the flowing sample stream. Prior to experimental verification of these results, the repeatability of the system was evaluated using the injection of a 100 ng/mL standard solution of PNL and APL in 0.5 mM H₃PO₄ for 3 min at 280 nL/s and 30 kV. The intraday repeatability % RSD (n=10) for peak area (corrected by migration time) were 19.9 and 7.2 % for APL and PNL, respectively. The interday repeatability % RSD (n=10) for peak area (corrected by migration time) were 11.2 and 14.2 % for APL and PNL, respectively. The repeatability %RSD (n=10) of the migration times were 2 and 2.3% for PNL and APL, respectively.

The repeatability of rebuilding the interface was assessed by disassembling and reassembling the entire interface 6 times and evaluated using the conditions above. The % RSD (n=6) for peak area (corrected by migration time) were 4.8 and 3.6 % for APL and PNL, respectively. The repeatability %RSD (n=10) of the migration times were 2.8 and 3.1% for PNL and APL, respectively.

Having established the repeatability of the system, an experimental study was performed with different voltages (5, 10, 15, 20 and 30 kV) and flow rates (123, 387 and 558 nL/s) with an injection time of 5 min. The data are shown in Figure 2.7 where it can be seen that, at a flow rate of 123 nL/s, the corrected peak area for PNL initially increases linearly ($R^2 = 0.9967$) until 20 kV after which the peak area does not increase any further. Significantly, this is exactly the same behavior observed in the simulations and the plateau is indicative of depletion of the analytes and indicates that nearly all of the ions are injected into the capillary.

Increasing the flow rate is expected to increase the depletion voltage, which is exactly what occurs and can be seen from the figure where the depletion plateau is not reached within the maximum 30 kV that can be applied in the instrument. The good agreement in the peak response predicted by the simulation and observed experimentally indicates that, despite the simplified geometry of the interface used in the simulations, it still accurately accounts for the physics of the hydrodynamic and electrophoretic transport of these solutes.

The data illustrate that most ions are injected at 30 kV and a flow rate of 558 nL/s. Injecting for 5.5 min at 558 nL/sec corresponds to 184 μ L which is less volume than the 295 μ L used earlier in the static vial but still gives a 3 times bigger SEF of 18,000. This suggests that FASI from a flowing sample is more efficient than from a static sample.

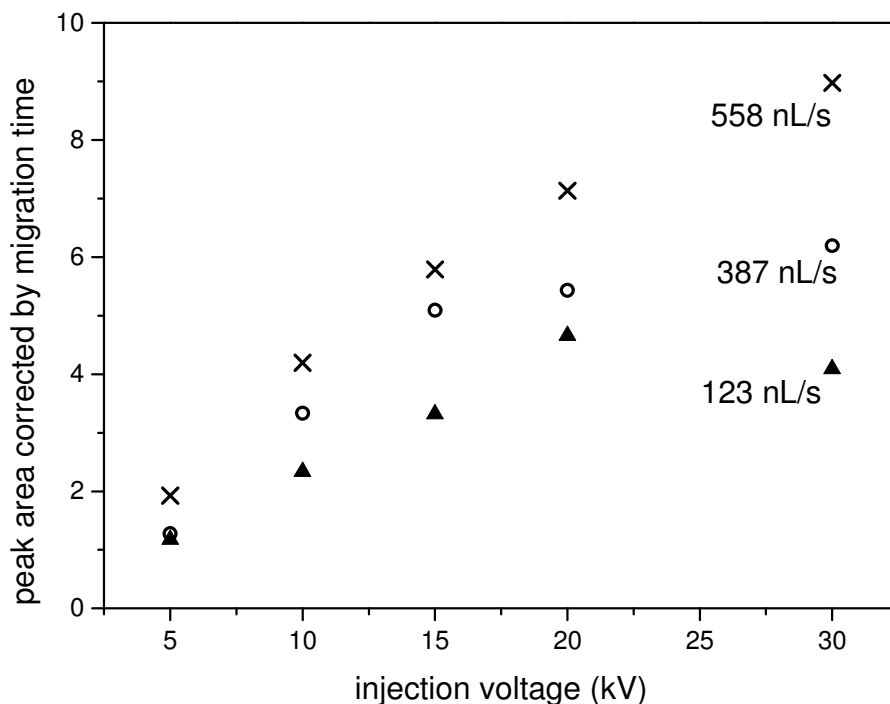


Figure 2.7 Experimental data on the effect of injection voltage and flow rate on corrected peak area of PNL when injecting at 5, 10, 15, 20 and 30 kV and 123 nL/s 387 nL/s and 558 nL/s; sample solution, 50 ng/mL of PNL, APL in 0.5 mM phosphoric acid; BGE, 200 mM phosphate buffer with 20% (v/v) acetonitrile (pH 2.0), SDS sweeping solution, 100 mM phosphate buffer (pH 2.0), 100mM SDS with 20% (v/v); separation voltage, 20 kV reversed polarity; capillary 50 μ m I.D. x 50 cm (20 cm to the detector); temperature, 25 $^{\circ}$ C ; detection, UV absorbance at 210 nm; CE instrument, Hewlett-Packard 3D CE, other explanations are in the text.

2.4 CONCLUSIONS

Using a flowing sample, four times more analyte is injected into the capillary than in a static system. Theoretical simulations investigating the effect of flow rate and injection voltage on the injected sample indicate that this is due to depletion of the ions from the flowing stream indicating near quantitative injection of all of the ions. Using a flow rate of 558 nL/s and an injection voltage of 30 kV, the sensitivity of two cationic drugs could be improved 18,000-fold with an injection time of 5.5 min. Future optimization of the interface design is likely to lead to even further enhancements and may also overcome the issue of injection bias associated with electrokinetic injection by choosing a flow rate and voltage that allows all ions, regardless of their mobility, to be injected. In the present work this was not studied in detail since the main aim was to gain an understanding of the underlying principle of the injection from a flowing stream. When dealing with real samples the field strength that is available for injection would change with differences in sample matrix conductivity. These differences could lead to analyte ions not being injected. To compensate for this a voltage above the depletion voltage needs to be used.

2.5 REFERENCES

- [1] L.G. Gagliardi, C.B. Castells, C. Ràfols, M. Rosés, E. Bosch, *Anal. Chem.* 79 (2007) 3180.
- [2] G.A. Blanco, Y.H. Nai, E.F. Hilder, R.A. Shellie, G.W. Dicoski, P.R. Haddad, M.C. Breadmore, *Anal. Chem.* 83 (2011) 9068.
- [3] J.P. Quirino, S. Terabe, *Anal. Chem.* 72 (2000) 1023.
- [4] T. Hirokawa, E. Koshimidzu, Z. Xu, *Electrophoresis* 29 (2008) 3786.
- [5] Z. Xu, K. Nakamura, A.R. Timerbaev, T. Hirokawa, *Anal. Chem.* 83 (2011) 398.

Chapter 3

MATHEMATICAL MODEL AND EXPERIMENTS

3.1 INTRODUCTION

In Chapter 2 it could be shown that electrokinetic injection from a flowing sample stream can lead to higher sensitivity enhancements than injecting from a static vial. The injection voltage and flow rate were optimized for the tee connector interface. The question now is how to get near quantitative injection from the biggest possible sample volume in the shortest possible time. Therefore it is necessary to investigate the influence of the interface dimensions on the highest possible flow rate that yields quantitative injection. Other reports investigated the use of different interface designs [1-8]. Despite this there is no systematic study that allows the influence of the various factors on the electrokinetic injection from a flowing sample stream to be understood.

This chapter firstly develops a simplified mathematical model from first principles to explain the influence of interface geometry on injection, and then provides experimental verification of the model in the second half.

3.2 DEVELOPMENT OF THE MATHEMATICAL MODEL

The first stage in developing a mathematical model is to define the setup and dimensions of the interface. Then the fundamental concept of electrokinetic transport from a hydrodynamic flow is developed. The main goal of the model is to find the depletion flow rate, defined as the flow rate at a defined voltage at which $> 90\%$ of all ions are injected. The depletion flow is specific to each set of experimental conditions, such as the interface and capillary dimensions as well as sample and background electrolyte properties. The model is used to understand the influence of each of these variables on the depletion flow rate to make recommendations for interface design to maximize the depletion flow rate.

3.2.1 DEFINITIONS AND DIMENSIONS

The scheme of the interface used for the mathematical model is presented in Figure 3.1. This is a flow through channel with a uniform inner diameter, D , with the capillary positioned in the middle. The liquid passes through the interface around the outer surface of the capillary. The electric field, E , is established between the cylindrical electrode in the interface and the electrode at the outlet end of the capillary.

The electric field strength depends on the length L_{Inf} between the capillary entrance and the electrode. It also depends on the interface diameter D because with a wider interface there is a longer path between the capillary inlet and the electrode. To account for this difference, the distance between the edge of the electrode and the symmetry axis of the capillary entrance was selected as the path of the electric field, seen in Figure 3.1 as L . The angle between the interface wall and the electric field line path was defined as θ .

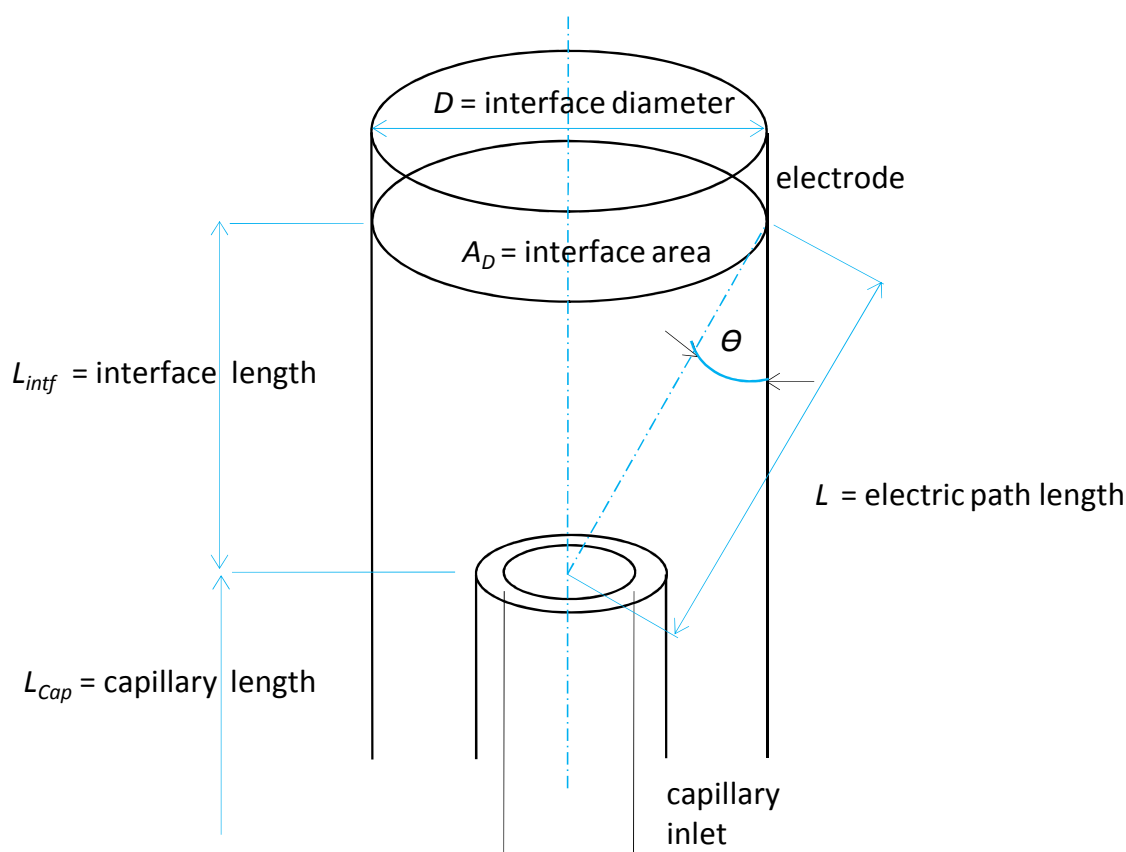


Figure 3.1 Scheme of interface for the mathematical model. The electric field strength is assumed to be uniform across the interface length L_{intf} . The field lines are assumed to be parallel to the interface walls. To account for the influence of the inner diameter on the field line pathway the distance between the lower edge of the electrode and the center of the capillary L was chosen as the electric path length.

3.2.2 ELECTROKINETIC AND HYDRODYNAMIC FORCES FOR ELECTROKINETIC INJECTION FROM A FLOWING SAMPLE STREAM

The sample flows through the interface in Figure 3.1 from the bottom of the figure around the capillary by pressure. In order to transport sample ions into the separation capillary inlet a high voltage is applied to the electrode in the capillary outlet which forms an electric field between

the tip of the capillary and the edge of the grounded ring electrode in the interface. Ions in-between the capillary and electrode are subjected to the applied electric field. They move with an electrophoretic velocity against the hydrodynamic movement of the sample stream. The direction of their resulting velocity defines whether they are transported into the separation capillary inlet or not. This is based on whether the hydrodynamic or electrophoretic forces dominate.

The electrophoretic velocity of the sample ions along the electric field line path is $v_{el,\theta}$ which is illustrated in Figure 3.2. The electrophoretic velocity $v_{el,\theta}$ is comprised of an electrophoretic velocity in radial direction $v_{el,r}$ which accounts for movement from the outer edge of the flow into the center of the flowing stream and the axial direction $v_{el,a}$ which accounts for movement of the ions from the electrode back towards the capillary entrance. Superimposed on $v_{el,a}$ is the hydrodynamic velocity of the sample stream v_{hydr} . The apparent velocity $v_{app,a}$ is the vector sum of the axial electrophoretic velocity $v_{el,a}$ and the hydrodynamic velocity v_{hydr} . When the apparent velocity is positive the ions move towards the capillary and are injected. When the apparent velocity is negative, the hydrodynamic velocity is dominant and not all of the ions are injected.

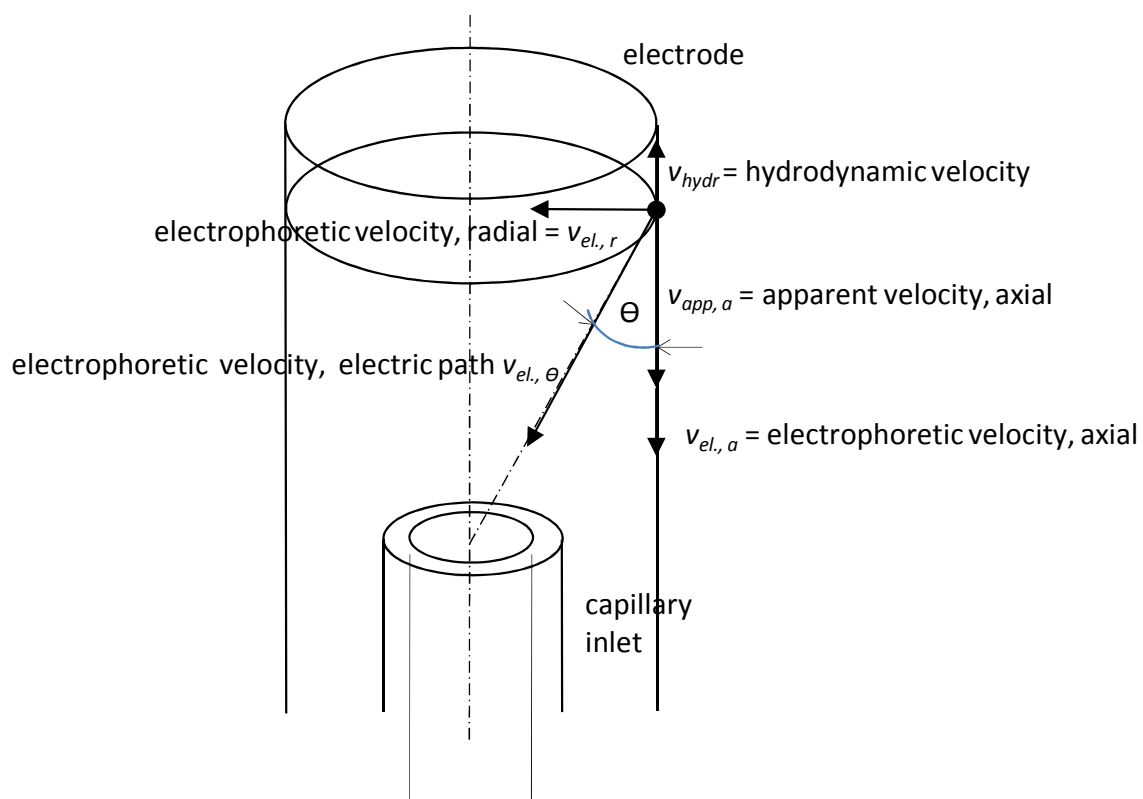


Figure 3.2 Scheme of the hydrodynamic, electrophoretic and apparent velocities in the continuous sample flow interface

3.2.2.1 APPARENT VELOCITY OF THE SAMPLE ION

Using geometry and the theory of electromigration, the apparent velocity $v_{app,a}$ can be expressed as a function of the interface dimensions, the sample mobility, injection voltage and the flow rate. The voltage available for injection U_{Intf} leads to the formation of an electric field in the interface, $E_{Intf,\theta}$, along the electric path length L (Figure 3.1) according to:

$$E_{Intf,\theta} = \frac{U_{Intf}}{L} \quad (3.1)$$

$E_{Intf,\theta}$ electric field strength along the electric field path in V/m
 U_{Intf} voltage available for injection in V
 L length of electric field path in m

The angle θ is defined by the length of the interface L_{Intf} and the electric field path L (see Figure 3.1). θ is also defined by the electrophoretic velocity of the sample ion along the electric field path $v_{el,\theta}$ and its axial component $v_{el,a}$ which is illustrated in Figure 3.2.

$$\cos \theta = \frac{L_{Intf}}{L} = \frac{v_{el,a}}{v_{el,\theta}} \quad (3.2)$$

$v_{el,\theta}$ electrophoretic velocity of sample ion in the direction of the electric field path in m/s
 $v_{el,a}$ electrophoretic velocity of the sample ion in axial direction in m/s
 L_{Intf} length of interface in m
 L length of electric field path in m

An ion with the electrophoretic mobility μ is acted upon by the electric field $E_{Intf,\theta}$ which causes it to accelerate until it reaches a constant velocity of $v_{el,\theta}$.

$$v_{el,\theta} = \mu \cdot E_{Intf,\theta} \quad (3.3)$$

$v_{el,\theta}$	electrophoretic velocity of sample ion along the electric field line path in m/s
μ	electrophoretic mobility of the sample ion in $m^2/(V*s)$
$E_{Intf,\theta}$	electric field strength along the electric field line path in V/m

At the same time the sample is being pushed through the interface with a hydrodynamic velocity v_{hydr} . The volumetric flow rate fl is given by:

$$v_{hydr} = \frac{fl}{A_D} = \frac{fl \cdot 4}{D^2 \cdot \pi} \quad (3.4)$$

v_{hydr}	hydrodynamic velocity of sample stream in m/s
A_D	cross section of interface in m^2
D	inner diameter of interface in m
fl	volumetric flow rate of sample stream in m^3/s

The apparent velocity of the sample ion $v_{app,a}$ is the sum of the electrophoretic velocity in axial direction $v_{el,a}$ and the hydrodynamic flow velocity v_{hydr} .

$$v_{app,a} = v_{el,a} - v_{hydr} \quad (3.5)$$

$v_{app,a}$	apparent electrophoretic velocity of sample ion in m/s
$v_{el,a}$	electrophoretic velocity of sample ion in axial direction in m/s
v_{hydr}	hydrodynamic velocity of sample stream in m/s

The above formula needs to be rearranged to contain only parameters of the interface setup which are independent from each other.

Using equation 3.2, the following expression for $v_{app,a}$ can be obtained:

$$v_{app,a} = v_{el,\theta} \cdot \frac{L_{Intf}}{L} - \frac{fl \cdot 4}{D^2 \cdot \pi}$$

Using $v_{el,\theta} = \mu \cdot E_{Intf,\theta}$ we obtain

$$v_{app,a} = E_{Intf,\theta} \cdot \mu \cdot \frac{L_{Intf}}{L} - \frac{fl \cdot 4}{D^2 \cdot \pi}$$

Further $E_{Intf,\theta} = \frac{U_{Intf}}{L}$ which gives

$$v_{app,a} = \frac{U_{Intf}}{L} \cdot \mu \cdot \frac{L_{Intf}}{L} - \frac{fl \cdot 4}{D^2 \cdot \pi}$$

and $L = \sqrt{L_{Intf}^2 + \left(\frac{D}{2}\right)^2}$ (3.6) which gives

$$v_{app,a} = \frac{U_{Intf}}{\sqrt{L_{Intf}^2 + \left(\frac{D}{2}\right)^2}} \cdot \mu \cdot \frac{L_{Intf}}{\sqrt{L_{Intf}^2 + \left(\frac{D}{2}\right)^2}} - \frac{fl \cdot 4}{D^2 \cdot \pi}$$

This can be rearranged to give the final equation describing $v_{app,a}$ as:

$$v_{app,a} = \frac{U_{Intf} \cdot \mu \cdot L_{Intf}}{L_{Intf}^2 + \left(\frac{D}{2}\right)^2} - \frac{fl \cdot 4}{D^2 \cdot \pi} \quad (3.7)$$

$v_{app,a}$	apparent electrophoretic velocity of sample ion in m/s
μ	electrophoretic mobility of the sample ion in $m^2/(V*s)$
L_{Intf}	length of interface in m
fl	volumetric flow rate of sample stream in m^3/s
D	inner diameter of interface in m
U_{Intf}	voltage available for sample injection in V

The injection voltage U_{inf} is the only dependent variable remaining in the formula. Therefore it is necessary to derive a formula that describes the injection voltage as a function of independent interface parameters.

3.2.2.2 DERIVATION OF THE INJECTION VOLTAGE

In order to understand how the various interface parameters influence the injection voltage an electric equivalent circuit was constructed.

The continuous flow interface and the capillary form an electric series circuit which can be calculated using Ohm's law and Kirchhoff's mesh rule. The equivalent electric circuit diagram is shown Figure 3.3 .

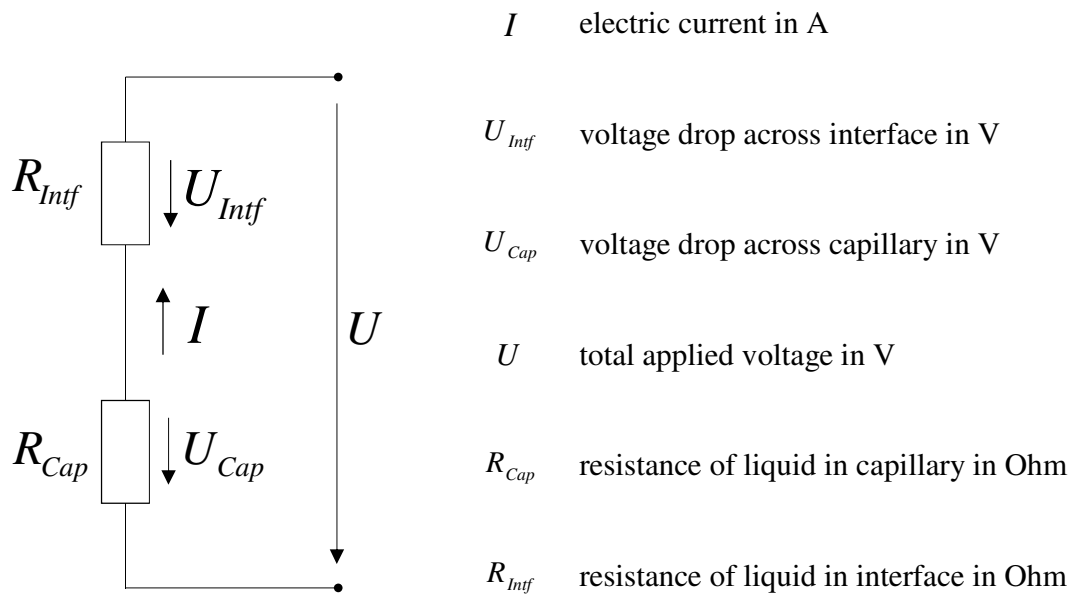


Figure 3.3 Electric equivalent circuit diagram for the continuous flow interface and the separation capillary. The electric resistance of the interface is connected in series to the capillary resistance. The total voltage is the voltage applied by the high voltage power supply. Part of this voltage will drop across the interface and the rest across the capillary. The current is the same in the interface and capillary.

The voltage drop in a series circuit can be calculated using Kirchhoff's mesh rule which states that the direct sum of any potential differences around any closed network is zero. Thus,

$$U = U_{Intf} + U_{Cap} \quad (3.8)$$

U_{Intf} voltage drop across interface in V

U_{Cap} voltage drop across capillary in V

U total applied voltage

The total resistance is equal to the sum of the individual resistances of the capillary and the interface according to equation 3.9:

$$R = R_{Intf} + R_{Cap} \quad (3.9)$$

R_{Intf} electric resistance of liquid in interface in Ohm

R_{Cap} electric resistance of liquid in capillary in Ohm

The electric current flowing through the liquid in the interface and in the capillary will follow Ohm's law. Therefore the capillary and the interface carry the same current.

$$I = \frac{U}{R} = \frac{U_{Intf} + U_{Cap}}{R_{Intf} + R_{Cap}} \quad (3.10)$$

I electric current in A

U_{Intf} voltage drop across interface in V

U_{Cap} voltage drop across capillary in V

R_{Intf} resistance of liquid in interface in Ohm

R_{Cap} resistance of liquid in capillary in Ohm

The interface resistance R_{Intf} is defined by the dimension of the interface and the properties of the electrolyte and can be calculated by:

$$R_{Intf} = \frac{\rho_{Intf} \cdot L_{Intf}}{A_D} \quad (3.11)$$

R_{Intf}	resistance of liquid in interface in Ohm
L_{Intf}	length of interface in m
ρ_{Intf}	electric specific resistivity of liquid in interface in Ohm*m
A_D	cross section of interface in m ²

Similarly, the resistance of the capillary can be calculated by:

$$R_{Cap} = \frac{\rho_{Cap} \cdot L_{Cap}}{A_d} \quad (3.12)$$

R_{Cap}	resistance of liquid in capillary in Ohm
L_{Cap}	length of capillary in m
ρ_{Cap}	electric specific resistivity of liquid in capillary in Ohm*m
A_d	cross section of capillary in m ²

The conductivity ratio between the liquid in the capillary and the interface is defined as:

$$k = \frac{\rho_{Intf}}{\rho_{Cap}} = \frac{\gamma_{Cap}}{\gamma_{Intf}} \quad (3.13)$$

k	conductivity ratio of liquid in capillary and interface
ρ_{Cap}	electric specific resistivity of liquid in capillary in Ohm*m
ρ_{Intf}	electric specific resistivity of liquid in interface in Ohm*m
γ_{Cap}	electric specific conductivity of liquid in capillary
γ_{Intf}	electric specific conductivity of liquid in interface

Rearranging Ohm's law for the voltage drop across the interface and capillary we get:

$$U_{Intf} = I \cdot R_{Intf} \quad (3.14)$$

$$U_{Cap} = I \cdot R_{Cap} \quad (3.15)$$

Given that the current is identical, then equating equations 3.14 and 3.15 yields:

$$U_{Intf} = \frac{U}{R_{Intf} + R_{Cap}} \cdot R_{Intf} \quad (3.16)$$

Adding in the specific resistivities, the interface dimensions, capillary dimensions and the conductivity ratio we obtain the following formula for the injection voltage,

$$U_{Intf} = \frac{U \cdot \frac{\rho_{Intf} \cdot L_{Intf} \cdot 4}{\pi \cdot D^2}}{\frac{\rho_{Intf} \cdot L_{Intf} \cdot 4}{\pi \cdot D^2} + \frac{\rho_{Intf} \cdot \frac{1}{k} \cdot L_{Cap} \cdot 4}{\pi \cdot d^2}} \quad (3.17)$$

This formula contains only independent variables all of which are parameters of the interface setup.

3.2.2.3 DEPLETION FLOW RATE FOR COMPLETE SAMPLE INJECTION

Intuitively, all ions are injected when the apparent ion velocity is towards the capillary inlet. From a practical perspective, maximizing the flow rate while still injecting all of the ions will yield the most significant enhancements in sensitivity in the shortest possible time. Therefore, the main goal is to find the depletion flow rate – the maximum flow rate at a defined voltage at which all sample ions are injected.

At a certain flow rate the axial component of the electrophoretic sample ion velocity and the hydrodynamic velocity are equal. At this flow rate, the depletion flow rate fl_0 , the apparent velocity in axial direction $v_{app,a}$ of the sample ion is zero. Below fl_0 the apparent velocity points towards the capillary inlet and all the sample ions are injected. Above fl_0 a certain proportion of the incoming sample ions are lost.

In order to find fl_0 , $v_{app,a}$ is set to zero in equation 3.7 to give:

$$v_{app,a} = \frac{U_{Intf} \cdot \mu \cdot L_{Intf}}{L_{Intf}^2 + \left(\frac{D}{2}\right)^2} - \frac{fl \cdot 4}{D^2 \cdot \pi} = 0$$

Rearranging this equation yields:

$$fl_0 = \frac{U_{Intf} \cdot \mu \cdot L_{Intf} \cdot D^2 \cdot \pi}{\left(L_{Intf}^2 + \left(\frac{D}{2}\right)^2\right) \cdot 4} \quad (3.18)$$

fl_0 is the volumetric flow rate where $v_{app,a}$ is zero. Combining this with equation 3.17 for U_{Intf} gives:

$$fl_0 = \frac{\frac{U \cdot \frac{\rho_{Intf} \cdot L_{Intf} \cdot 4}{\pi \cdot D^2} \cdot \mu \cdot L_{Intf} \cdot D^2 \cdot \pi}{\frac{\rho_{Intf} \cdot L_{Intf} \cdot 4}{\pi \cdot D^2} + \frac{\rho_{Intf} \cdot \frac{1}{k} \cdot L_{Cap} \cdot 4}{\pi \cdot d^2}}{\left(L_{Intf}^2 + \left(\frac{D}{2}\right)^2\right) \cdot 4}$$

, which can be rearranged to

$$fl_0 = \frac{\pi \cdot U \cdot L_{intf}^2 \cdot \mu}{4 \cdot \left(\frac{L_{intf}}{D^2} + \frac{1}{k} \cdot \frac{L_{cap}}{d^2} \right) \cdot \left(L_{intf}^2 + \left(\frac{D}{2} \right)^2 \right)} \quad (3.19)$$

fl_0 volumetric depletion flow rate
where $v_{app,a}$ is zero in m^3/s

U total applied voltage in V

k conductivity ratio of liquid in
capillary and interface

D inner diameter of interface in m

L_{intf} length of interface in m

L_{cap} length of capillary in m

d inner diameter of capillary in m

μ electrophoretic mobility of sample
ion in m^2/Vs

For any flow rate $fl < fl_0$ all of the sample ions get injected

3.2.3 SENSITIVITY ANALYSIS OF THE DEPLETION FLOW RATE

In the following sections the influence of each variable on the depletion flow rate is examined. The formula for fl_0 contains 8 variables that can be varied within certain practical constraints with a sensitivity analysis performed by changing each parameter individually. For the following calculations the parameters have been chosen as they appear in the experimental

setting in section 3.3 in this chapter. The variables were: $U = 15$ kV, $k = 400$, $L_{mf} = 5$ mm, $L_{cap} = 32.6$ cm, $d = 50$ μ m, $\mu = 23 \cdot 10^{-9}$ m²/Vs, $D = 1000$ μ m.

3.2.3.1 INFLUENCE OF INTERFACE DIAMETER

Varying the diameter of the interface will have two effects. First, based on equation 3.11 an increase in interface diameter D will reduce interface resistance as there is a bigger cross sectional area available for the current to pass through, thus a lower resistance. This will lead to a lower injection voltage. Second, the electric path L is increased with a bigger D . The combination of decreased injection voltage and a longer electric path length should cause a reduction in the electric field strength and a decrease in the axial component of the electrophoretic velocity $v_{el.,a}$. Thus $v_{el.,a}$ will decrease with increasing interface diameters. This means that at higher interface diameters the hydrodynamic velocity for complete sample injection should decrease. However, it is important to realise that the flow rate through the interface does not decrease in the same manner as the hydrodynamic velocity. This is due to the fact that the flow rate decreases quadratically with the interface diameter. For example: if the interface diameter is doubled the hydrodynamic velocity is reduced by 4 to keep the same flow rate through the interface. This means if the axial component of the electrophoretic sample velocity decreases also decreases by a factor of 4, complete sample injection at this flow rate is possible. If $v_{el.,a}$ decreases less than a factor of 4, this will mean that there is a lower flow rate fl_0 for complete sample injection. If $v_{el.,a}$ decreases more than a factor 4 complete sample injection, then a higher fl_0 is possible.

In Figure 3.4 the change of fl_0 with the interface diameter D is shown. As can be seen from the graph fl_0 starts out with a sharp rise from 0.1165 μ L/s at 50 μ m to the maximum of 0.8110

$\mu\text{L/s}$ at $1100 \mu\text{m}$. f_{l_0} is decreasing after the maximum at a less sharp slope to $0.4155 \mu\text{L/s}$ at $10,000 \mu\text{m}$. Between $450 \mu\text{m}$ and $2750 \mu\text{m}$ interface inner diameter the depletion flow rate decreases only around 5% of its maximum value at $1100 \mu\text{m}$. Therefore interface diameters should be chosen within the relatively flat top of the graph to ensure a high depletion flow rate. All other parameters were defined as previously stated.

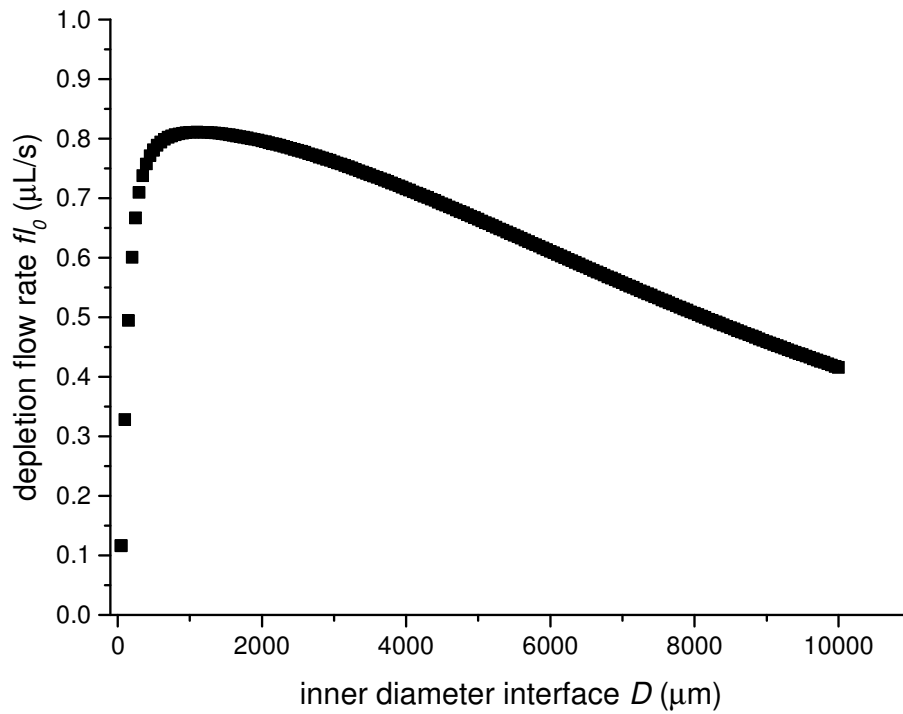


Figure 3.4 Change of fl_0 with the interface diameter D . Above the depletion flow rate fl_0 sample gets lost and below sample gets injected. The depletion flow rate has a maximum at 1100 μm interface inner diameter. The variables chosen were: $k = 400$, $L_{mf} = 5$ mm, $L_{Cap} = 32.6$ cm, $d = 50$ μm , $\mu = 23 \cdot 10^{-9}$ m^2/Vs , $U = 15$ kV. The inner diameter of the interface D was varied from 50 to 10,000 μm .

3.2.3.2 EFFECT OF TOTAL APPLIED VOLTAGE AND SAMPLE MOBILITY

A higher total applied voltage is expected to increase the electric field strength and allow higher depletion flow rates. From the formula for fl_0 it is clear that increasing the applied total voltage leads to a directly proportional increase in fl_0 . fl_0 increases proportionally at 0.05400 $\mu\text{L/s}$ per 1 kV. The variables chosen were: $k = 400$, $L_{inf} = 5$ mm, $L_{Cap} = 32.6$ cm, $d = 50$ μm , $D = 1000$ μm , $\mu = 23 \cdot 10^{-9}$ m^2/Vs . Within the chosen constraint of 1-30 kV the depletion flow rate increases from 0.05400 to 1.621 $\mu\text{L/s}$. With an increased electrophoretic sample mobility the samples travel towards the capillary inlet at higher velocities which allows for higher depletion flow rates. The depletion flow rate increases 3.524 $\cdot 10^7$ $\mu\text{L/s}$ per 1 m^2/Vs and increases from 0.7048 to 3.524 $\mu\text{L/s}$ when varying the electrophoretic sample mobility from 10-100 $\cdot 10^{-9}$ m^2/Vs . The variables chosen were: $k = 400$, $L_{inf} = 5$ mm, $L_{Cap} = 32.6$ cm, $d = 50$ μm , $D = 1000$ μm , $U = 15$ kV.

3.2.3.3 INFLUENCE OF CONDUCTIVITY RATIO

Other important factors that will affect fl_0 are the conductivities of the BGE and the sample. This is expressed as the conductivity ratio k between the liquid in the capillary and the liquid in the interface and will affect the distribution of the voltage across the interface and capillary. For these calculations, the interface is assumed to be filled with sample and the capillary with BGE. Intuitively, a higher conductivity ratio should cause an increased field strength in the interface and therefore enable a higher depletion flow rate fl_0 .

This is reflected in the formula for fl_0 where it can be seen that increasing k leads to a directly proportional increase in fl_0 . Within the chosen constraint of 200-1000 for k the depletion flow rate increases from 0.4084 to 1.981 $\mu\text{L/s}$ proportionally at 0.001970 $\mu\text{L/s}$ per conductivity

ratio unit. This suggests that a high conductivity difference between sample and background electrolyte will yield higher depletion flow rates. The variables chosen were: $L_{inf} = 5$ mm, $L_{Cap} = 32.6$ cm, $d = 50$ μ m, $D = 1000$ μ m, $\mu = 23 \cdot 10^{-9}$ m²/Vs, $U = 15$ kV.

3.2.3.4 INFLUENCE OF INTERFACE LENGTH

Increasing the interface length L_{inf} should increase the interface resistance R_{inf} (see equation 3.11) and the voltage drop across the interface U_{inf} , which is the injection voltage (see equation 3.16). The interface resistance R_{inf} can be assumed to be negligibly small in the denominator of equation 3.16 at short interface lengths L_{inf} . This means the injection voltage U_{inf} will increase nearly directly proportional with the interface resistance R_{inf} and therefore the interface length L_{inf} when using a short interface. With the interface getting longer the capillary resistance R_{Cap} in the denominator in equation 3.15 can be assumed to be negligibly small. In this case the injection voltage will not increase any further when increasing the interface resistance and therefore the interface length. Therefore the injection voltage will start out with a sharp incline at small interface lengths and reach a plateau value at bigger interface diameters. The electric path length L as a function of interface length L_{inf} (see equation 3.6) on the other hand will start out relatively flat and reach a near linear dependence at long interface lengths. The resulting electric field strength $E_{Inf,\theta}$ along the electric path length L is defined as the ratio of U_{inf} / L . Therefore $E_{Inf,\theta}$ and the axial component of the electrophoretic velocity $v_{el,a}$ will reach a maximum as function of the interface length. This means that the hydrodynamic velocity for complete sample injection, v_{hydr} and the depletion flow rate fl_0 should show the same dependence on the interface length.

Figure 3.5 illustrates the dependence of fl_0 on the interface length L_{Intf} . As expected the depletion flow rate increases from 0.7775 uL/s at 2mm interface length, reaches a maximum of 0.8107 uL/s at 5.5 mm and then declines to 0.7826 at 20 mm. Between the chosen interface diameters of 2 mm and 20 mm the depletion flow rate varies only around 5%. Therefore the influence of the interface length on the depletion flow rate is negligible for the chosen constraints of the interface length.

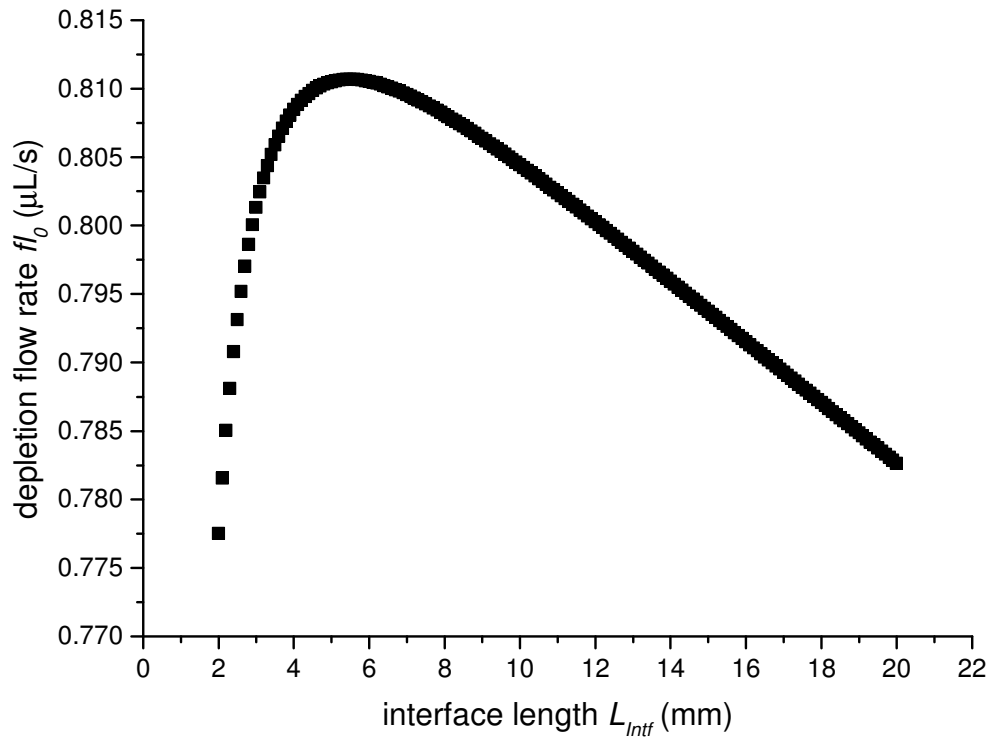


Figure 3.5 Change of f_{l_0} with the interface length L_{Intf} . The depletion flow rate shows a maximum of 0.8107 $\mu\text{L/s}$ at 5.5 mm interface length. The variables chosen were: $k = 400$, $L_{Cap} = 32.6$ cm, $d = 50$ μm , $D = 1000$ μm , $\mu = 23 \cdot 10^{-9}$ m^2/Vs , $U = 15$ kV. The interface length L_{Intf} was varied from 2 to 20 mm.

3.2.3.5 INFLUENCE OF CAPILLARY DIMENSIONS

The separation capillary and the interface form an electric series circuit. Part of the total voltage will drop across the interface and the majority across the capillary. By reducing the voltage drop across the capillary more voltage is available for injection in the interface. Reducing the length of the separation capillary is expected to leave more voltage for injection in the interface. Thus a reduction in capillary length should increase f_{i0} exponentially according to equation 3.17. From equations 3.16 and 3.17 it can be seen that tripling the inner diameter of the capillary d decreases the capillary resistance R_{Cap} by a factor of $3^2 = 9$. Therefore increasing the inner diameter is expected to increase the injection voltage and f_{i0} exponentially.

It can be seen from Figure 3.6 that this is indeed the case. With a shorter capillary the depletion flow rate f_{i0} increases exponentially. At 2 cm capillary length the depletion flow rate is 10.73 $\mu\text{L/s}$ and falls to 0.2269 $\mu\text{L/s}$ at 100 cm. Figure 3.7 shows that a decrease in capillary inner diameter increases the depletion flow rate exponentially from 8.230×10^{-3} $\mu\text{L/s}$ at 5 μm to 3.101 $\mu\text{L/s}$ at 100 μm capillary i.d.

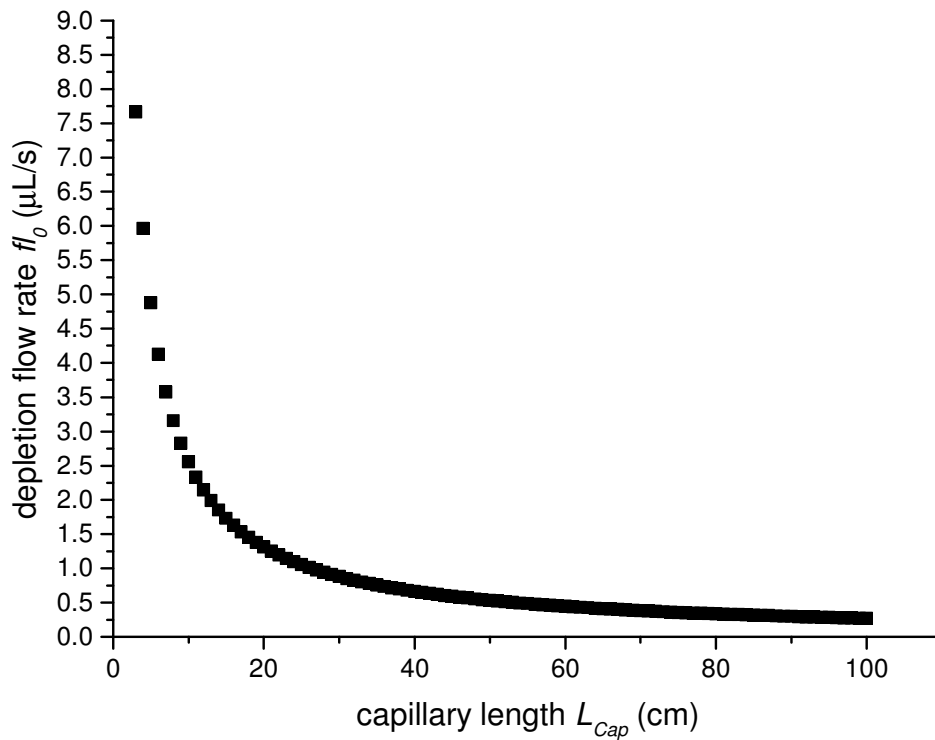


Figure 3.6 Effect of capillary length on depletion flow rate f_{l0} . A shorter separation capillary allows for higher depletion flow rates. The variables chosen were: $k = 400$, $L_{inj} = 5$ mm, $d = 50$ μm , $D = 1000$ μm , $\mu = 23 \cdot 10^{-9}$ m^2/Vs , $U = 15$ kV. The capillary length was varied from 2 to 100 cm.

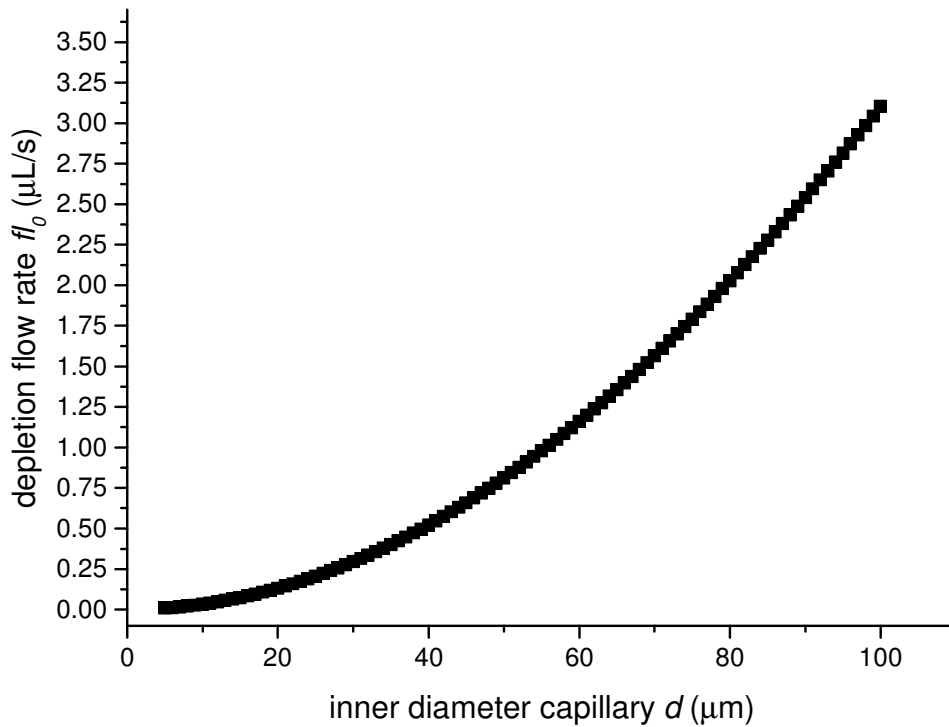


Figure 3.7 Effect of capillary inner diameter on depletion flow rate f_{l_0} . A bigger capillary i.d. allows for higher depletion flow rates. The variables chosen were: $k = 400$, $L_{mf} = 5$ mm, $L_{Cap} = 32.6$ cm, $D = 1000$ μm , $\mu = 23 \cdot 10^{-9}$ m^2/Vs , $U = 15$ kV. The capillary inner diameter was varied from 5 to 100 μm .

3.2.3.6 GUIDELINES FOR INTERFACE DESIGN FROM THE MATHEMATICAL MODEL

In order to maximise the depletion flow rate, the following guidelines can be determined from the examination above: the total applied voltage, the electrophoretic sample mobility and the conductivity ratio between the liquid in the interface and the capillary should be as high as practically possible to give high depletion flow rates. The conductivity ratio will be determined by the limitations of the stacking method and the electrophoretic sample mobility will be determined by the analyte of interest in an experimental setup. Limitations due to high currents will arise when choosing the highest possible applied voltage. The results propose that there is an optimum interface diameter and length at which the depletion flow rate reaches a maximum. It should be noted that varying the interface length between 2 to 20 mm changes the depletion flow rate only around 5% of its maximum of 0.8107 $\mu\text{L/s}$. Within a range of 450 to 2750 μm of interface diameter the depletion flow rate changes around 5% of its maximum at 0.8110 $\mu\text{L/s}$. The capillary inner diameter should be as big as current limitations allow and increases the depletion flow rate exponentially. Out of all parameters a reduced capillary length showed the biggest improvements in depletion flow rate up to 10.73 $\mu\text{L/s}$ at a capillary length of 2cm. This again limited because the voltage needs to be reduced accordingly when using a short separation capillary to avoid high currents. The mathematical model represents a simplified version of a continuous flow interface and did not capture all physical effects. For example in the mathematical model the liquid velocity across the interface chamber was assumed to be uniform. In reality the velocity profile in the interface chamber is parabolic. This means, that in reality the velocity of the liquid at the center of the channel is relatively high, while the velocity close to the walls is relatively slow. Another aspect is that the electric field lines are assumed to be parallel

throughout the interface channel. In reality the field lines have to go from the ring electrode in the interface channel into the separation capillary entrance. Therefore the field line density must increase in close proximity to the capillary entrance. Despite these simplifications the mathematical model should allow to predict correct trends for the depletion flow rate as a function of interface parameters.

3.3 EXPERIMENTAL VALIDATION OF THE MATHEMATICAL MODEL

The mathematical model established an understanding of how the various interface parameters affect the depletion flow rate when performing EKI from a flowing sample stream. In this section the influence of the flow interface dimensions on the depletion flow rate is examined in an experimental setup and then compared with the mathematical model predictions.

3.3.1 EXPERIMENTAL

3.3.1.1 MATERIALS AND INSTRUMENTATION

To monitor the electrokinetic injection from a flowing sample stream a fluorescent dye was used. The suitable buffers were set to pH 7.9 in order to have maximum fluorescent intensity while preventing damage of the Zero EOF coated capillary. HCL, TRIS, HEPES and Fluorescein sodium salt were purchased from Sigma-Aldrich (St. Louis, MO). KOH was purchased from Merck Millipore (Darmstadt, Germany). Stock solutions of 100 $\mu\text{g}/\text{mL}$ sodiumfluorescein, 400 mM Tris in water adjusted to pH 7.9 with HCl and 400 mM HEPES in water adjusted to pH 7.9 with KOH were prepared. Dilutions of sodium fluorescein in Tris-HCl or HEPES-KOH buffer were prepared by mixing an appropriate amount of purified water with the 100 $\mu\text{g}/\text{mL}$ sodium fluorescein solution and the 400 mM Tris-HCl or the 400 mM HEPES-KOH stock, respectively. All solutions were filtered through a 0.45 μm filter from MicroScience (Co Durham, UK) and sonicated for 10 min prior to use. The background electrolyte (BGE) was prepared by diluting the stock solutions with the appropriate amount of water to 40 mM Tris-HCl or 40 mM HEPES-KOH, respectively. Water was purified using a Milli-Q system from Millipore (Bedford, MA). The *pH* was measured using an Activon Model 210 pH meter (New South Wales, Australia).

3.3.1.2 HOMEMADE CE SYSTEM

The setup of the CE system was designed to allow a controlled flow of sample and adjustment of all liquid levels to prevent sample matrix injection. The interface was a straight channel in a block of polymer to avoid formation of unwanted turbulences and mixing of sample and BGE at the boundary. The capillary was positioned *in-line* with the axis of the sample flow and the ring electrode. This created a symmetrical electric field and a uniform electric field line density for injection. An eppendorf 200 μL pipette tip was used to connect the capillary which was surrounded by the sample stream to the BGE filled interface. This approach maintained a clean sample-BGE front prior to reaching the capillary inlet.

All capillary electrophoresis experiments were conducted on a homemade system (see Figure 3.8) equipped with a fluorescence microscope detector (AM4133T-GFBW Dino Lite Premier Digital Fluorescence Microscope), a high voltage power supply (Spellman Model SMS60P60/24), a pump (milli GAT, Model i-24273-GF) with a connector (MFORCE 3AMP Microdrive Plus MFI3CD17N4-EE). The power supply and pump were controlled via a lab view program (Student Edition) and connected via a National Instruments controller (NI-USB-6212 16 Inputs, 16-bit, 400 GS/s, Multifunction I/O). A Zero EOF neutral coated capillary (50 μm inner and 365 μm outer diameters, respectively) from MicroSolv Technology (New Jersey, USA) was used. The total length was 32.6 cm. A Y connector was used to join the sample stream with the capillary (see Figure 3.9). In order to connect the separation capillary to the Y connector a low pressure standard union (P 603, Upchurch Scientific) with the supplied fittings and ferrules (Upchurch Scientific), a polyethyletherketone (PEEK) tubing (F -158 x) and a 3 cm piece of transparent plastic tubing (060610, Dionex) was used. The separation capillary was connected to the Y connector so that no liquid could leak through between the barb of the Y connector and the

capillary (see Figure 3.9) In order to establish a connection from the Y-connector to the continuous flow interface a 3 cm piece of plastic tubing (060610, Dionex) with a pipette tip at the end was used (for details see Figure 3.10). The interface which can be seen in Figure 3.11 was custom made from a block of polymethyl methacrylate (PMMA). The electrodes were custom made from stainless steel. The waste tube was a 9 cm piece of plastic tubing (060610, Dionex).

The ethylene-tetrafluorethylene (EFTE) tubing (1528 XL, Upchurch Scientific) between the sample vial and pump was 30 cm in length with 1.6 mm outer and 0.75mm inner diameter. In order to connect the EFTE tubing to the Y-connector (P-860 x, IDEX Health & Science) a low pressure standard union (P 603, Upchurch Scientific) with the supplied fittings and ferrules (Upchurch Scientific) and a 3 cm piece of transparent plastic tubing (060610, Dionex) were used.

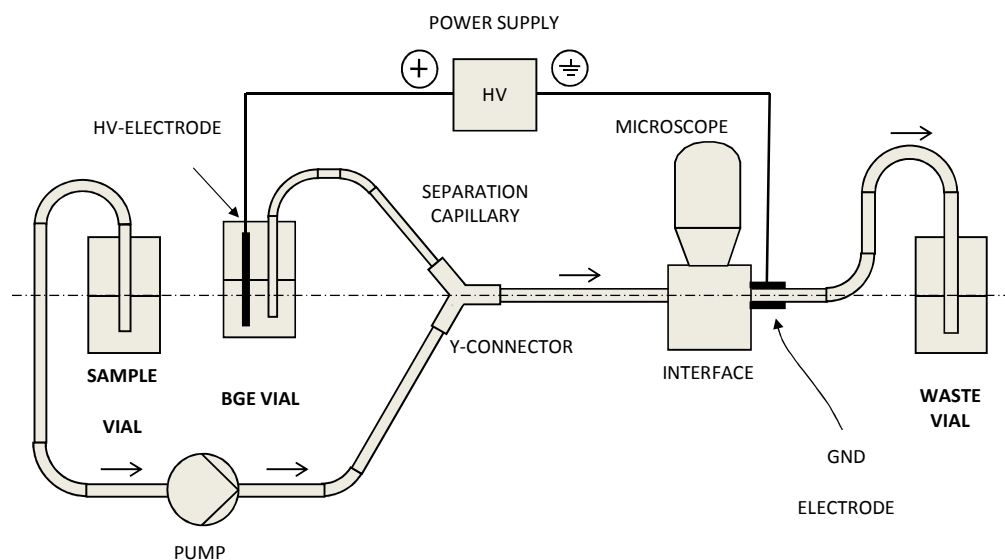


Figure 3.8 Scheme of the continuous flow interface setup. The pump delivers the sample liquid through the Y connector and the interface towards the waste vial. The capillary's inlet is placed inside the interface where the GND electrode is positioned while the other end is inside the BGE vial with the HV wire electrode. The BGE vial is elevated 8 mm above the liquid levels of the sample and waste vial to counterbalance the hydrostatic sample injection. A detailed description of the Y connector and the interface can be found in Figure 3.9 and Figure 3.10; for further explanation see text.

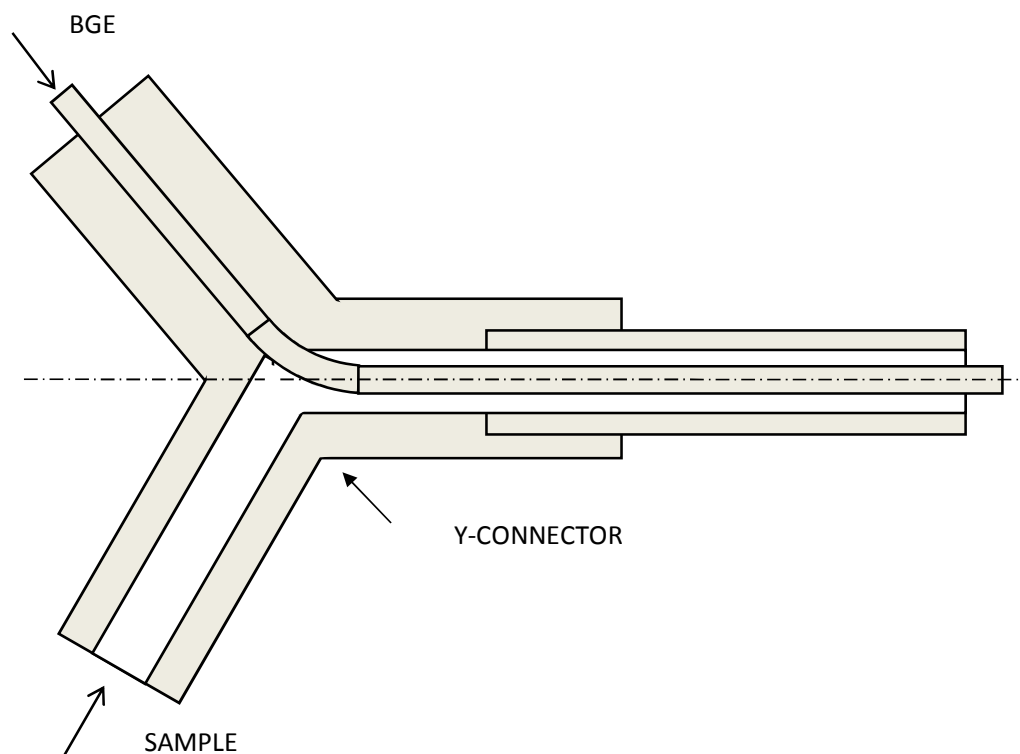


Figure 3.9 Scheme of the Y connector; the sample stream coming in from the lower end surrounds the separation capillary that is coming in from the top. The separation capillary which is surrounded by the flowing sample stream is further connected to the sample interface via a pipette tip (see Figure 3.10 and Figure 3.11). A connector was used to connect the capillary to the Y connector without allowing liquid to pass through between the top Y barb and the capillary; further explanations are in the text.

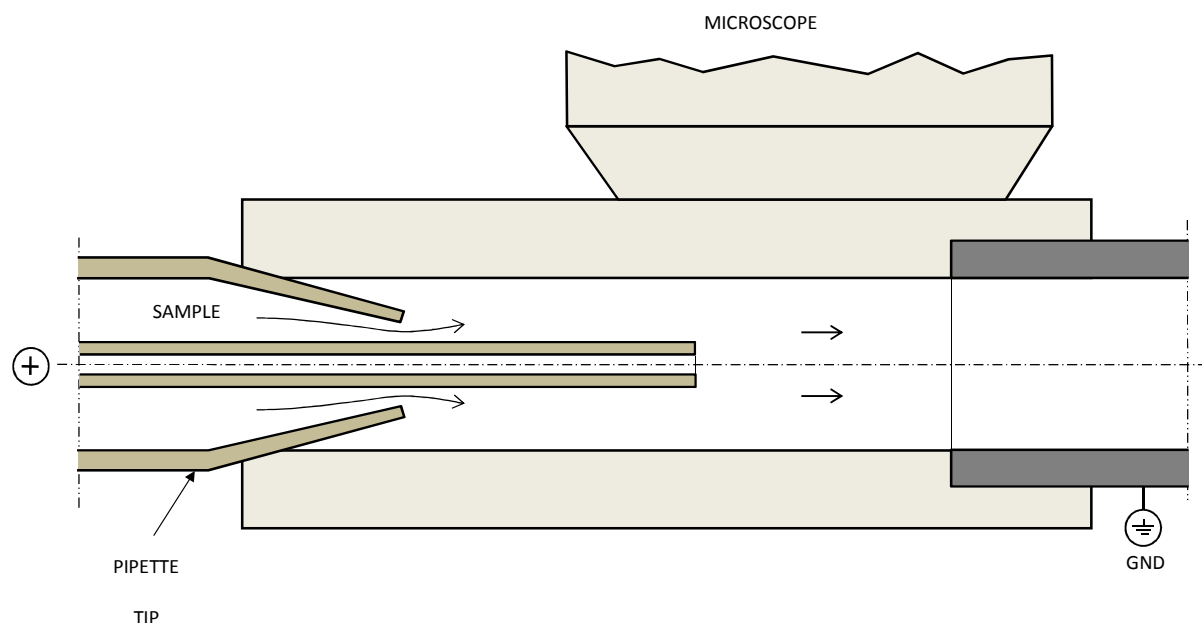


Figure 3.10 Scheme of the continuous sample flow interface; a pipette tip was used to connect the capillary which is surrounded by the sample stream to the interface. The capillary was positioned *in-line* with the symmetry axis of the interface and the pipette tip. Voltage was applied between the GND electrode and the outlet of the BGE filled capillary. The distance between the GND electrode and the outlet of the BGE filled capillary. The distance between the capillary entrance tip and the GND electrode was kept constant at 5 mm. The interface consisted of a block of transparent PPMA with a thru hole of i.d's of 500 μm , 1000 μm and 1500 μm . The entire length of the interface was 30 mm and 10 mm in height. The stainless steel electrode had a total length of 20 mm with 10 mm being inside the interface. The microscope was positioned flat on the polished interface, and recorded the area between electrode and capillary inlet (see Figure 3.11), for further explanation see text.

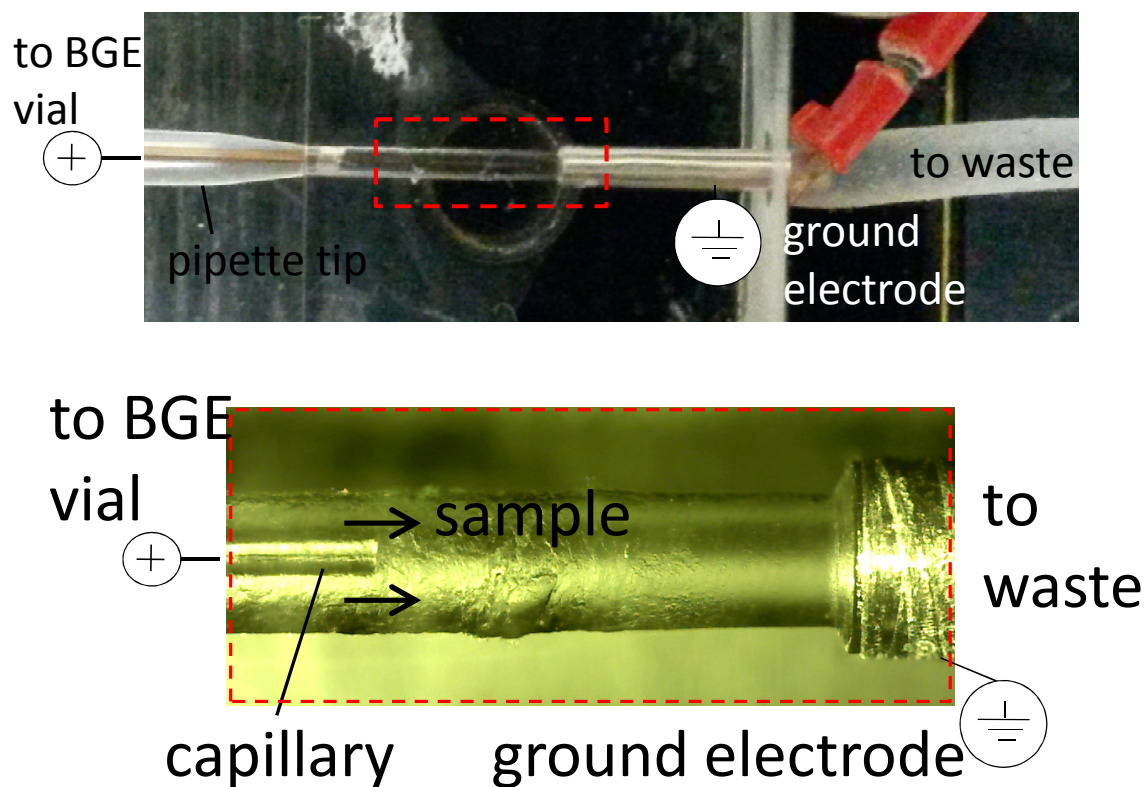


Figure 3.11 Top view of the sample interface. A hole drilled into a block of PMMA accommodates the ground electrode and the pipette tip which contains the sample stream that surrounds the capillary. A close up view recorded from the microscope can be seen in the picture below.

3.3.1.3 DETERMINATION OF INJECTED SAMPLE PROPORTION

To compare different injections the recorded fluorescence images were processed using Image J (version 1.49 m). The mean gray value over a defined area in the interface (see Figure 3.12) was recorded. It is a measure for the fluorescence intensity emitted by the fluorescein sample. The % injection was calculated by taking the ratio between the mean gray value of the 0 kV image of the blank run and the 15 kV image and expressing it as % of the 0 kV image and then subtracting it from 100% using the following formula:

$$\%injection = 100 - 100 \cdot \frac{\text{mean gray value of 0 kV blank run}}{\text{mean gray value of 15 kV run}}$$

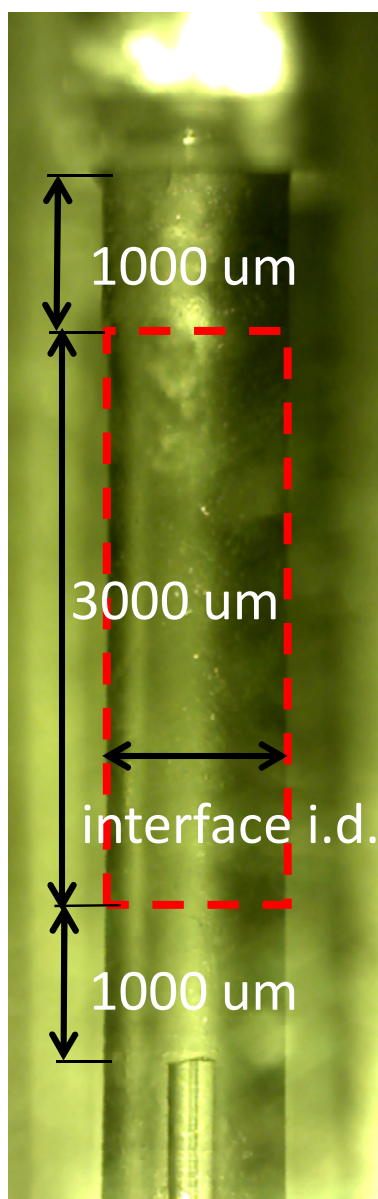


Figure 3.12 The mean gray value of the emitted fluorescence intensity of the fluorescein sample was recorded over the area inside the red dotted line. The intensity was used to calculate the % injection value.

3.3.1.4 ELECTROPHORETIC PROCEDURES

New capillaries were conditioned by flushing with background electrolyte (BGE) for 20 min at 1 bar and purified water for 5 min at 1 bar followed by a final run of BGE for 5 min at 1 bar. Zero EOF coated capillaries have been used in order to minimize the EOF. The capillary was stored in water overnight. The first step before sample injection was to disconnect the capillary tip which contains the separation capillary surrounded by the sample stream (see Figure 3.10). This allows to fill the interface with BGE first and then reconnect the pipette tip to push sample through the interface while applying voltage. The following steps described the process in detail: (1) before each injection the pipette tip in Figure 3.10 was disconnected and the separation capillary was conditioned by flushing with BGE for 5 min, (2) the sample lines were flushed for 1 min at 20 $\mu\text{L/s}$ with sample, (3) the continuous flow interface was filled with BGE using a syringe, (4) the separation capillary surrounded by the sample stream was connected to the interface via a pipette tip, (5) the position of the capillary axis was manually aligned with the interface symmetry axis, (6) the capillary inlet was positioned 5 mm away from the GND electrode in the interface, (7) the injection voltage of 15 kV was switched on and the sample was pushed through the interface. This way a sample-BGE front started moving through the interface. The corresponding flow rate and injection voltage were switched on at the same time the video started recording. For all injections, the sample was injected at 15 kV at different sample flow rates with the anode being at the capillary outlet. Recordings of the 0 kV blank runs consisted of the same steps as described in (1) to (7) except that that no voltage was applied.

3.3.1.5 HYDROGEL PREPARATION

To control unwanted hydrostatic injection a hydrogel was prepared following the procedure of Wuethrich et al. [8]. 600 μL polyacrylamide solution (average M_w 10,000, 50 wt% in H_2O , Sigma Aldrich) was mixed with 60 μL 5 wt% potassium sulfate (ACS reagent, $\geq 99.0\%$, powder, Sigma Aldrich) and 120 μL mM Tris-HCl (pH adjusted to 7.9 with HCl) and 320 μL Milli-Q purified water in a glass container. The container was placed in a 60 $^\circ\text{C}$ hot water bath for 10 min.

3.3.2 RESULTS AND DISCUSSION

During the efforts to systematically study the various interface parameters, the developed mathematical model showed that the depletion flow rate can be maximized by choosing the appropriate interface diameter. The aim of the present work was to investigate the relation between depletion flow rate and the interface diameter experimentally and to verify the predictions of the mathematical model. Therefore the injections from three different interfaces with 500, 1000 and 1500 μm interface diameter were compared with each other. As a starting point the depletion flow rate was determined in the 1000 μm interface and then in the 1500 and 500 μm interface.

3.3.2.1 FLOW STUDIES

In order to understand the electrokinetic component of the injection it is important to reduce the hydrodynamic and hydrostatic sample injection onto the capillary. First the prevention of hydrodynamic and hydrostatic injection by physically blocking the outlet of the separation capillary with a hydrogel was examined.

3.3.2.1.1 PREVENTION OF SAMPLE MATRIX INJECTION USING A HYDROGEL

One way to prevent the bulk flow of liquid into the separation capillary that is caused by hydrodynamic and hydrostatic forces is to use a hydrogel. This approach was based on work by Wuethrich et al. [8] who demonstrated the use of a hydrogel to suppress the bulk flow of liquid that is caused by the EOF inside a capillary. A hydrogel was prepared and placed at the outlet end of the separation capillary together with the electrode. The BGE used in the capillary was 40 mM Tris-HCl at pH 7.9. The sample used was 150 ng/mL sodium fluorescein in 0.04 mM BGE. The interface channel had an inner diameter of 1000 μm . In the present work no successful injection could be achieved when using a hydrogel due to a current drop within the first few minutes of the injection. We suspect that electrolysis bubbles get trapped between the capillary outlet and the hydrogel which then cause a current drop. As this approach was consistently unreliable, an alternative approach of using hydrostatic pressure was examined.

3.3.2.1.2 PREVENTION OF SAMPLE MATRIX INJECTION BY ADJUSTING LIQUID LEVELS

To counterbalance and prevent the hydrodynamic and hydrostatic injection experiments were performed using differential hydrostatic pressure created through the relative liquid level heights. This was achieved by setting all liquid levels in the setup to the correct height difference. The height difference here is defined as the relative height between the liquid level in the waste reservoir and the liquid level in the background electrolyte (BGE) container. The liquid level in the waste container was set to be at the same height with the symmetry axis of the flow interface (see Figure 3.11). By changing the height of liquid level in the BGE container we expected to see a change in the amount of liquid introduced into the separation capillary.

The movement of a fluorescent dye inside the capillary at increasing height differences was measured. The liquid inside the interface was kept stationary at a flow rate of 0 $\mu\text{L/s}$. This

allowed to study the contribution of sample matrix injection due to hydrostatic pressure differences between the in- and out-let of the separation capillary. In Figure 3.13 it can be seen that at +0.8 cm no movement of liquid could be observed after 10 s. There is a flux of liquid into the capillary at 0 cm and a flux of liquid out of the capillary at + 3cm. Therefore + 0.8 cm was chosen as the optimum height difference to avoid hydrostatic sample injection or loss. In a subsequent study shown in Figure 3.14 the movement of a fluorescent dye inside the capillary at + 0.8cm height difference after 10 min was measured. This was done to ensure that + 0.8 cm is the right height since the experiments at 10 s served only as a guideline on which height is close to the optimum height difference.

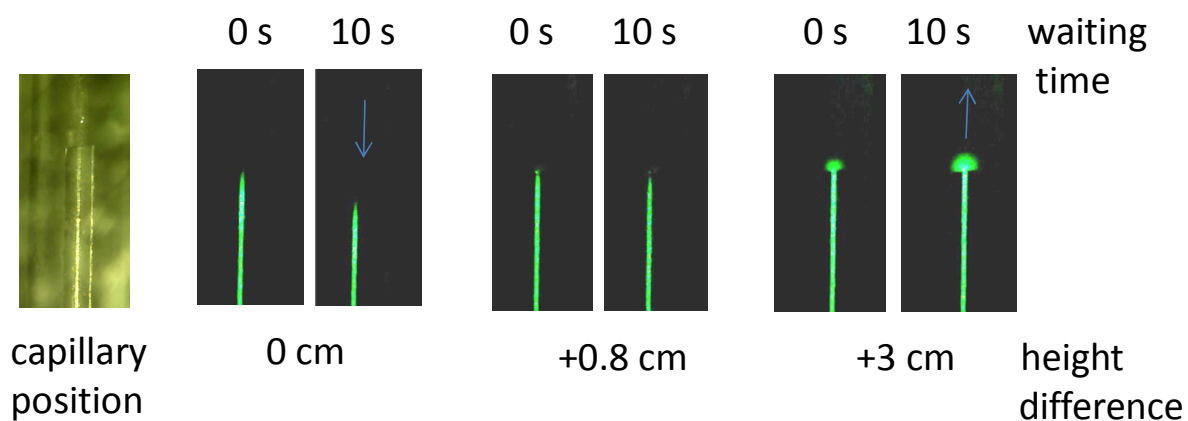


Figure 3.13 Effect of the height difference between the liquid levels of BGE vial and waste vial on the hydrostatic injection into the separation capillary. At +0.8cm the hydrostatic sample injection is at a minimum. The left image shows the position of the capillary. The images at 0cm, +0.8cm and +3 cm show the movement of the fluorescent dye inside the capillary depending on the height difference. The position of the fluorescent dye at 0s at the start of the experiment and after 10s is shown. The blue arrow indicates the direction of liquid movement inside the capillary.

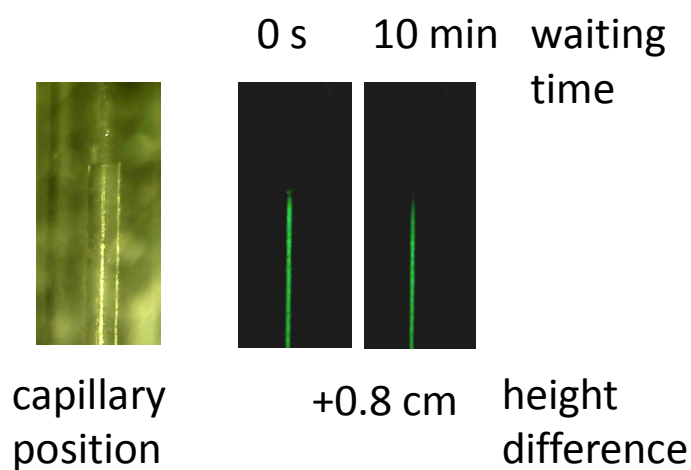


Figure 3.14 Effect of a longer waiting time of on the hydrostatic injection into the separation capillary at the optimized height difference. The left image shows the position of the capillary. The images at +0.8cm shows the position of the fluorescent dye inside the capillary at 0s at the start of the experiment and that there is no significant movement of the dye after 10 min.

3.3.2.1.3 EFFECT OF FLOW RATE ON SAMPLE MATRIX INJECTION

In addition to hydrostatic flow, there is also hydrodynamic flow arising from the flowing sample which exerts pressure on the separation capillary inlet and can cause sample matrix to enter into the capillary. Therefore the contribution of the hydrodynamic pressure at +0.8 cm height difference was investigated.

In the first step the separation capillary was filled with fluorescent sample and the interface with a solution that exhibits less fluorescence. This allowed observing the liquid movement in the separation capillary entrance. In the next step the interface was flushed with liquid at either 0 $\mu\text{L/s}$ or 0.8 $\mu\text{L/s}$ flow rate for 5 min. The results in Figure 3.15 show that at a height difference of + 0.8 cm there is no significant hydrodynamic introduction of sample matrix into the separation capillary entrance after 5 min at flow rates of 0.8 $\mu\text{L/s}$ for the 500 μm , 1000 μm and 1500 μm i.d. interfaces. For all following experiments the height difference was set to + 0.8 cm since this proved to prevent hydrostatic and hydrodynamic injection of liquid into the separation capillary.

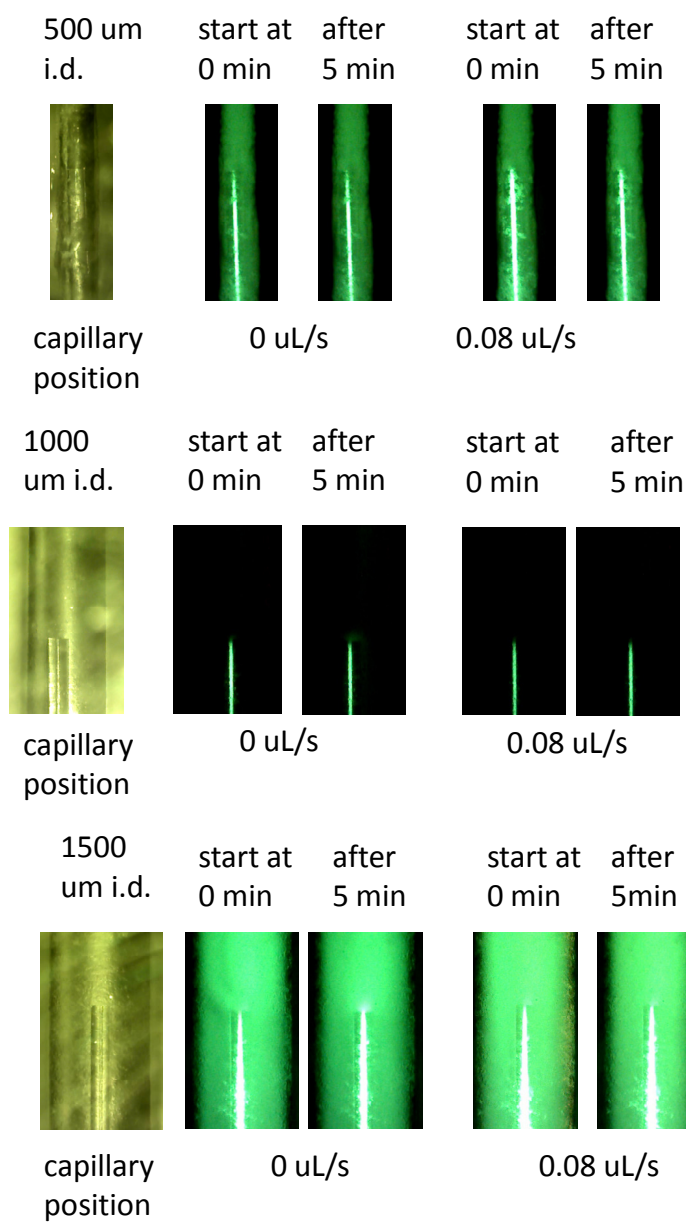


Figure 3.15 Effect of flow rate on the hydrodynamic sample matrix injection into the separation capillary entrance when using different interfaces. The liquid in the 1000 μm i.d. interface was water. For the 500 μm and 1500 μm i.d interface 250 and 150 $\mu\text{g/L}$ sodiumfluorescein in 0.04 mM Tris-HCl at pH 7.9 were used, respectively.

3.3.2.2 LINEARITY

To study the electrokinetic injection from a continuous sample flow interface a suitable sample concentration had to be chosen. The most suitable sample concentration for each interface was chosen to be within the linear range and to be ten times higher than the lowest concentration that could be noticed as a green color in the image recorded by the fluorescence microscope. For each interface the fluorescence intensity at different sample concentrations was recorded. This was done by filling the interface manually with the desired sample solution. Sample solutions used were diluted in 0.04 mM Tris-HCl adjusted to pH 7.9. The linear ranges and the corresponding calibration curves can be seen in Figure 3.16. The 1500 μm i.d. interface shows the steepest slope of 0.6658 mean intensity units / concentration unit. This is caused by the bigger path length in the 1500 μm channel compared to the smaller interfaces. At concentrations higher than 250 $\mu\text{g/L}$ the mean intensity does not show a linear response to a change in concentration for the 1500 μm i.d. interface. This is because the sample fluorescence intensity is out of the linear range of the used fluorescence microscope. The 1000 μm i.d interface has a smaller pathlength than the 1500 μm i.d. interface and therefore a smaller slope of 0.2263 intensity units / concentration unit. Additionally sample concentrations of up to 375 $\mu\text{g/L}$ are within the linear range due to its smaller pathlength. Due to its shorter pathlength the 500 μm i.d interface is expected to have a slope significantly smaller than the bigger 1000 μm i.d. interface. But the 500 μm i.d interface shows a slope of 0.225 intensity units / concentration unit which is similar to the 1000 μm i.d interface. This was caused by a very rough wall surface of the channel in the 500 μm i.d interface which led to adsorption of dye to the channel wall. This enhanced the fluorescent intensities in the 500 μm i.d interface. For the 1000 and 1500 μm

interface the sample concentration chosen for observing the sample injection was 150 $\mu\text{g/L}$ and for the 500 μm i.d. interface the chosen sample concentration was 250 $\mu\text{g/L}$.

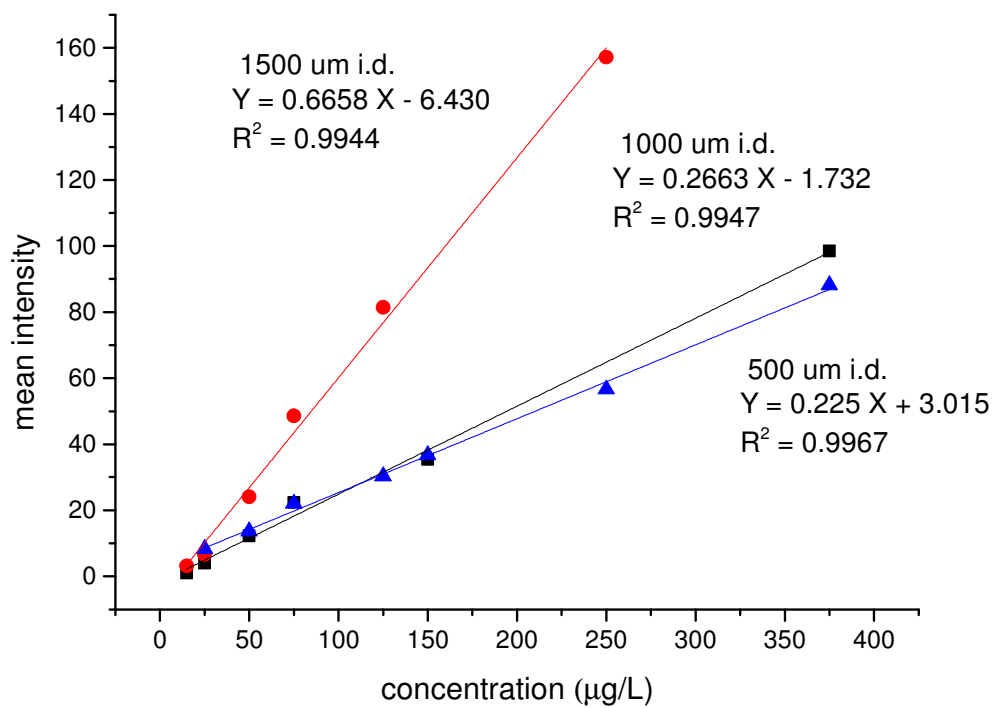


Figure 3.16 Linear ranges of the 500, 1000 and 1500 μm i.d. interfaces. The sample was sodiumfluorescein in 0.04 mM Tris-HCl at pH 7.9 buffer. The linear ranges were 25-375 $\mu\text{g/L}$, 15 -375 $\mu\text{g/L}$ and 15 -250 $\mu\text{g/L}$ for the 500, 1000 and 1500 μm i.d. interfaces, respectively.

3.3.3 DEPLETION FLOW RATE IN THE 1000 μm DIAMETER INTERFACE

In the interest of finding the depletion flow rate as a function of interface diameter the 1000 μm diameter interface is chosen as a starting point. The depletion flow rate in the experimental setup was defined as the flow rate at a given voltage at which $> 90\%$ of all sample ions are being injected. Finding the depletion flow rate requires the determination of the injected sample proportion at different flow rates.

3.3.3.1 INJECTION OF A FLUORESCENT DYE

The interface setup built in Figure 3.10 is expected to allow injection of sample from a flowing sample stream. To check this and to see what phenomena occur during the injection process sodium fluorescein was chosen as a sample which allowed monitoring the injection. At 15 kV the incoming sample stream was expected to be injected and preconcentrated in the separation capillary entrance. At 0 kV in contrast the sample was expected to pass through the interface without injection.

At the beginning of injection the whole interface and the separation capillary are filled with BGE. To perform electrokinetic injection from the flowing sample interface a sample plug was pushed through the BGE filled interface. The voltage and flow rate are turned on at the same time the recording starts. When performing the blank run at 0 kV, which is shown in Figure 3.17, the sample does not get injected and is pushed through the interface towards the waste. When applying a voltage of 15 kV the non-fluorescent BGE is replaced by an incoming plug of fluorescent sample which can be seen in Figure 3.17, 15 kV. As expected, sample ions are injected as the highly conductive BGE is replaced by the lower conductive sample indicating that as expected the electric field strength increases. This can be seen in Figure 3.17, 15 kV where

there is fluorescent sample in the area between the capillary and electrode at 1.5 min. The time was defined as 0 min when the parabolic sample-BGE front reached the separation capillary entrance. At 4.5 min the area between the electrode and the capillary entrance is black since all incoming sample ions are being injected into the capillary. The fluorescence intensity inside the separation capillary also increases over time, which indicates that sample ions are being injected into the capillary. Since the observed injection changes with time it is necessary to investigate the injection as a function of time in more detail.

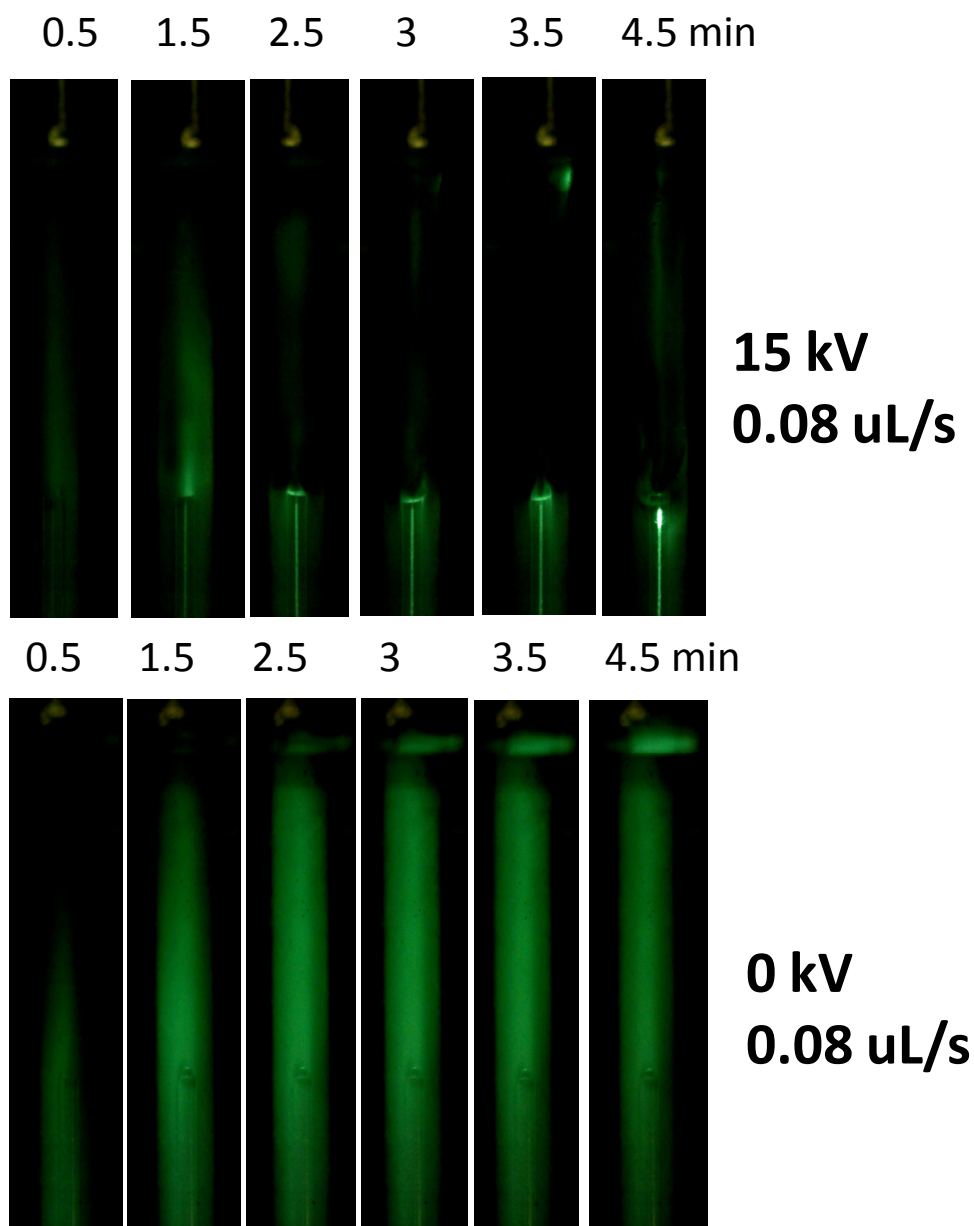


Figure 3.17 Injection of a fluorescent dye at 0 kV and 15 kV at 0.08 $\mu\text{L/s}$ flow rate in the 1000 μm i.d. interface. The sample was sodium fluorescein in 0.04 mM Tris-HCl, pH adjusted to 7.9 with HCl. The BGE was 40 mM Tris-HCl, pH adjusted to 7.9 with HCl. The corresponding recorded intensities can be found in Figure 3.18. The calculated percentage of injected sample amount can be found in Figure 3.19. The time was measured from the moment the sample-BGE front reaches the separation capillary entrance which was set as 0 min.

3.3.3.2 INJECTION AS A FUNCTION OF TIME

In order to better understand the injection process as a function of time the recorded injection of fluorescence sample was quantified.

The area in the fluorescence images that is between the capillary entrance and the electrode (see Figure 3.13) was used for quantification. The mean gray value of the fluorescence emission intensity was determined in the area between capillary and electrode. It is a measure for the sample amount present. For the 15 kV injection the mean gray value was expected to represent the amount of sample that is not being injected and getting lost. For the 0 kV blank injections this should equate to the total amount of sample that is entering the interface.

The recorded intensity for the area in the 15 kV injections (Figure 3.18, 15 kV) is increasing till 1.5 min with the fluorescent sample entering the interface. After 1.5 min the sample starts being injected into the capillary and thus the intensity starts decreasing till 3.5 min. After 3.5 min the intensity increases again slightly since parts of the incoming sample start getting lost and are being pushed through the interface to the waste outlet.

The recorded intensities of the 0 kV blank run are plotted against the injection time in Figure 3.18, 0 kV. The intensity increases till 2.5 min due to the incoming fluorescent sample stream that replaces the BGE in the interface. It reaches a maximum at 2.5 min due to residual amounts of BGE that mix with the incoming sample and cause an increase in fluorescence emission. The intensity is then decreasing from 2.5 min till 7 min since the BGE residues are flushed out of the interface. The change in fluorescence emission caused by mixing with BGE suggests that the ionization state of the sample changes as it gets pushed through the interface. Therefore the blank injection at 0 kV needs to be used as a reference when determining the proportion of injected sample amount in the 15 kV injections.

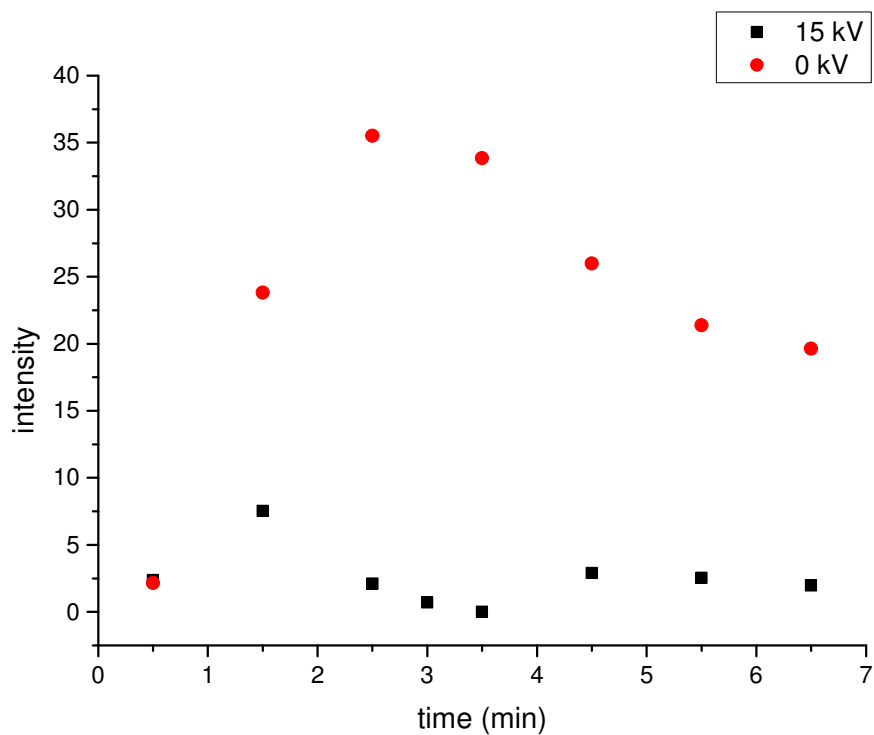


Figure 3.18 Progress of the recorded intensity with time at a 15 kV injection and a blank run at 0 kV, both at 0.08 $\mu\text{L/s}$. The corresponding images and calculated % of injected sample amount can be found in Figure 3.17 and Figure 3.19, respectively. The time was measured from the moment the sample-BGE front reaches the separation capillary entrance which was set as 0 min. Other explanations are in the text.

3.3.3.3 PROPORTION OF INJECTED SAMPLE AMOUNT

Before the depletion flow rate can be determined the proportion of injected sample amount (% injection) as a function of time for the 1000 μm i.d. interface at 0.08 $\mu\text{L/s}$ flow rate needs to be investigated. The findings in 3.3.3.1 suggested that the field strength across the interface increases with time. Therefore the injected sample proportion is expected to increase with longer injection times.

As shown in 3.3.3.2 the blank run at 0 kV needs to be considered when determining the proportion of injected sample. The determination of the injected sample proportion in % injection is explained in 3.3.1.3 in detail. In Figure 3.19 the proportion of injected sample (expressed as % injection) was plotted against the injection time when a flow rate of 0.08 $\mu\text{L/s}$ was used. The injected sample proportion increases within 2.5 min to above 90% and then stays at > 80 % till 6.5 min. Figure 3.17 and Figure 3.18 both show that at around 2.5 min injection time the majority of the BGE in the interface has been replaced with sample. Therefore the extent to which the BGE is being replaced with sample has an influence on the injected sample proportion. A representative value for the proportion of injected sample needs to be determined. Therefore the mean value of the % injection was chosen when the majority of BGE has been replaced by sample which is at 2.5, 3 and 3.5 min. This yielded an average of 97.3% injection (relative standard deviation = 3 %, n = 3) for the 15kV injection from the 1000 μm i.d. interface at 0.08 $\mu\text{L/s}$ flow rate.

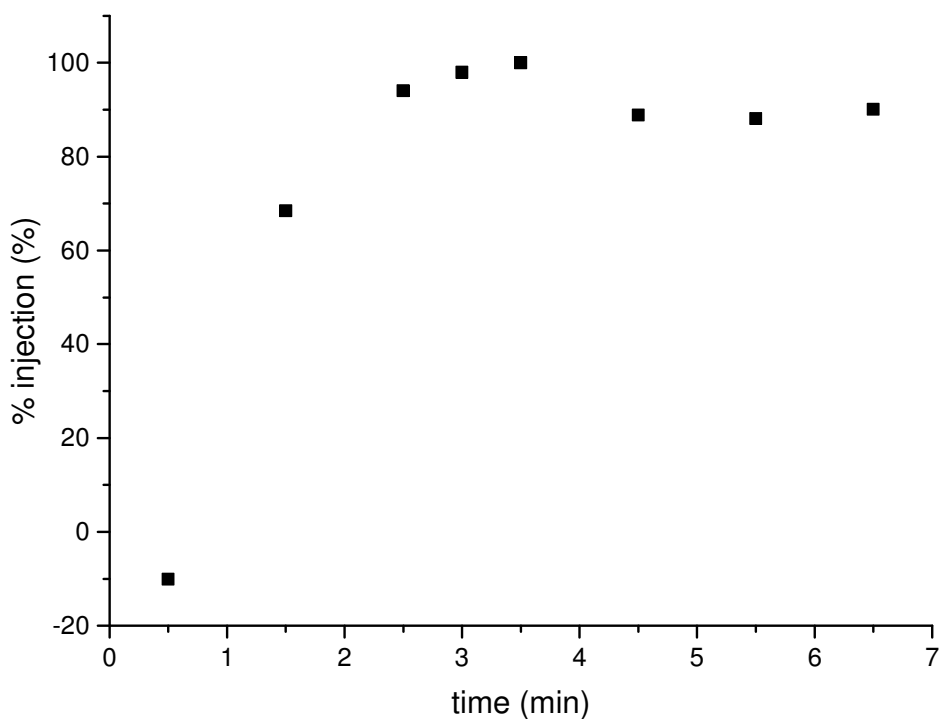


Figure 3.19 Proportion of the incoming sample stream that is being injected into the separation capillary in % injection as a function of injection time at $0.08 \mu\text{L/s}$ in the $1000 \mu\text{m}$ i.d. interface. The time was measured from the moment the sample-BGE front reaches the separation capillary entrance which was set as 0 min.

3.3.3.4 DEPLETION FLOW RATE DETERMINATION

The amount of injected sample as a function of injection voltage and flow rate was already examined in chapter 2. It was shown that a depletion voltage for a given flow rate exists above which the amount of sample injected could not be increased any further. Additionally it could be seen that increasing the flow rate required a higher depletion voltage. Thus the flow rate and the voltage both needed to be increased accordingly in order to inject the entire available sample. Further it showed that at a given applied voltage the proportion of sample injected decreased when higher flow rates were used. In the present setup the applied voltage is kept constant and the % of injected sample is recorded as a function of flow rate. Based on the findings in chapter 2 the % injection is expected to be >90% at flow rates below the depletion flow rate and <90% above the depletion flow rate.

In Figure 3.20 a representative image of the sample being injected at each flow rate is shown in the top, with the proportion of the incoming sample stream that is injected (% injection) plotted against flow rate shown in the bottom. The average % injection is 99.2% (%RSD = 0.891%, n=3) at a flow rate of 0.04 $\mu\text{L/s}$ and 94.7% (%RSD=3.11%, n=3) at 0.06 $\mu\text{L/s}$. This means that the total applied voltage of 15 kV is above the depletion voltage for the flow rates of 0.04 and 0.06 $\mu\text{L/s}$ according to the findings in chapter 2. The depletion flow rate was determined as 0.08 $\mu\text{L/s}$ where 97.3% were injected (%RSD= 3.03, n=3) for the 1000 μm i.d. interface. As expected past the depletion flow rate the average % injection decreased to 72.3% (%RSD = 3.31%, n = 3) at 0.12 $\mu\text{L/s}$ and 54.5% (%RSD = 8.56%, n = 3) at 0.16 $\mu\text{L/s}$. This correlates with the findings in chapter 2 which suggest that an increased flow rate would require a higher applied voltage for complete sample injection to happen. To find the % of injection for

each flow rate the average of three % injection values at three different injection times was calculated. The time points were chosen when the majority of BGE was replaced by sample as described in 3.3.3.3. At 0.04 $\mu\text{L/s}$ flow rate the timeframes chosen were 5, 5.5 and 6 min, at 0.06 $\mu\text{L/s}$ 3, 3.5 and 4 min, at 0.08 $\mu\text{L/s}$ 2.5, 3 and 3.5 min and at 0.12 $\mu\text{L/s}$ 1.5, 2 and 2.5 min. The time it takes to replace the majority of the BGE with sample is decreasing with higher flow rates. This stands in agreement with the findings in 3.3.3.3 that the flow rate determines the exchange of BGE with sample.

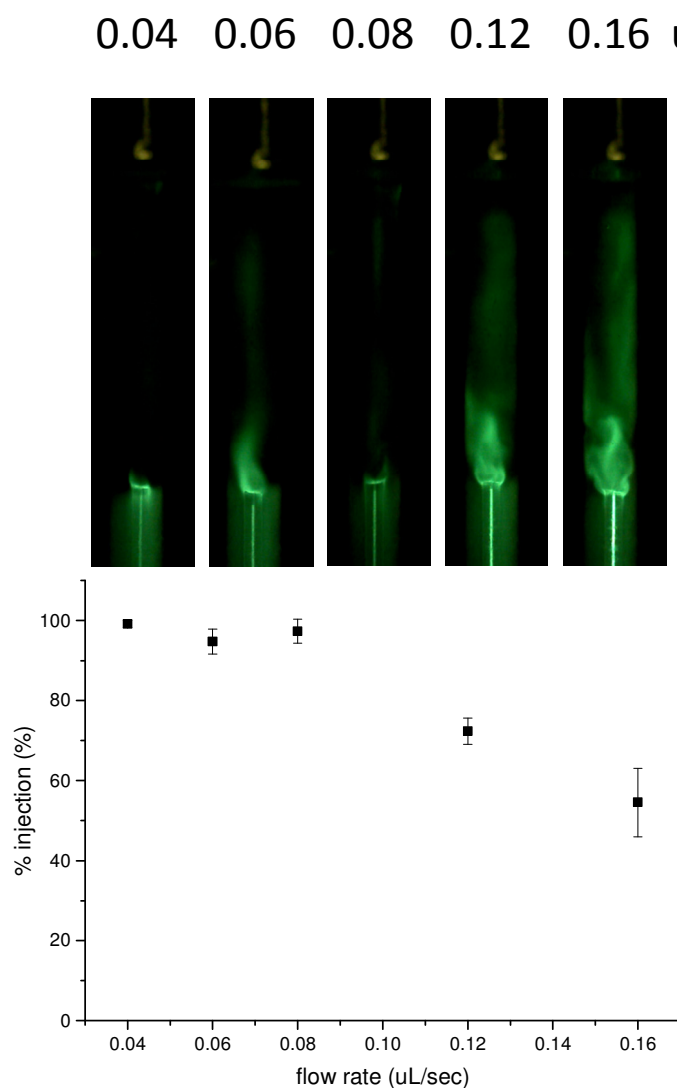


Figure 3.20 Determination of depletion flow rate from proportion of injected sample (in % injection) as a function of flow rate in a $1000 \mu\text{m}$ i.d. interface. The images are representative for the injection at the given flow rate. The time was measured from the moment the sample-BGE front reaches the separation capillary entrance which was set as 0 min.

The question is if a higher depletion flow rate can be achieved by using different interface diameters. The mathematical model predictions in paragraph 3.2.3.1 used the parameters of the experimental setup: $U = 15$ kV, $k = 400$, $L_{intf} = 5$ mm, $\mu(\text{fluorescein}) = 23 \cdot 10^{-9}$ m²/Vs [9], $L_{cap} = 32.6$ cm, $d = 50$ μm . It predicted that the depletion flow rate reaches a maximum at 1100 μm as shown in Figure 3.4. In the experimental setup only three different interface diameters of $D = 500, 1000$ and 1500 μm have been used. The depletion flow rates have been calculated for these three i.d's using the mathematical model and the result is shown in Figure 3.21. The mathematical model predicts that the depletion flow rate increases slightly from 0.78 $\mu\text{L/s}$ at 500 μm to 0.81 $\mu\text{L/s}$ at 1000 μm . When the interface diameter is increased from 1000 to 1500 μm the depletion flow rate decreases to 0.8074 $\mu\text{L/s}$. This is a change of around 4 % in depletion flow rate when changing the interface diameter from 500 to 1500 μm . Therefore changing the interface diameter is expected to have only a minor influence on the depletion flow rate.

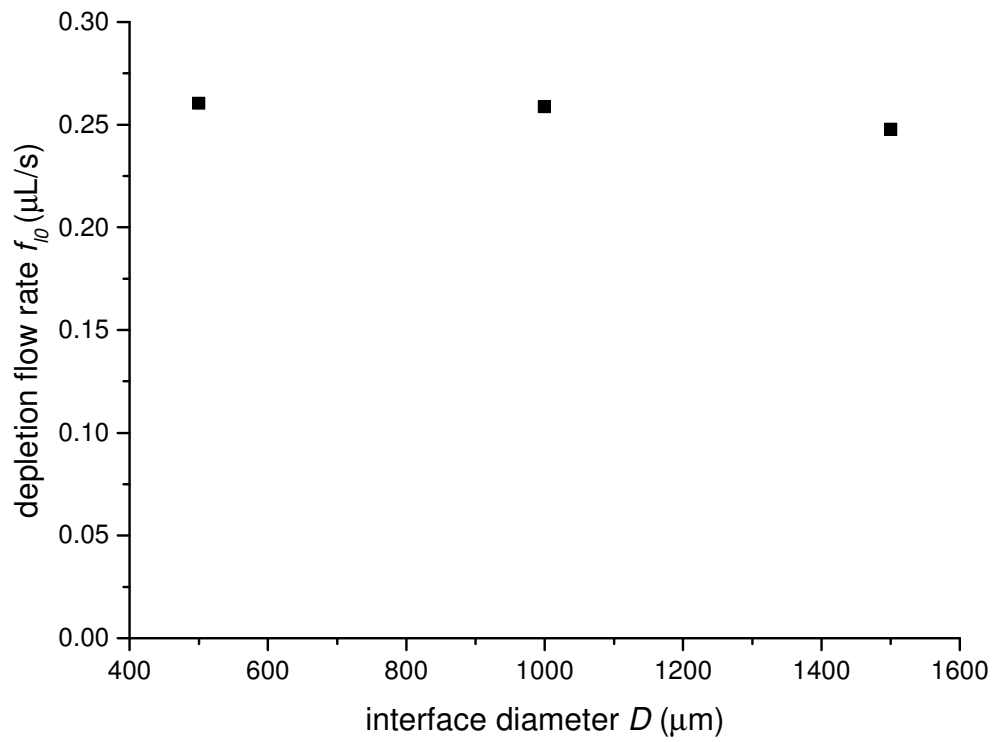


Figure 3.21 Mathematical model predictions for the relation between interface diameter and depletion flow rate at interface diameters of 500, 1000 and 1500 μm .

3.3.4 DEPLETION FLOW RATE IN A 1500 μm DIAMETER INTERFACE

When injecting from 1500 μm i.d. interface the trend for % injection vs. flow rate is expected to look similar to Figure 3.20. The only difference being that the depletion flow rate is expected to be lower than the 0.08 $\mu\text{L/s}$ from the 1000 μm i.d interface. The mathematical model predicts a <1 % decrease in depletion flow rate when performing injections from a bigger 1500 μm i.d. interface.

The depletion flow rate is determined as described in 3.3.3.4. from the % injection vs. flow rate plot as the maximum flow rate at which > 90% sample injection occurs. Injections at 15 kV from a 1500 μm i.d. interface were performed at flow rates of 0.01, 0.02, 0.04 and 0.08 $\mu\text{L/s}$. Unfortunately electrolysis bubbles started to form before stable stacking conditions could be reached within 30 min of injection time for the 0.01, 0.02 and 0.04 $\mu\text{L/s}$ injection. Therefore it was not possible to get a representative % injection value at 0.01, 0.02 and 0.04 $\mu\text{L/s}$. When injecting at 15 kV from a sample stream that flows at 0.08 $\mu\text{L/s}$ stable injection conditions could be reached within the 30 min injection time and yielded 27.3% injection (%RSD = 3.97%, n=3). The three timepoints chosen to determine the % injection were 30, 30.5 and 31 min. Due to the lack of injections at different flow rates no depletion flow rate could be determined. Despite this a comparison between the injection at 0.08 $\mu\text{L/s}$ in the 1000 and 1500 μm i.d. interface can be made. The mathematical model suggests that the depletion flow rate in the 1500 μm interface should be insignificantly lower than 0.08 $\mu\text{L/s}$. This would mean that in the 1500 μm i.d. interface at 0.08 $\mu\text{L/s}$ the % injection should lower than 97.3%, which is the % injection at the depletion flow rate in the 1000 μm i.d. interface. This is based on the assumption that the % injection vs flow rate trend for the 1500 μm i.d. interface follows the same trend as Figure 3.20.

As expected 27.3% injection for the 1500 μm i.d. interface is lower than 97.3% injection (%RSD= 3.03, n=3) in the 1000 μm i.d. interface.

To investigate the bubble formation at lower flow rates in the 1500 μm i.d interface a comparison of injections between the 0.01 $\mu\text{L/s}$ and 0.08 $\mu\text{L/s}$ injection was made (see Figure 3.22). At 0.08 $\mu\text{L/s}$ the injection starts to happen visibly after 10 min. At the slower flow rate of 0.01 $\mu\text{L/s}$ bubbles obstruct the interface before the injection starts to happen. Based on the results in Figure 3.19 the progress of injection and the time it takes to reach stable stacking conditions depends on the extent at which the BGE has been replaced by the sample plug. The majority of the BGE in the interface needs to be replaced for the injection to reach stable stacking conditions. The replacement of BGE with sample in the 1500 μm i.d. interface was observed by pushing the fluorescent sample plug through the BGE filled interface without applying voltage. The change in fluorescent intensity with time was recorded over a defined area between the electrode and capillary inlet (see **Error! Reference source not found.** for details) as shown in Figure 3.23. It can be seen that for the 0.08 $\mu\text{L/s}$ run at 0 kV in a 1500 μm i.d. interface it takes around 10 min to reach the maximum fluorescent intensity which is also when the injection starts in Figure 3.22. At the slow flow rate of 0.01 $\mu\text{L/s}$ the maximum was not reached within the recorded 30 min. Therefore it takes longer than 30 min to replace the majority of BGE with sample for an injection at 0.01 $\mu\text{L/s}$. This leads to bubble formation and does not allow to reach stable stacking conditions.

The next interesting step is to investigate the injection from a smaller i.d. interface which is expected to reach stable injection conditions earlier.

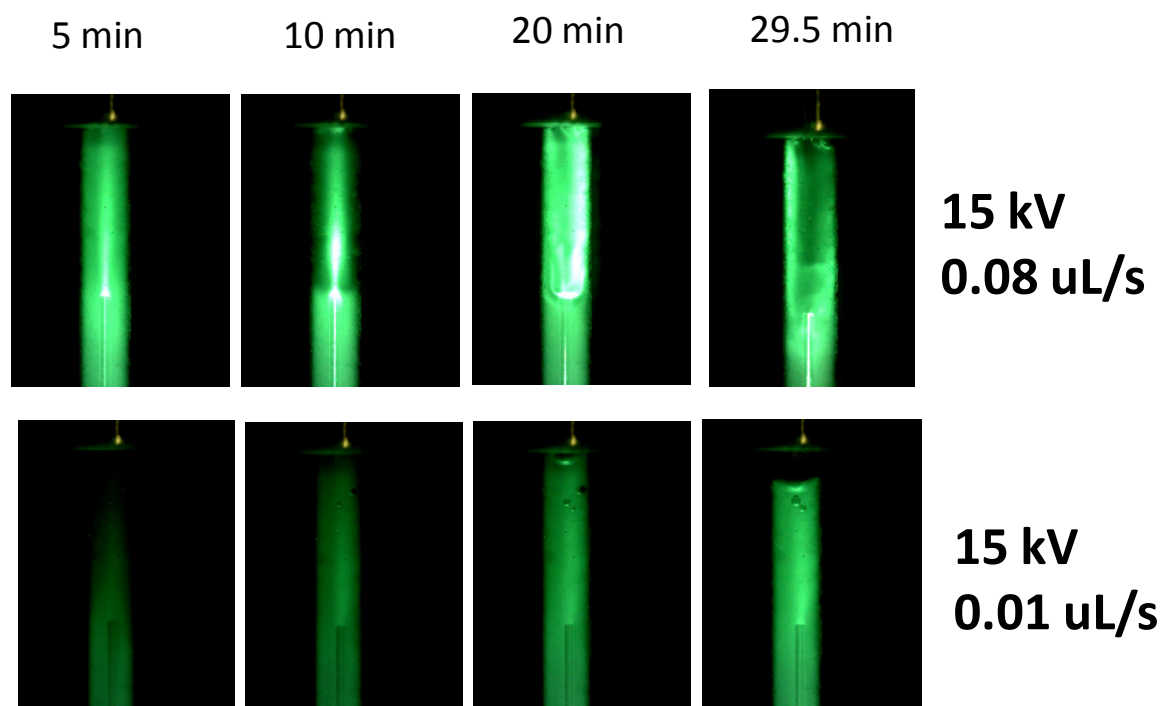


Figure 3.22 Comparison of injections at two different flow rates in the 1500 μm i.d. interface. It can be seen that at a faster flow rate of 0.08 $\mu\text{L/s}$ the injection of sample into the capillary takes place within the recorded time frame whereas at the slower flow rate the injection does not happen and an agglomeration of electrolysis bubbles at the electrode obstructs the interface.

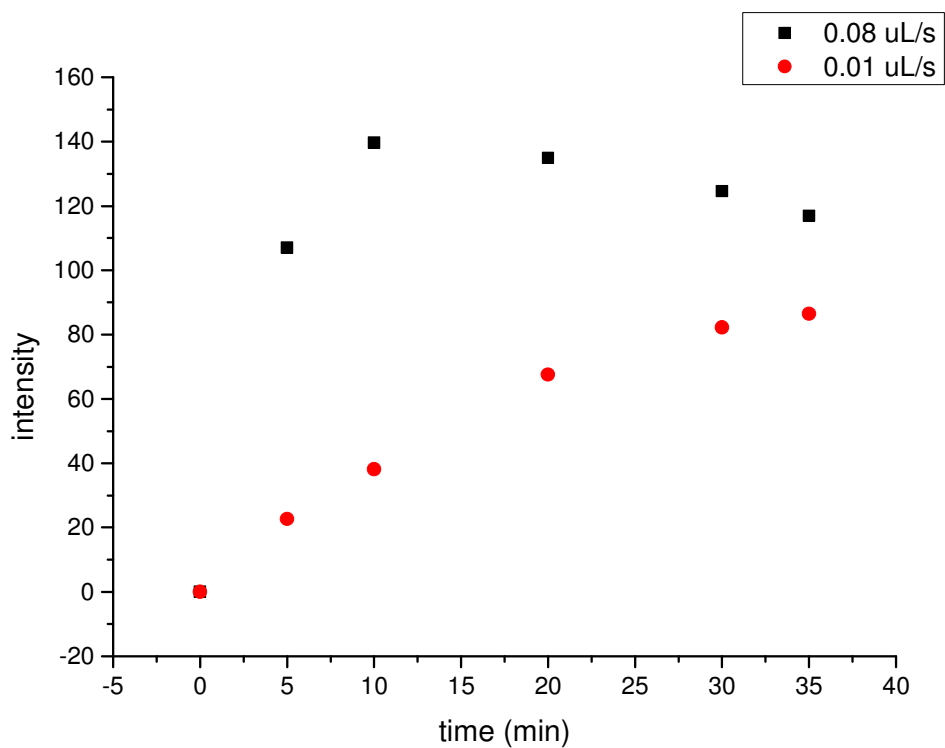


Figure 3.23 Change in intensity over time when the fluorescent sample is pushed through the 1500 μm i.d. interface at 0 kV using a slow and fast flow rate.

3.3.5 DEPLETION FLOW RATE IN A 500 μm DIAMETER INTERFACE

The mathematical model predicts a decrease of around 4 % in depletion flow rate when decreasing the interface diameter from 1000 to 500 μm . Also the time it takes to reach stable stacking conditions is expected to be shorter due to higher linear velocities of the sample liquid. A shorter injection time should prevent a negative impact from electrolysis bubble formation.

Figure 3.24 shows an injection performed at 0.08 $\mu\text{L/s}$ in a 500 μm i.d. interface. When performing an injection at 0.04, 0.12 and 0.16 $\mu\text{L/s}$ the current dropped during the injection to zero before the injection had reached stable conditions. The current interruption was due to bubble formation caused by overheating of the small volume between the electrode and the capillary entrance. The position of bubble formation and aggregation within the interface was not predictable. Due to bubble formation not enough successful injections at different flow rates could be performed in the 500 μm i.d. interface. Therefore it was not possible to determine a depletion flow rate. Only for an injection at 0.08 $\mu\text{L/s}$ stable injection conditions could be reached before heat bubbles caused current interruption. The injection at 0.08 $\mu\text{L/s}$ flow rate allowed 100 % sample injection. This is in contrast to the mathematical model predictions which suggested that the depletion flow rate decreases slightly for smaller i.d. interfaces. This would also mean that the % injection in the 500 μm i.d. interface should be lower than the 97.3 % injection at 0.08 $\mu\text{L/s}$ in the 1000 μm i.d. interface. This can be explained by the fact that bubbles agglomerated during the course of injection around the electrode and obstructed the entire 500 μm wide interface before the injection reached stable conditions. With the interface being obstructed the electric field distribution might be changed. The bubble formation was attributed to heat generation as they appeared throughout the entire interface channel and not only around the electrode as in the case of electrolysis bubbles.

At higher flow rates of 0.12 and 0.16 $\mu\text{L/s}$ heat generated bubbles are expected to be flushed out of the interface. This is expected because of higher hydrodynamic velocities of the sample stream. Despite this it was found that the flow rate could be increased up to 40 $\mu\text{L/s}$ and bubbles attached to the wall could still not be flushed out. This was attributed to the surface roughness of the interface wall caused by the drill that was used to create the interface channel.

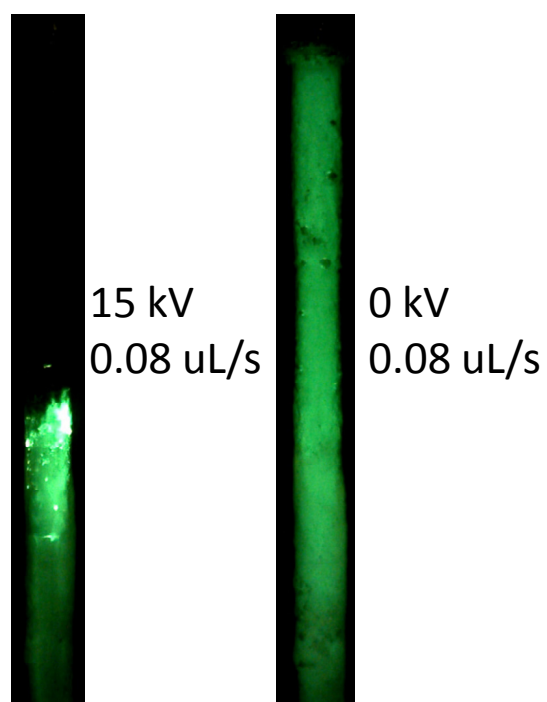


Figure 3.24 Comparison of an injection from a 500 μm i.d. interface at 15 kV and 0.08 $\mu\text{L/s}$ with the blank run at 0 kV. 100 % of all sample ions are being injected into the capillary during the course of injection at 15 kV.

3.3.6 AVOIDING BUBBLE FORMATION

One of the key findings from the above study was that electrolysis and heat generated bubble formation appeared before stable stacking conditions could be reached. Stacking conditions were found to be stable when the majority of the BGE in the interface was exchanged with sample. Shortening the time it takes for the sample to exchange the BGE in the interface is expected to avoid bubble formation.

3.3.6.1 INJECTION WITH A SAMPLE FILLED INTERFACE AS STARTING CONDITION

A possible way to shorten the sample-BGE exchange time is to have sample present in the interface as a starting condition. Then the voltage and flow rate are turned on simultaneously at the time the recording started. This is expected to allow studying the trend of % injection versus flow rate and determining the depletion flow rate even at bigger diameters and low linear velocities. For the smaller i.d. interfaces it is expected to allow injection before the solution starts to overheat and bubble formation appears.

To perform this experiment sample was present in the 1000 μm i.d. interface at the start of the injection. The results in Figure 3.25 show the injection events within the first 180 s for the 0.08 $\mu\text{L/s}$ injection. A bright plug of stacked sample forms in the entrance region of the capillary within the first 2 s. Within 10 s the stacked sample plug moves towards the capillary outlet. When continuing the injection till 180 s no visible injection happened. Experiments at flow rates of 0.04, 0.06, and 0.12 $\mu\text{L/s}$ did not lead to any injection either and the same phenomena could be observed.

With the present approach the stacked zone moved towards the capillary outlet after 10 sec. Based on previous results this usually marked the end of an injection, presumably due to a

reduction in the electric field over the interface due to the liquid in the capillary having a lower conductivity. Injected sample ions replace the chloride ions from the TRIS-HCl buffer which are moving towards the capillary outlet. This creates a low conductivity – high electric field strength zone inside the capillary. Under the influence of the increased field strength the sample plug moves towards the capillary outlet. To stabilize the stacked sample zone in the capillary entrance the formation of a low conductivity zone in the capillary entrance area during injection needs to be prevented.

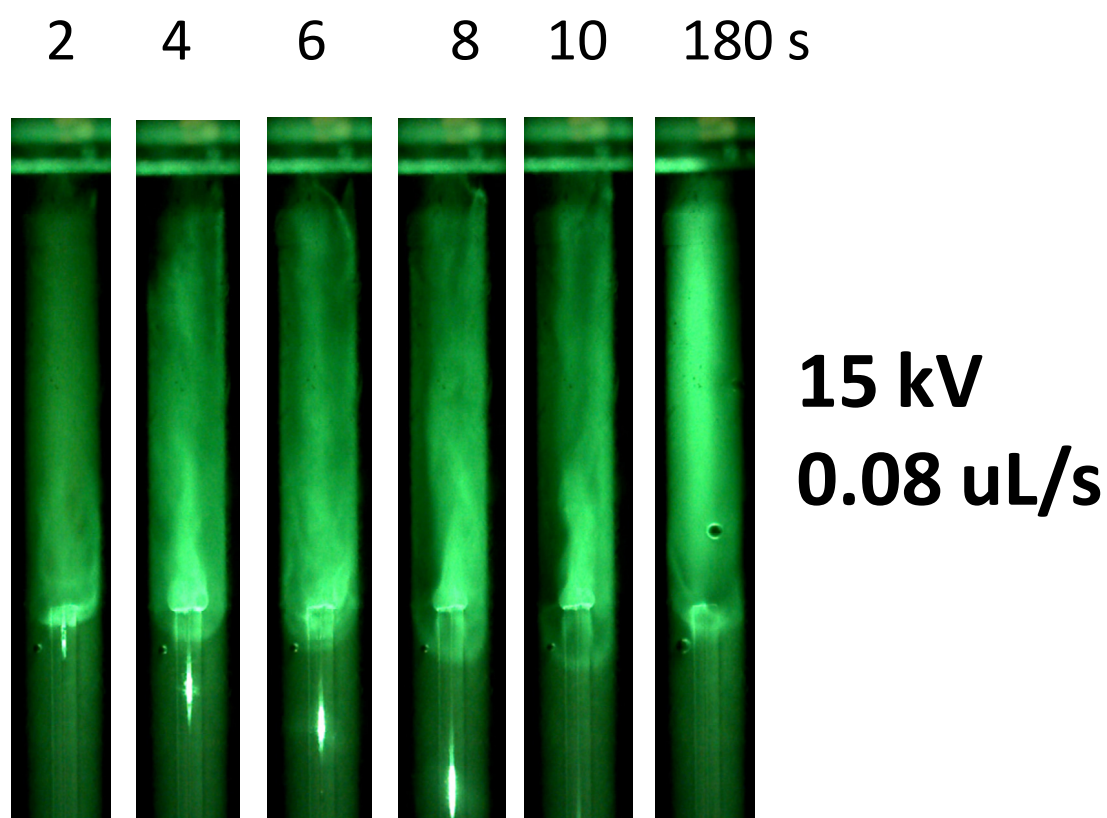


Figure 3.25 Injection with the sample in the 1000 μm i.d. interface as a starting condition. Within 10 s the stacked sample zone moves towards the capillary outlet and prevents further injection. After 180 s no further sample is getting injected; the sample was 150 $\mu\text{g/L}$ sodiumfluorescein in 0.04 mM Tris-HCl; for further explanation see text.

3.3.6.2 INJECTION WITH A HEPES-KOH BUFFER

HEPES was chosen as an anion with lower mobility to replace the fast moving chloride ions. It is expected to increase the timeframe before the low conductivity zone in the capillary entrance prevents further injection.

The results in Figure 3.26 show the injection events within the first 180 s when using a 40 mM HEPES-KOH buffer at pH 7.9 in the capillary and a sample dissolved in 0.04 mM HEPES-KOH buffer at pH 7.9 in the interface. At the start of the injection 15 kV are applied and the sample liquid is moving at 0.08 $\mu\text{L/s}$ through the interface. At 2s bright plug of stacked sample forms outside of the entrance region of the capillary within 10 s. When continuing the injection till 180 s no visible injection of the stacked sample into the capillary happened. A possible reason for stacking outside the entrance could be that the hydrodynamic velocity counterbalances the electrophoretic velocity. This can be easily investigated by performing an experiment with the sample diluents being water. This should allow a bigger voltage drop across the interface and therefore a higher electrophoretic velocity. An experiment with the sample in water resulted in sample stacking outside the capillary without injection into the capillary, too. Further investigations are necessary to find the right combination of BGE and sample diluents to achieve stacking of the sample zone inside the capillary entrance long enough so that the injections can reach stable stacking conditions.

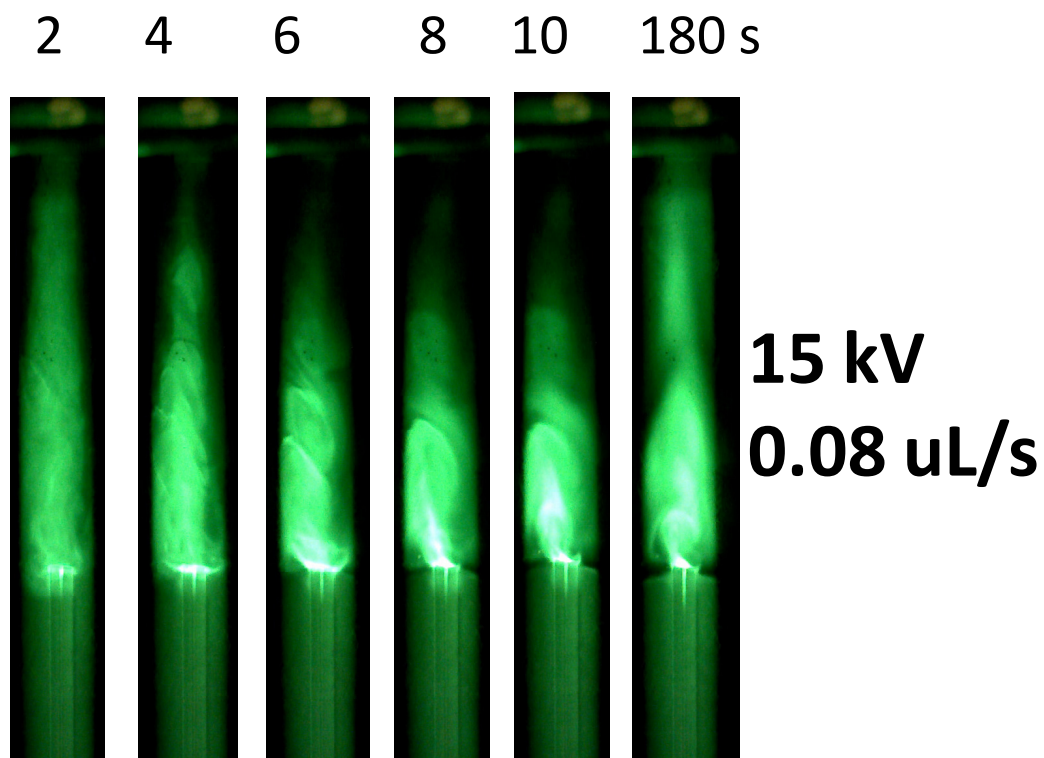


Figure 3.26 Injection with the sample in the 1000 μm i.d. interface as a starting condition and a slower anion in the BGE (40 mM HEPES-KOH, pH adjusted to 7.9). Within 10 s the sample stacks outside the capillary entrance and prevents further injection. After 180 s no further sample is getting injected; the sample was 150 $\mu\text{g/L}$ sodiumfluorescein in 0.04 mM HEPES-KOH; for further explanation see text.

3.4 CONCLUSIONS

Within the present work a set of guidelines for continuous sample flow interface parameters to enhance the sensitivity of electrokinetic injection from a flowing sample stream is proposed. The literature lacks a simple fundamental understanding of the underlying theoretical principles of a continuous flow interface. To address this need a simplified mathematical model was developed and experimentally verified. This model allowed gaining understanding on how the applied voltage, conductivity ratio and the interface and capillary dimensions affect the injection process.

From the results of the mathematical model a few design recommendations could be derived. For a potential application of the continuous flow interface to real samples the sample mobility and matrix will be given factors. The conductivity difference between the sample and the BGE in the capillary will be affected by the stacking system. The distance between the ring electrode and the capillary entrance was found to be of minor importance and should be chosen so that small variations do not affect the depletion flow rate. The capillary length should be as short as practically possible and is limited by the increase in current which could lead to heat generated bubble formation. Knox et al. [10] provide a table on maximum allowed field strengths that allow separation without being negatively affected by Joule heating under several operating conditions.

The applied voltage should be chosen as high as possible without the formation of bubbles due to overheating. The mathematical model predicted that the capillary inner diameter should be as big as possible to enhance the depletion flow rate. Certainly this has practical limitations such as bubble formation caused by an increase in current. The mathematical model is able to provide a range for the interface diameter and length that leads to a depletion flow rate that is above 95 % of its maximum. The presented design recommendations and guidelines on how to choose the

interface parameters are a set of intuitive rules that can be applied to a variety of interface designs. The developed mathematical model is specifically derived for the used interface geometry. Despite this the simple principles used for developing the model can be easily adjusted and applied to different interface setups. We anticipate that the present work will enable the reader to easily adapt the mathematical model to their own needs. In an experimental setup bubble formation due to overheating and electrolysis of sample solutions can be a limiting factor. Despite all derived guidelines and rules the practical limitations will be the ultimate governing factors that direct the interface design. These presented ideas should be seen as a rough guideline that aid in interface design. They can be used in the planning stage when developing a continuous sample flow interface. Experiments and laboratory testing together with the presented rules will enable a directed and efficient approach for interface design.

In the experimental part the aim was to investigate how the interface diameter can increase the depletion flow rate. Three different interfaces with 500, 1000 and 1500 μm i.d. were built and the injection process was monitored using a fluorescent sample. The mathematical model predicted a less than 4 % change in depletion flow rate when increasing the interface diameter from 500 to 1500 μm . These predictions were experimentally investigated by attempting to determine the depletion flow rate at each diameter. In the 1000 μm i.d. interface the depletion flow rate was determined as 0.08 $\mu\text{L/s}$. In the 1500 μm i.d. interface electrolysis bubbles and in the 500 μm i.d. interface heat generated bubbles appeared before stable stacking conditions could be reached. This prevented the determination of a depletion flow rate. Therefore it was necessary to reach stable stacking conditions earlier. Therefore the sample was placed in the interface at the start of the injection. This caused the stacked sample zone to move towards the capillary outlet within the first 10 s of injection. To stabilize the stacked sample zone the slower anion HEPES was

chosen which led to the opposite effect. The sample stacked outside the capillary entrance and did not enter the capillary entrance. To verify the mathematical model experimentally it is necessary to find a suitable stacking mechanism. It needs to allow a stable stacking zone at the capillary entrance for long enough so that the depletion flow rate can be determined for different interface i.d's. This could be achieved by using a different type of anion with a suitable mobility that lies between the mobility of Chloride and HEPES.

Another interesting aspect is how the injection voltage is affected by a change in sample matrix. This might require optimization of the interface for the slowest occurring electrophoretic velocity. Near quantitative electrokinetic injection without mobility bias will be achieved when optimizing the presented interface for a set of analytes and matrix conditions. The anticipation is that the correct interface geometry combined with suitable stacking methods will lead to improvements for a variety of existing stacking techniques.

3.5 REFERENCES

- [1] A.A. Alhusban, A.J. Gaudry, M.C. Breadmore, N. Gueven, R.M. Guijt, *J. Chromatogr. A* 1323 (2014) 157.
- [2] G.A. Blanco, Y.H. Nai, E.F. Hilder, R.A. Shellie, G.W. Dicoski, P.R. Haddad, M.C. Breadmore, *Anal. Chem.* 83 (2011) 9068.
- [3] L.Y. Fan, H.L. Chen, X.G. Chen, Z.D. Hu, *J. Sep. Sci.* 26 (2003) 1376.
- [4] J. Samskog, S.K. Bergström, M. Jönsson, O. Klett, M. Wetterhall, K.E. Markides, *Electrophoresis* 24 (2003) 1723.
- [5] B. Santos, B.M. Simonet, B. Lendl, A. Ríos, M. Valcárcel, *J. Chromatogr. A* 1127 (2006) 278.
- [6] N. Teshima, T. Hino, T. Sakai, *Anal. Sci.* 23 (2007) 751.
- [7] D.D. Wang, F. Li, X.P. Yan, *J. Chromatogr. A* 1117 (2006) 246.
- [8] A. Wuethrich, P.R. Haddad, J.P. Quirino, *Analyst* 139 (2014) 3722.
- [9] D. Milanova, R.D. Chambers, S.S. Bahga, J.G. Santiago, *Electrophoresis* 32 (2011) 3286.
- [10] J.H. Knox, *Chromatographia* 26 (1988) 329.

Chapter 4

COMPUTATIONAL FLUID DYNAMICS MODEL OF THE CONTINUOUS FLOW INTERFACE

4.1 INTRODUCTION

In chapter three a mathematical model was derived to gain a deeper understanding of the fundamental principles that determine the depletion flow rate f_{l0} for complete injection. The mathematical model is a simplification that allows prediction of trends and provides a guideline on which parameters to choose. It does not take into account the exact electric field line distribution and it does not take into account the parabolic flow of sample through the interface. In order to get a more accurate prediction of trends and better guidelines for interface development a simulation model has been developed. Hirokawa et al. [1] extensively used simulations to increase the injected sample amount. His group studied different electrode to capillary setups in static sample vials which was discussed in chapter 1. Despite this no systematic study of the effect of interface parameters on the injection in a continuous flow interface was undertaken.

In the chapter which follows, a simulation model that was based on the interface design used in the experimental part in chapter 3 is discussed. It is demonstrated that the concentration profiles across the interface outlet in a 5 kV and a 0 kV blank injection can be used to calculate the proportion of the injected sample stream. Different flow rates were simulated to determine

the depletion flow f_{i0} rate for the sample injection in a 2.5 mm i.d. interface. Simulations at different interface diameters were used to study the change in depletion flow rate with different interface i.d.'s. The simulation model results were verified using the mathematical model developed in chapter 3. Significant differences between the simulation and mathematical model predictions are demonstrated. The possible reason for the observed differences was attributed to unexpected stacking at the capillary entrance without a conductivity discontinuity in the simulation model. Stacking at the capillary entrance without a conductivity discontinuity could be experimentally verified. A mechanism for the unexpected stacking phenomena is proposed which presents an exciting direction in the field of stacking from a continuous sample flow interface.

4.2 COMPUTATIONAL FLUID DYNAMICS MODEL

In the simulation model some simplifications had to be made to allow reasonable computational times and allow the simulation to converge to a stable solution. This means that the simulation model parameters differ from the experimental parameters. The multiphysics software COMSOL (version 4.3b) was used to simulate and explain how the interface diameter affects the injected sample amount. The governing equations were a variation of the Navier Stokes equation and the Nernst-Planck equation. At the start of each simulation the interface was filled with BGE which was then exchanged with the incoming sample at a tenfold lower concentration to simulate FASI conditions. The interface length was chosen so that the capillary entrance and electrode can be accommodated 5 mm apart from each other. The incoming sample stream enters at the bottom of the interface surrounding the capillary and exits the interface in the direction of the ring electrode. The capillary i.d. and o.d. were chosen to be the same as the

capillary used in the experiment. The length chosen was relatively short at 2 mm since a longer capillary requires computational times that would not allow the simulations to be completed in a reasonable time. The simulation model interface diameters were different from the experiments since the simulations did not converge to a stable solution at smaller interface diameters.

Figure 4.1 shows the basic 2D-axisymmetric geometry of the flow interface used in this simulation. The cylindrical flow interface surrounds the capillary. The cylindrical cathodic electrode is located on the wall of the flow cell 5 mm away from the capillary entrance. The simulated sample in the reservoir was iodate (diffusion coefficient set to $1.448 \times 10^{-9} \text{ m}^2/\text{s}$) with a mobility of $56 \times 10^{-9} \text{ m}^2/\text{Vs}$, with an initial concentration of 0.1 mmol/L. The counterion was 0.1 mmol/L sodium (diffusion coefficient set to $1.334 \times 10^{-9} \text{ m}^2/\text{s}$). The interface and capillary were filled with 1 mmol/L sodium nitrate (diffusion coefficient set to $1.902 \times 10^{-9} \text{ m}^2/\text{s}$) at the start of each simulation. The voltage applied was 5000 volts between the anodic end of the capillary end and the electrode. It builds up an electric field between the anodic end of the capillary and the electrode which is displayed in Figure 4.2. The field strength is indicated by the arrow length and the direction of the field lines is indicated by the arrow and its direction. Towards the capillary entrance the electric field line direction points to the capillary entrance which causes the electric field line density to increase. This leads to an increase in electric field strength which is represented by a longer arrow. Despite this the majority of the field lines are parallel and uniform in length in the simulated interface. The EOF was assumed to be zero. The simulation was continued till twice the time it takes to fill the entire interface with sample. The time it takes to fill the interface with sample was calculated from the interface length and the linear velocity of the sample stream. All simulations were carried out on a supercomputer (SGI Altix ICE 8200 Cluster) with an 8 GHz clock.

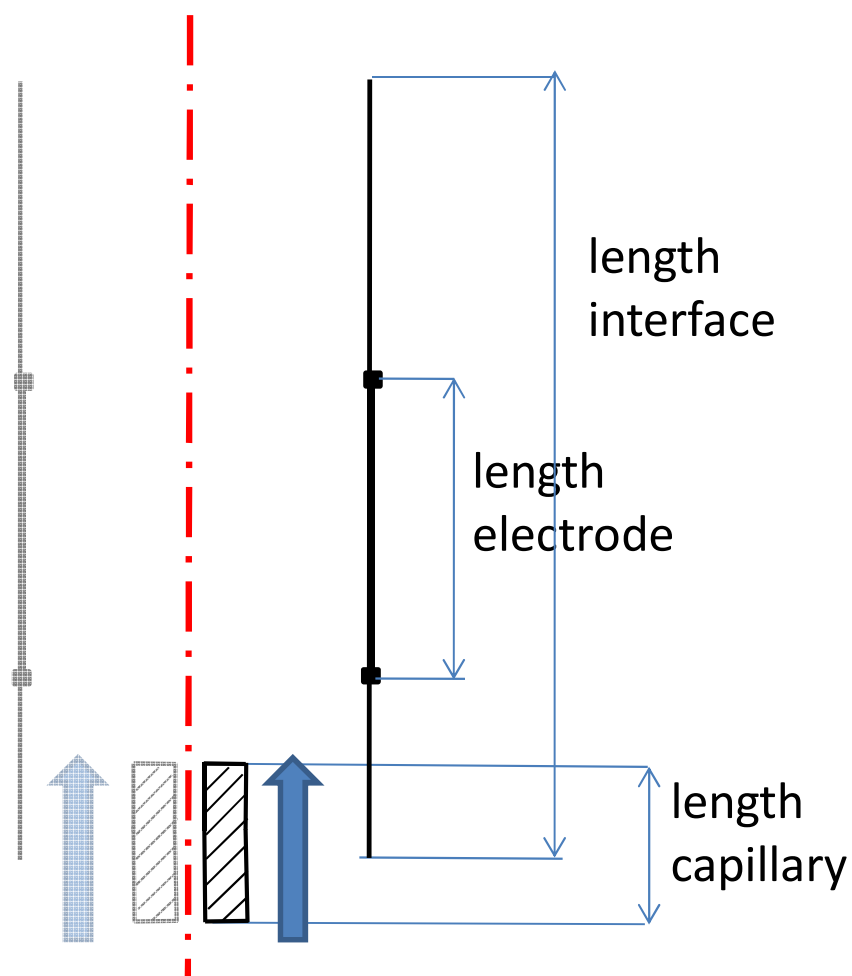


Figure 4.1 Schematic of the continuous sample flow interface used for simulations. The i.d's of the interfaces used for simulation were 2.5 mm, 10 mm, 50 mm and 100mm. The interface length was 12mm, electrode length 500 μm , capillary ID 50 μm , capillary OD 365 μm and the capillary length was 2mm. The blue arrows indicate the direction of the flow of liquid. In the shown image the incoming sample stream is directly injected into the tip of the separation capillary. The electric field is built up by applying a voltage between the ground electrode and the outlet of the capillary. For further explanation, see text.

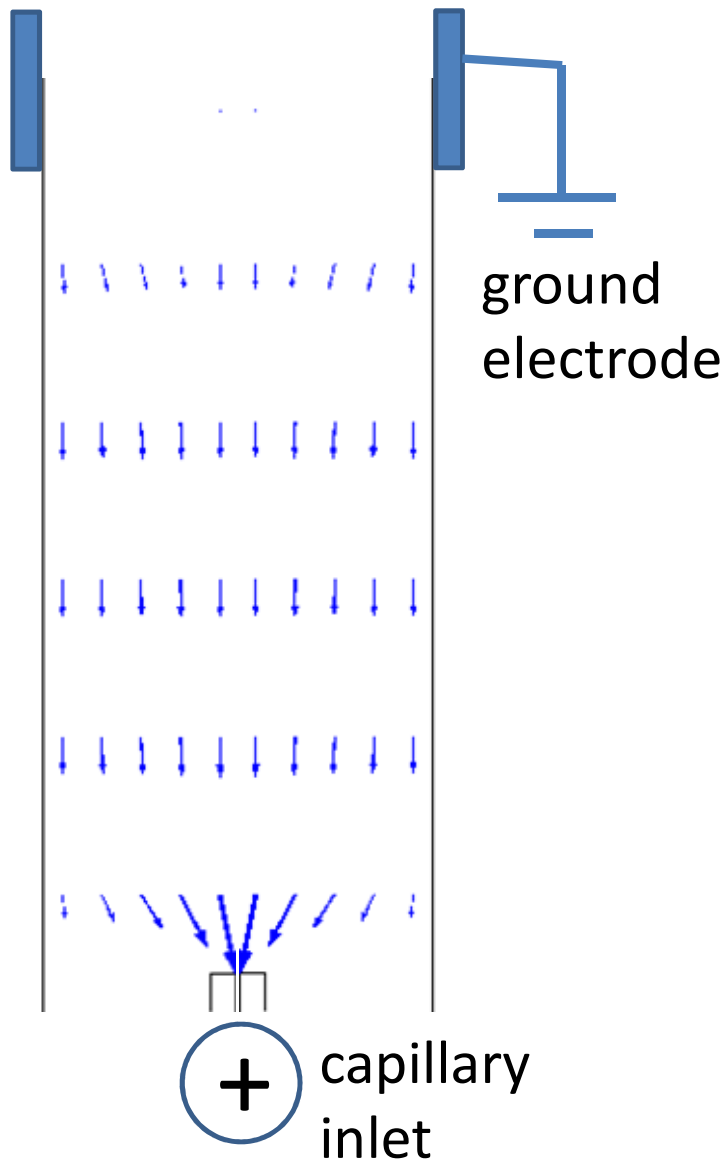


Figure 4.2 Simulation of the electric field distribution in the interface used for simulations. The arrow surface indicates the electric field strength at different points in the interface. Throughout the majority of the interface the electric field strength is uniform which is represented by the arrow length. The field line direction is mostly parallel.

4.3 RESULTS AND DISCUSSION

The mathematical model suggested that the various interface parameters need to be adjusted accordingly to maximize the depletion flow rate f_{10} . The simulation model is expected to provide more accurate guidelines on how the individual interface parameters can maximize the depletion flow rate and sensitivity enhancement.

4.3.1 DEPLETION FLOW RATE f_{10} FOR 2.5 mm INTERFACE DIAMETER

The depletion flow rate f_{10} is the highest flow rate at a given voltage at which > 90 % of the sample is being injected into the separation capillary. In order to find this flow rate in the 2.5 mm inner diameter interface the % of injection at different flow rates need to be determined. 2.5 mm inner diameter was used as the starting interface diameter since for smaller interface diameters the simulation did not converge towards a stable solution.

4.3.1.1 INJECTED SAMPLE PROPORTION

When the sample stream enters the continuous flow interface a certain proportion will be injected into the capillary and the rest should exit the capillary. The concentration of the sample stream that exits the continuous flow interface should therefore be a measure for the injected sample proportion. In this section the injected sample proportion is determined as % injection. To determine the % injection in the simulation concentration profiles were recorded across the interface outlet in the 0 kV blank run and the 5 kV run. Then the area under the concentration profile was determined and used to calculate the % injection. For a 0 kV blank injection the concentration profile across the interface outlet is expected to be equal to the incoming sample concentration of 0.1 mmol/L NaIO₃. The area under the concentration profile for the 5 kV

injection is expected to be lower than the area under the 0 kV concentration profile. This is because part of the incoming sample stream is expected to be injected.

The concentration profile obtained from the simulation in Figure 4.3 shows that at 0 kV the concentration is 0.1 mmol/L across the interface outlet which corresponds to 0 % injection. The corresponding picture above shows the concentration distribution inside the interface channel for the 0 kV injection. It can be seen that the interface is entirely filled with 0.1 mmol/L NaNO₃ since no sample has been injected. When injecting at 5 kV the concentration decreases below 0.1 mmol/L towards the interface wall and increases above 0.1 mmol/L towards the middle of the interface as can be seen from the concentration profile and the corresponding image of the interface channel. Close to the capillary entrance the electric field lines point towards the capillary entrance and increase in magnitude (see Figure 4.2). Since the sample ions will follow the direction of the electric field lines the concentration of sample will increase towards the middle and decrease towards the wall of the interface. Integration of the concentration profile resulted in 23.3 % injection. The % injection was calculated by taking the difference between the integrated area of the 0 kV and the 5 kV concentration profile and expressing it as % of the 0 kV concentration profile using the following formula:

$$\%injection = 100 - 100 \cdot \frac{\text{area_of_cncetration_profile_0kV blank run}}{\text{area_of_cncetration_profile_5kV run}} \quad (4.1)$$

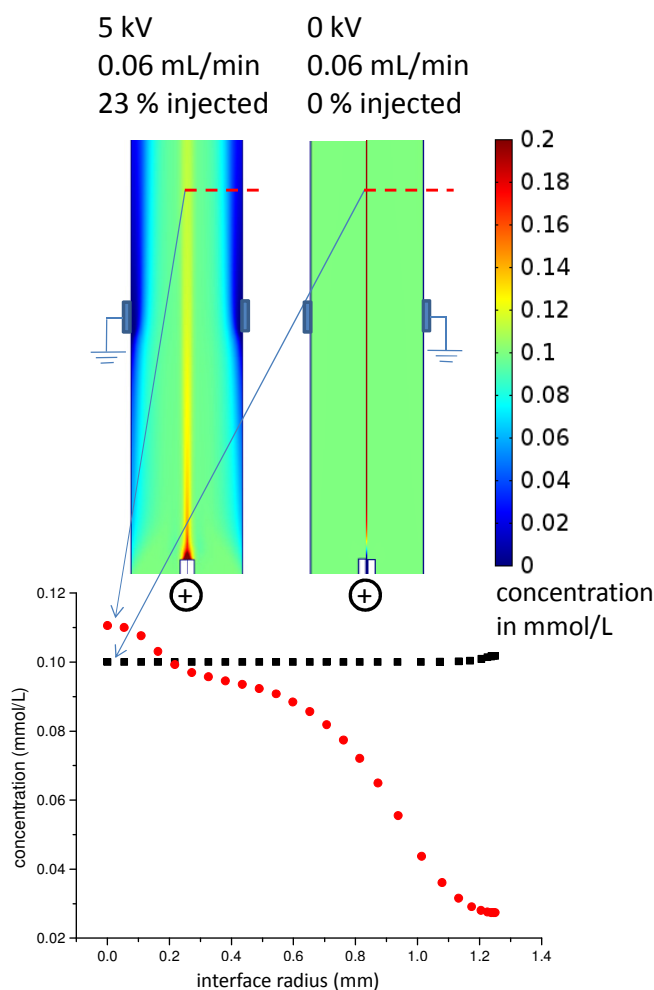


Figure 4.3 Sample concentration profiles recorded along the red dotted line in the top interface images. The concentration was recorded from the interface center at 0 mm to the interface channel wall at 1.25 mm. At 0 kV the interface is filled with the sample at its initial concentration of 0.1 mmol/L which is reflected by the concentration profile and image at 0 kV. At 5 kV part of the sample gets lost which is reflected in the concentration profile at the outlet and the image showing that only 23.3 % sample gets injected. The sample stream enters from the bottom surrounding the capillary. The cathode ring electrode in the interface is grounded and the anode is set to 5 kV at the capillary end. The profiles were recorded at 180 sec which is more than twice the time it takes to fill the interface with sample.

4.3.1.2 DEPLETION FLOW RATE f_{10}

By calculating the % injection for different flow rates in the 2.5 mm i.d. interface the depletion flow rate can be determined. The concentration profiles across the outlet are used to calculate the % injection as described in the previous section. At low flow rates the expected sample ion concentration profile across the outlet should be 0 mmol/L due to 100 % injection. With increasing flow rate the % injection is expected to decrease and the concentration profile across the interface outlet is expected to increase.

Figure 4.4 depicts the concentration profile across the outlet for different flow rates. At low flow rates of 0.02 and 0.1 mL/min the concentration across the outlet is 0 mmol/L since all incoming sample ions are injected. At 0.2 mL/min the concentration in the center of the interface channel is around 0.06 mmol/L and decreases closer to the interface wall to zero. This indicates that part of the incoming sample stream gets lost and is not injected. At the highest flow rate the concentration is around 0.11 mmol/L in the center and decreases to around 0.05 mmol/L at the interface wall.

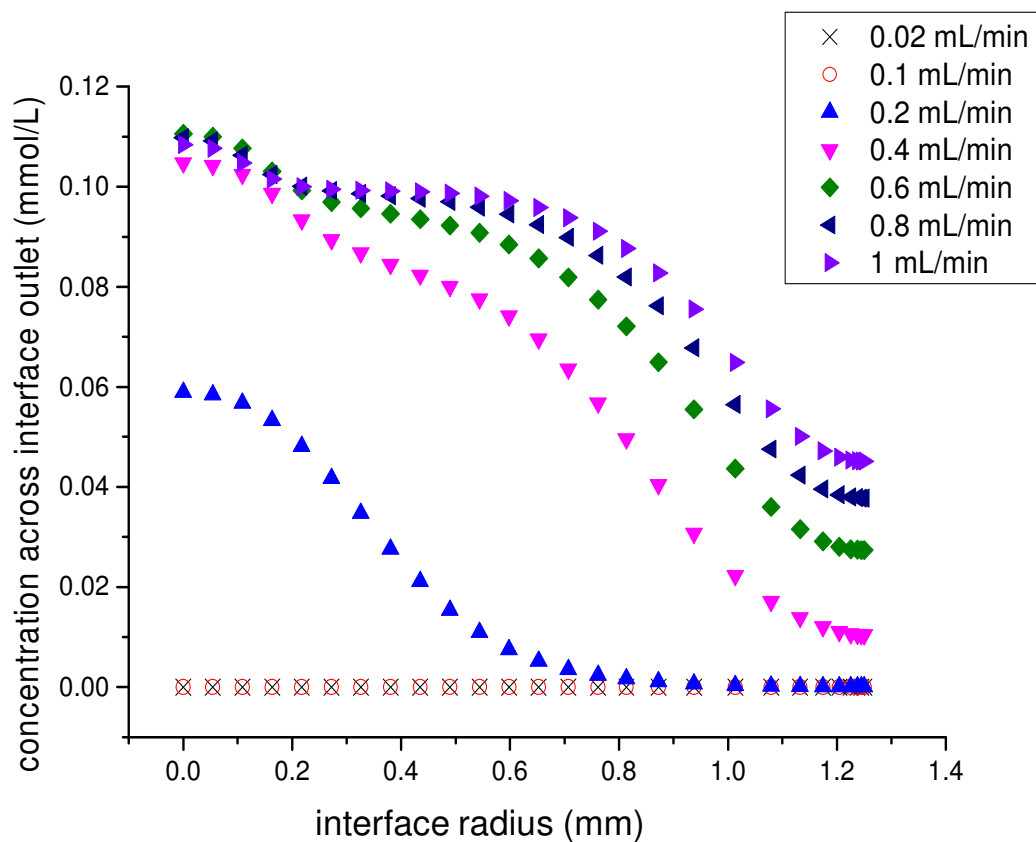


Figure 4.4 Concentration profiles recorded across the interface outlet in the 2.5 mm i.d. interface at a 5 kV injection are shown for different flow rates. The profiles were recorded at 180 sec which is more than twice the time it takes to fill the interface with sample.

The % injections for the different flow rates in Figure 4.4 are determined as described in 4.3.1.1 using equation 4.1. For each flow rate the corresponding concentration profile across the interface outlet of the 0 kV blank run was used. When plotting the % injection vs. the flow rate 100 % injection is expected at low flow rates. This is expected because the electrophoretic velocity of the sample ion is bigger than the linear hydrodynamic velocity at low flow rates. Above the depletion flow rate the % injection is expected to decrease. This is due to the electrophoretic velocity of the sample ion getting smaller than the linear hydrodynamic velocity.

Figure 4.5 shows that the % injection at different flow rates and a corresponding image of the injection above. 100% of all sample is being injected at 0.02 and 0.1 mL/min. At 0.2 mL/min the % injection drops to around 70 % and when doubling the flow rate to 0.4 mL/min less than 50 % are being injected. At 1.0 mL/min all sample ions pass by the capillary without being injected. With 2.5 mm interface i.d. the maximum flow rate at which >90% injection occurs lies in between 0.1 and 0.2 mL/min. Simulations at smaller flow rate increments would be necessary to determine the maximum flow rate at which >90% injection occurs. This would lead to very long simulation times. In order to use the simulation results for design guidelines it was assessed as being sufficient to chose the depletion flow rate as the highest simulated flow rate at which >90% injection occurs from the limited number of simulations. Therefore f_{10} was chosen to be 0.1 mL/min for the 2.5 mm i.d. interface.

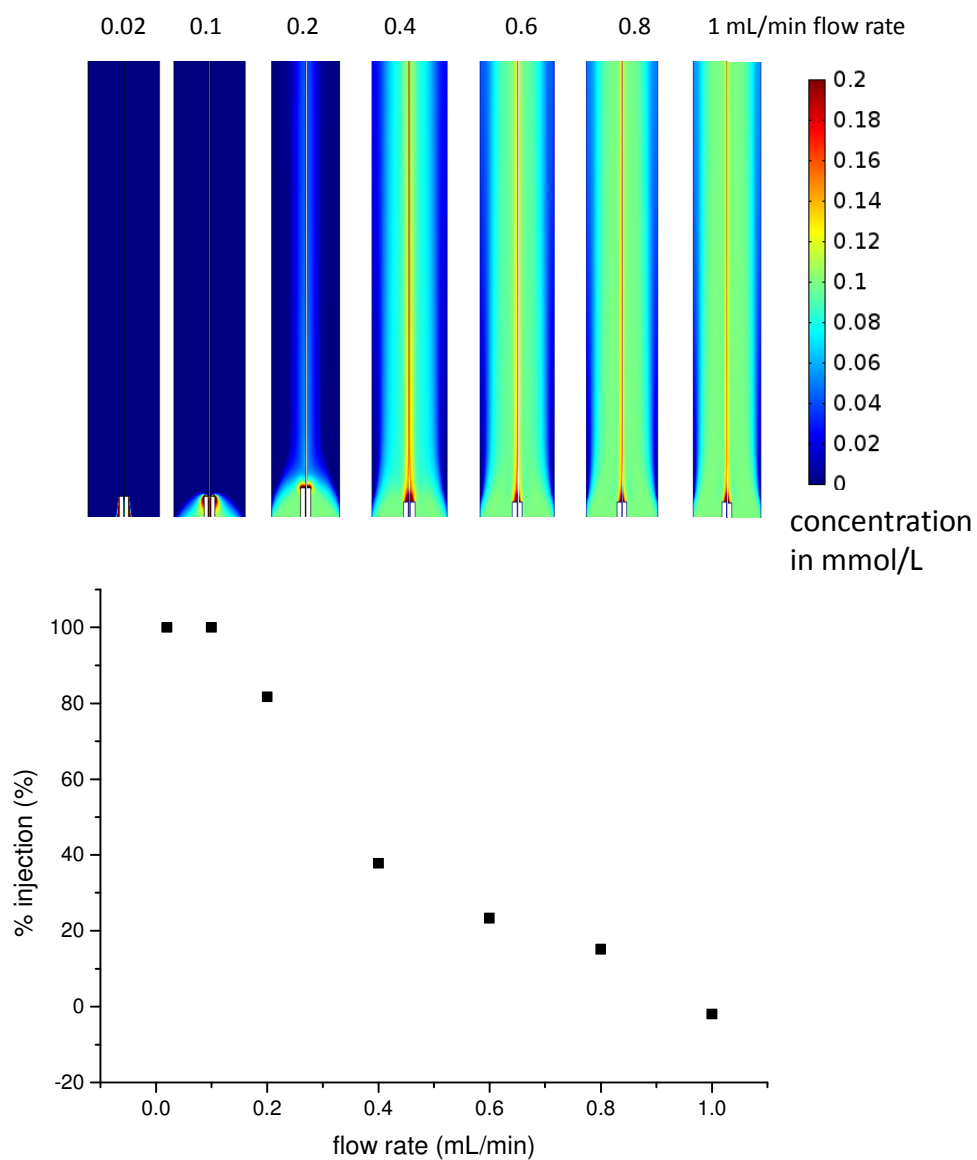


Figure 4.5 % injection as a function of flow rate with corresponding injection pictures in a 2.5 mm i.d. interface at 180 sec. The % injection decreases with flow rate. The sample concentration distribution is illustrated at different flow rates; sample solution, 0.1 mmol/L of IO_3^- ; capillary 50 μm i.d. The inlet flow enters at the bottom, outside the capillary, and leaves at the top of the interface.

4.3.2 MAXIMIZING THE DEPLETION FLOW RATE f_{10}

The mathematical model suggested that the depletion flow rate f_{10} can be maximized when interface and capillary dimensions, conductivity ratio, total applied voltage and sample mobility are changed accordingly. In the simulation model the influence of the interface inner diameter on f_{10} was examined first as this is one of the more complex variables.

To find the depletion flow rate the % injection was plotted against flow rate for the different interface i.d's as can be seen in Figure 4.6. From these graphs the depletion flow rates f_{10} for each interface i.d. were obtained as described in 4.3.1.2. At 2.5 mm, 10 mm, 50 mm and 100 mm interface i.d. the depletion flow rates were 0.1 mL/min, 0.6 mL/min, 1.5 mL/min and 1.75 mL/min, respectively.

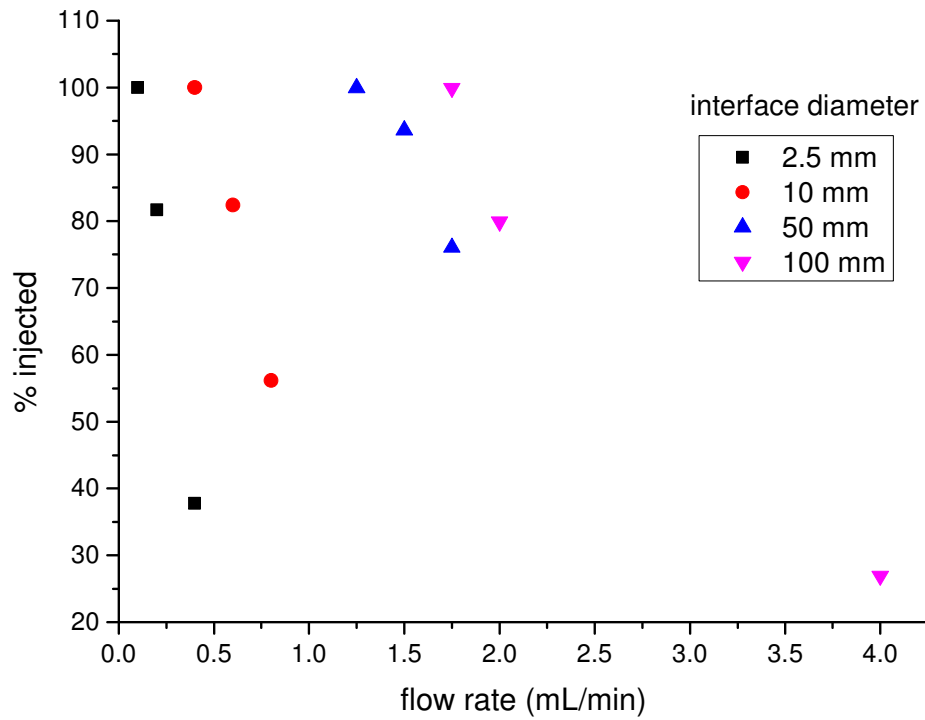


Figure 4.6 Proportion of injected sample amount as a function of flow rate for different interface i.d.'s. Only the flow rates where a transition from >90% to <90% injection is happening are shown.

The obtained depletion flow rates are plotted against the interface i.d. in Figure 4.7. Based on the mathematical model predictions the depletion flow rate is expected to be low at smaller i.d.'s, reach a maximum and then decline again. In contrast the simulation results show that a bigger interface diameter leads to a higher depletion flow rate. The slope at which f_{l_0} rises declines towards the bigger interface i.d.'s. This increase in depletion flow rate with i.d. is counterintuitive and stands in contrast to the trends predicted by the mathematical model. To verify these results a comparison with the mathematical model needs to be performed by using the exact same variables that have been employed in the simulation model.

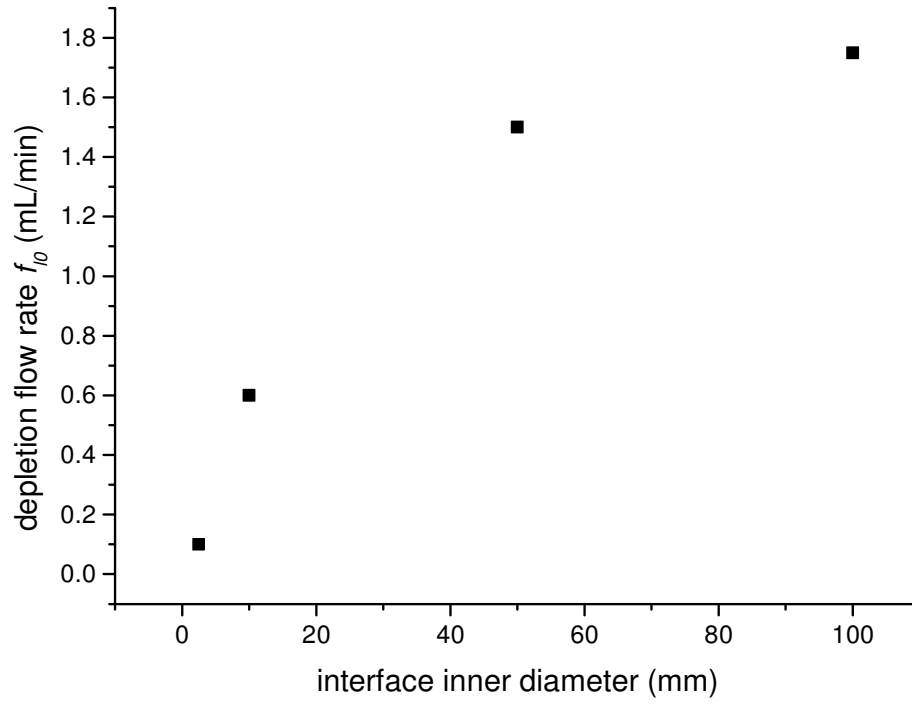


Figure 4.7 Depletion flow rate as a function of interface diameter in the simulation model.

4.3.3 COMPARISON OF THE SIMULATION MODEL WITH THE MATHEMATICAL MODEL

When using the parameters of the simulation model in the mathematical model the same trend for the depletion flow rate f_{l_0} vs. interface i.d. is expected.

Equation 3.19 in chapter 3 was used to plot the depletion flow rate as a function of interface diameter. The following parameters were used: $U = 5$ kV, $k = 11.66$, $L_{inf} = 5$ mm, $L_{cap} = 2$ mm, $d = 50$ μ m, $\mu = 56 \cdot 10^{-9}$ m²/Vs, interface i.d. = 2.5, 10, 50 and 100 mm. k was calculated using equation 3.13 in chapter 3 and the conductivities of the sample and BGE solution. The conductivity of the 0.1 mmol/L NaIO₃ sample solution was $1.06 \cdot 10^{-3}$ S/m and the 1 mmol/L NaNO₃ BGE was $12.4 \cdot 10^{-3}$ S/m. These values were taken from the simulation model. The results in Figure 4.7 show that the mathematical model predicts that the f_{l_0} decreases with bigger interface diameters. This contradicts the simulation model trend. Also the flow rates in the simulations are one order of magnitude larger than in the mathematical model. One possibility could be that the simulation results are not correct. To quantitatively assess the quality of the solution the level of convergence of the solution needs to be considered. It was found that it shows at least 3 to 4 orders of magnitude reduction in the norm of the residual. A grid sensitivity test was not performed since the grid used in the present simulations is already set to be fine and very dense especially around the corners of the capillary entrance. The number of domain elements was 23599. This is a much higher number of mesh elements than what is typically used in electrophoresis simulations [2]. Therefore the mesh number was deemed to be suitable.

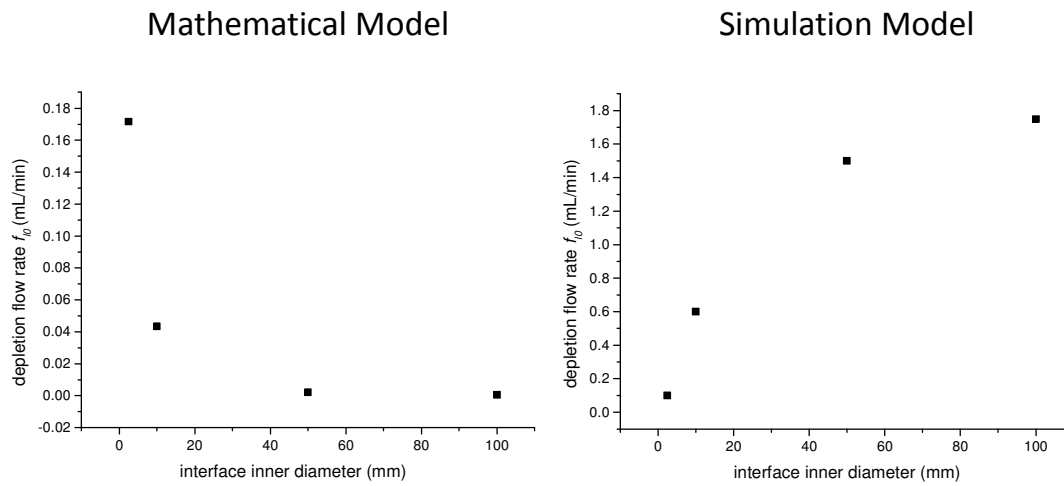


Figure 4.8 Comparison between mathematical model and simulation model predictions. The trends for the depletion flow rate vs. interface diameter are opposite. Also the flow rates in the simulations are one order of magnitude larger than in the simulation model. For further explanation see text.

4.3.3.1 COMPARISON OF THE INJECTION VOLTAGES

In order to understand the differences between the results predicted by simulations and the mathematical model a closer look at the voltage drop over the interface, which is the injection voltage, in both approaches is taken. For the sample ions to be injected the injection voltage needs to be high enough so that the sample ions moves against the flow of liquid into the capillary. Given the higher depletion flow rates in the simulation model for a given diameter it is expected that the simulation model shows a bigger injection voltage than the mathematical model.

To calculate the injection voltage for the mathematical model equation 3.17 in chapter 3, which is based on Ohms law, was used. As can be seen in Figure 4.9 the injection voltage in the mathematical model is predicted to decline exponentially from around 65V at 2.5 mm to around 3 V at 100 mm interface diameter. In contrast the injection voltage obtained from the simulation model shows a slight increase from around 130 V at 2.5 mm to 170 V at 100 mm interface diameter. The simulation model suggests that the voltage drops across the interface is bigger than the ones proposed by the mathematical model. Another significant difference is that the injection voltage is increasing with bigger interface diameters in the simulation model. The voltage drops in the simulation model are influenced by the conductivities that COMSOL uses which therefore need to be investigated.

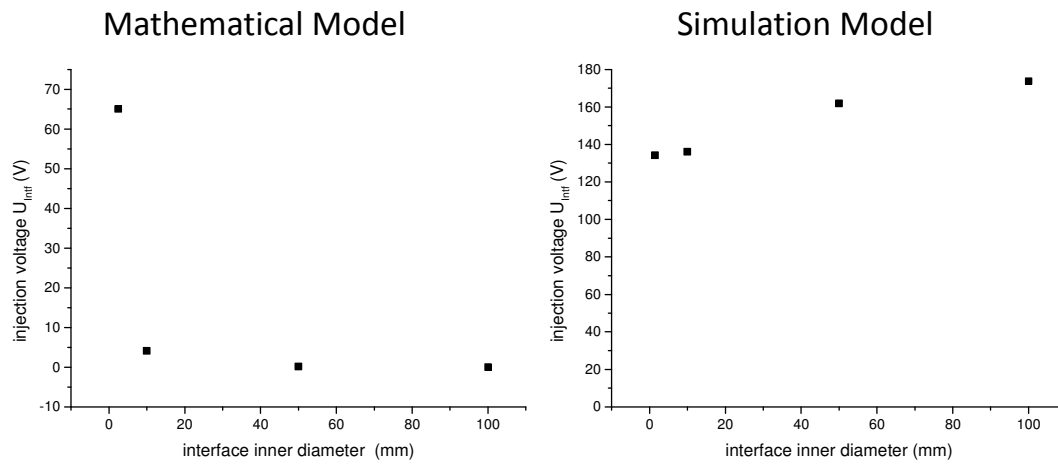


Figure 4.9 Difference in the injection voltage in the mathematical model and the simulation model. The voltage drop over the interface in the simulation was recorded at 0.6 mL/min flow rate for all different interface diameters at 180s, 600s, 15000s and 20000s injection time for the 2.5mm, 10mm, 50 mm and the 100 mm i.d. interface, respectively.

4.3.3.2 CONDUCTIVITY COMPARISON

For the mathematical model it was assumed that the IO_3^- sample ions replace the NO_3^- ions inside the capillary following Kohlrausch's regulating function [3]. This should not alter the conductivity inside the capillary significantly. Therefore in the mathematical model the conductivities were assumed to be given by the 1 mmol/L NaNO_3 BGE in the capillary and the 0.1 mmol/L NaIO_3 sample solution in the interface.

In the simulation model the interface and capillary are filled with 1 mmol/L NaNO_3 BGE at 0 s. The 0.1 mmol/L NaIO_3 sample stream enters at the bottom of the interface moving in the direction of the interface ring electrode. Once the sample stream has reached the capillary entrance the sample injection starts. The differences in injection voltages between the two models suggest that the simulation model injection is not restricted by Kohlrausch's regulating function [3]. Considering Kirchhoff's mesh rule, which is expressed in equation 3.8 in chapter 3, the voltage drop across the interface and the voltage drop across the capillary must be equal to the total applied voltage of 5 kV. An increased injection voltage in the simulation model must therefore result in a decreased voltage drop across the capillary. The voltage drop across the capillary is determined by the conductivity of the solution in the capillary following equation 3.12 in chapter 3. A decreased voltage drop across the capillary suggests that the conductivity of the solution inside the capillary has increased above the initial BGE conductivity of $12.4 \cdot 10^{-3}$ S/m in the simulation model.

This could be confirmed by plotting the conductivities at the capillary entrance area at 0s, 10 s, 30 s and 600 s injection time for a 5 kV injection in the simulation model (see Figure 4.10 5 kV injections). It can be seen that at 0 s the interface and capillary are filled with BGE and the conductivity is 0.0124 S/m. The conductivity increases as expected above its initial concentration

to around 0.2 S/m in the majority of the capillary at 10 s. When looking at a 0 kV injection shown in Figure 4.10 0 kV injections it is clear that at 10 s injection time the sample-BGE front, which is represented by rainbow colored area, has not even reached the capillary entrance. This means that at 10 s injection time there is no conductivity difference between the liquid in capillary and in the interface. Therefore no increase in conductivity should occur according to Kohlrausch's regulating function. Therefore the increased conductivity of around 0.2 S/m in the 5 kV injection at 10 s clearly shows that the concentrations in the simulation model are not regulated by Kohlrausch's regulating function.

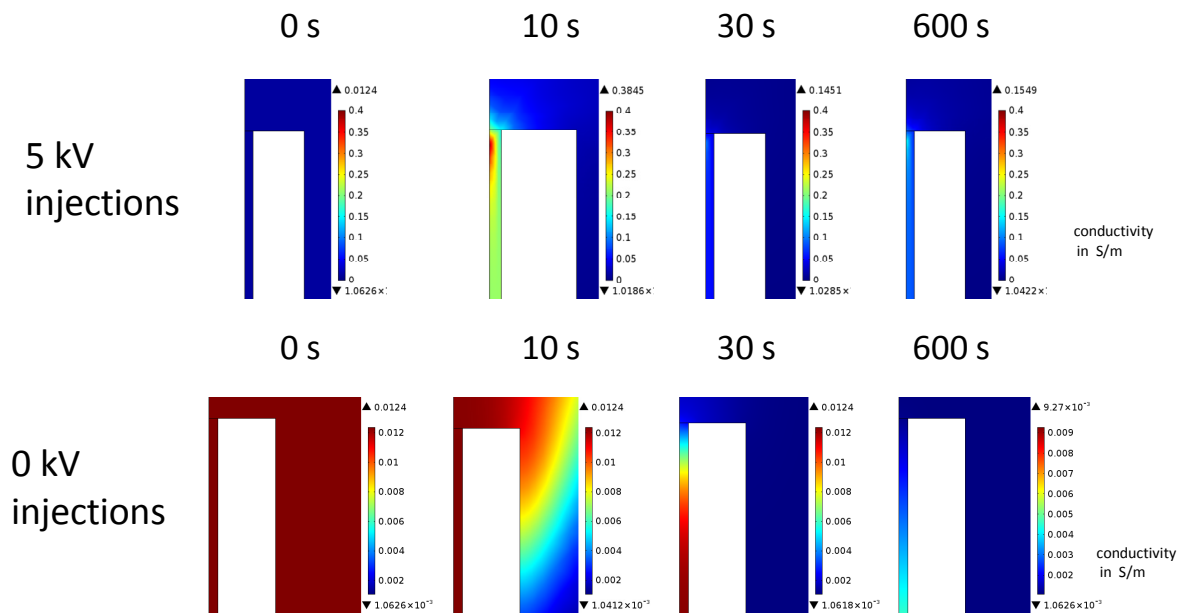


Figure 4.10 Change of conductivity (in S/m) around the capillary entrance area at 0s, 10s, 30s and 600s during a 5 kV injection and a 0 kV injection in the 10 mm i.d. interface at 0.6 mL/min flow rate. The white rectangular area represents the capillary wall. The symmetry axis of the capillary center is on the left side of the images. For further explanation, see text.

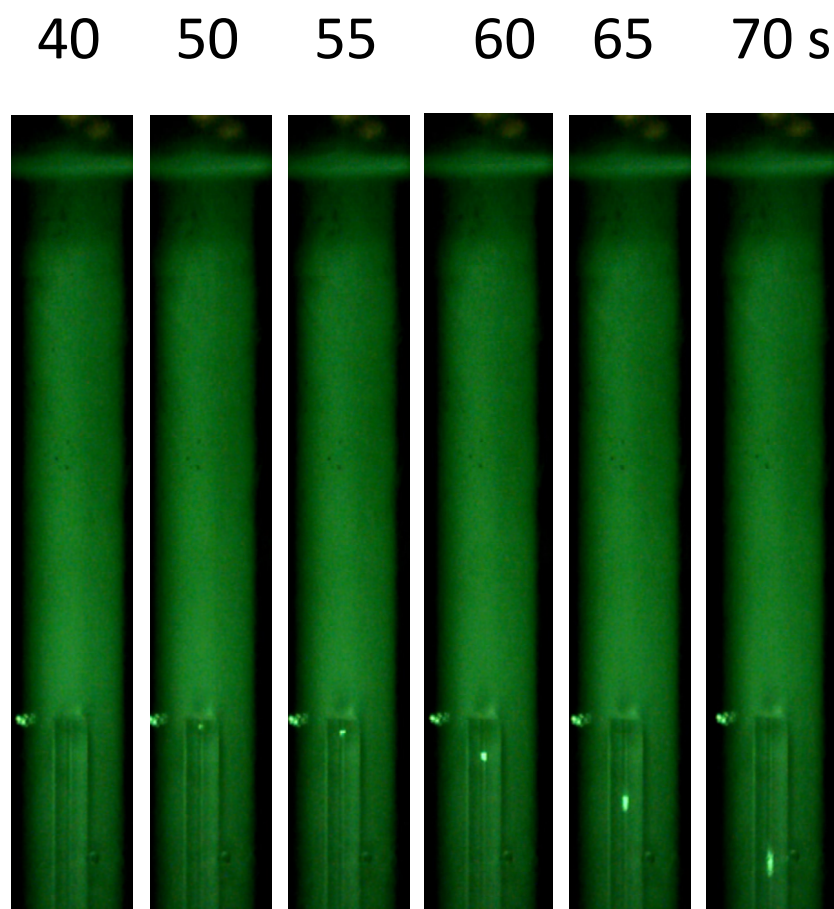
One possible reason for the preconcentration at the capillary entrance despite the lack of a conductivity difference could be that there is hydrodynamic flow of liquid into the capillary during the injection process. The sodium ions would then migrate against the hydrodynamic flow out of the capillary into the interface. Once the sodium ions enter the interface they experience a decrease in electric field strength. The hydrodynamic flow into the capillary reduces their total velocity even further and causes them to preconcentrate at the capillary entrance.

When investigating the flow of liquid inside the capillary in the simulation model it could be confirmed that there is hydrodynamic flow of liquid into the capillary at a velocity of around 3.9×10^{-8} m/s. Despite this the velocity seems too small to cause preconcentration of the sodium ions.

To understand this phenomenon experiments were undertaken using the experimental setup described in chapter 3. To achieve no conductivity difference between capillary and interface the same sample solution was placed inside the capillary and the interface. The same sample solution that was used in the capillary and the interface was flushed through the interface during the application of voltage. In the experimental setup the hydrodynamic flow of liquid into the capillary is negligibly small. Based on the simulation model predictions there should be preconcentration in the capillary entrance.

This could be confirmed experimentally and is shown in Figure 4.11. The interface and the capillary are filled with fluorescent sample solution so that there is no conductivity difference. At 0 s the flow rate of 0.08 μ L/s and a voltage of 15 kV were applied. After 40 s no preconcentration could be observed. At 50 s injection time a small plug of increased concentration has formed at the capillary entrance. The preconcentrated plug becomes more

visible at 55 s and moves towards the capillary outlet which is shown in the images taken at 60 s, 65 s and 70 s.



15 kV, 0.08 $\mu\text{L/s}$, sample solution in capillary and interface

Figure 4.11 Sample preconcentration without a conductivity difference as a function of time. A sample solution of 150 ng/mL of sodiumfluorescein in 0.04 mM Tris-HCl buffer (pH 7.9) was placed inside the capillary and in the 1000 μm i.d. interface. The same sample solution used in the capillary was flushed through the interface at 0.08 $\mu\text{L/s}$ flow rate and a voltage of 15 kV was applied. The formation and movement of a preconcentrated sample zone at 40s, 50s, 55s, 60s, 65s and 70s is shown. The bright spot on the left side of the interface channel was attributed to an impurity on the outside of the interface. Other explanations are in the text.

The simulation model shows that the conductivity in the capillary entrance increases to around 30 times of its initial value in the 10 s image in Figure 4.10 5 kV injections. After that the conductivity decreases again to around 5 times above its initial value at 30 s and 600 s. As stated above the conductivity increase was attributed to the stacking of sodium ions, with the counter-anion also stacking to maintain charge neutrality. Therefore at 10 s where the conductivity has increased 30 times more stacking must happen than compared to 30 s and 600 s. The stacking is influenced by the change in velocity that the sodium ions experience when reaching the capillary entrance. This would suggest that the sodium ions experience a bigger decrease in velocity at 10s compared to 30 s and 600s. This can be explained by the fact that at 10 s the sample-BGE front has not yet reached the capillary entrance and the majority of the interface is filled with BGE. The sodium ions will stack due to the decreased electric field strength in the interface and the hydrodynamic flow into the capillary. At 30s and 600s the interface is already filled with the lower conductive sample. This means the sodium ions will experience a smaller decrease in field strength upon exiting the capillary entrance. Thus the stacking effect is bigger before the interface has reached the capillary entrance and causes a peak in conductivity at around 10 s injection time.

Another finding in the simulation model was that the injection voltage increases slightly with increasing interface diameters as shown in Figure 4.9 in the simulation model. This is only possible if the conductivity of the liquid inside the capillary increases with the interface diameter. Looking at the simulation model data it could be confirmed that the conductivity inside the capillary increases from around 0.01 S/m at 2.5 mm interface i.d. to 0.07 S/m at 10 mm i.d., 0.65 S/m at 50 mm i.d. and 0.8 S/m at 100 mm i.d. This change in conductivity, and hence

change in the distribution of the electric field over the interface during injection is not included in the mathematical model previously developed.

To explain the reason for the higher conductivities inside the capillary at larger interface diameters a closer look at the change of conductivity with injection time needs to be taken. As stated above the stacking effect is greater before the sample – BGE front has reached the capillary inlet. In the 100 μm interface it takes 1600 times longer compared to the 2.5 μm i.d interface for the sample-BGE front to reach the capillary inlet. This means in the bigger interface there is more time for the conductivity to increase inside the capillary. Thus the conductivity inside the capillary is higher at larger interface diameters. This will mean that the voltage will adjust to provide a higher proportion over the interface than the capillary, which is what the simulation model shows. Unfortunately, the effect of the interface diameter on the conductivity change in the capillary entrance could not be experimentally confirmed yet but will be an exciting starting point for future research projects on electrokinetic injection from a flowing sample stream

4.4 CONCLUSIONS

Within the present work a computational fluid dynamics simulation model is presented. Insight into the simulation parameters and setup as well as a comparison to the mathematical model is provided. A number of publications provide simulation models that investigate the electrode capillary setup for maximum sensitivity in static injection vial. The literature lacks a simulation model that aids in the understanding of the underlying theoretical principles of a continuous flow interface. To address this need a simplified simulation model was developed. The aim of the simulation model was to derive a more accurate and refined set of rules and guidelines for interface design compared to the mathematical model developed in chapter three. To verify the simulation model predictions it was compared with the mathematical model. It was found that the simulation model predictions contradict the mathematical model results. The mathematical model proposed a decrease of depletion flow rate with bigger interface diameters and was based on the assumption that all concentrations are regulated by the Kohlrausch function. In contrast the simulation model proposed that the depletion flow rate increases with bigger interface i.d's. It was found that the simulation model predicts sample preconcentration of ions at the capillary entrance even without a conductivity difference between the solutions in the capillary and interface. Therefore the concentrations in the simulation model were not regulated by the Kohlrausch function. The explanation was that a hydrodynamic flow into the capillary could be observed in the simulation model. It was anticipated that the hydrodynamic flow of liquid counterbalances the electrophoretic migration of sodium ions out of the capillary entrance and causes them to stack at the capillary entrance. It could be confirmed experimentally that stacking of sample can occur without a conductivity difference in the presence of a small hydrodynamic flow into the capillary. Since this could be experimentally confirmed it is

anticipated that the simulation model predictions are correct. This means that with bigger interface diameters higher depletion flow rates can be achieved which can enhance the sensitivity of CE equipment when used with a continuous flow interface. This will have to be further investigated in future work as it is a promising direction in the field of electrokinetic injection from a flowing sample stream.

4.5 REFERENCES

- [1] T. Hirokawa, E. Koshimidzu, Z. Xu, *Electrophoresis* 29 (2008) 3786.
- [2] W. Thormann, J. Caslavska, M.C. Breadmore, R.A. Mosher, *Electrophoresis* 30 (2009) 16.
- [3] F. Kohlrausch, *Ann. Phys. Chem.* 62 (1897) 209.

Chapter 5

GENERAL CONCLUSIONS AND FUTURE DIRECTIONS

5.1 GENERAL CONCLUSIONS

The present literature lacks a systematic study on the electrokinetic injection from a flowing sample stream. This need was addressed in the present thesis by the development of continuous sample flow interfaces for stacking in capillary electrophoresis in combination with a simulation and a mathematical model. The following general conclusions can be made regarding the developed interfaces and models.

In chapter two a tee connector in a commercial capillary electrophoresis instrument was used to investigate the effect of field amplified sample injection from both flowing and static sample volumes. FASI with sweeping followed by micellar electrokinetic chromatography (FASI-sweep-MEKC) was used for sample injection comparison from a static system and a flowing stream. It was shown that under identical conditions (40 min electrokinetic injection at 5 kV from a sample volume of 295 μL) the limit of detection is 4 times lower when using the continuous sample flow interface compared to an injection from a static vial. The effect of flow rate and injection voltage on the injected sample amount was also investigated using a 2D axisymmetric simulation (COMSOL 4.3b) and verified experimentally. Conditions under which there is near-quantitative injection of the sample target ions could be confirmed. Using the continuous flow interface and electrokinetic injection at 30 kV at a flow rate of 558 nL/s for 5.5

min (corresponds to 184 μL of sample) the same enhancement compared to injection from 295 μL for 40 min injection in a static vial could be achieved. Compared to a hydrodynamic injection this sensitivity enhancement factor corresponded to four orders of magnitude improvement.

In chapter three the aim was to improve the electrokinetic injection from a flowing sample stream further by investigating the influence of the capillary and interface dimensions, the conductivity ratio of BGE and sample, the total applied voltage and the sample mobility on the injection. A mathematical model was presented and a set of guidelines for designing an interface that allows for high depletion flow rates was proposed. It was found that the total applied voltage, the electrophoretic sample mobility and the conductivity ratio between the liquid in the interface and the capillary should be as high as practically possible to yield high depletion flow rates. In an experimental setup the conductivity ratio will be determined by the limitations of the stacking method and the electrophoretic sample mobility will be determined by the analyte that is to be investigated. The highest possible applied voltage will be limited by the highest practically possible current. The model suggests further that an optimum interface diameter and length exist at which the depletion flow rate reaches a maximum. When varying the interface length between 2 to 20 mm the depletion flow rate changed only around 5% of its maximum value at 0.8107 $\mu\text{L/s}$. Between 450 to 2750 μm of interface diameter the depletion flow rate changed around 5% of its maximum at 0.8110 $\mu\text{L/s}$. The capillary inner diameter increases the depletion flow rate exponentially and should be maximized but will be limited by the current. A reduction in capillary length showed the biggest improvement in depletion flow rate up to 10.73 $\mu\text{L/s}$ at a capillary length of 2cm. The voltage needs to be reduced accordingly when using a short separation capillary to avoid high currents.

In the second part of chapter three a simple flow through channel interfaces was developed. Out of all possible variables the effect of different interface diameters on the electrokinetic injection from a flowing sample stream was investigated first.

In the experimental part the aim was to investigate how the interface diameter can increase the depletion flow rate. Interfaces with 500, 1000 and 1500 μm i.d. were investigated and the injection process was monitored using a fluorescent sample. A change of less than 4% in depletion flow rate was predicted by the mathematical model when increasing the interface diameter from 500 to 1500 μm experimentally. To verify these predictions it was attempted to determine the depletion flow rate at each diameter. The depletion flow rate in the 1000 μm i.d. interface was determined as 0.08 $\mu\text{L/s}$. Electrolysis bubbles in the 1500 μm i.d. interface and heat generated bubbles in the 500 μm i.d. interface appeared before stable stacking conditions could be reached which prevented the determination of a depletion flow rate. To reach stable stacking conditions before bubble formation appears the sample was placed in the interface at the start of the injection. With this approach the stacked sample zone migrated towards the capillary outlet within the first 10 s of injection. The slower anion HEPES was chosen in an attempt to stabilize the stacked sample zone. As a result the sample stacked outside the capillary entrance and did not enter the capillary entrance. For future work it is necessary to fine tune the stacking mechanism. This is expected to create a stable stacking zone at the capillary entrance for long enough so that the depletion flow rate can be determined for different interface i.d.'s.

Finally a simulation model was developed in chapter 4. This was done to get more accurate predictions than compared to the mathematical model. In the simulation model simplifications had to be made in order to allow for reasonable computational times. In particular the capillary length in the simulation had to be shortened to 2 mm instead of the 36.4 cm which was used

experimentally. To verify the simulation model predictions it was compared with predictions of the mathematical model. The simulation model predicted an increase in depletion flow rate with interface diameter whereas in the mathematical model a decrease was predicted. The mathematical model was based on the assumption that all concentrations are regulated by the Kohlrausch function. It was found that the concentrations in the simulation model are not regulated by the Kohlrausch function and preconcentration of ions seems to occur at the capillary entrance even without a conductivity difference. This was attributed to a hydrodynamic flow of liquid into the capillary entrance which counterbalanced the electrophoretic movement of sodium ions out of the capillary and led to preconcentration. The preconcentration of sample in the absence of a conductivity difference with of a small hydrodynamic flow into the capillary could be experimentally confirmed. This opened up new directions for exiting future research projects as it suggests that an increase in interface i.d. in a continuous flow interface increases the depletion flow rate and could therefore improve the sensitivity of CE.

5.2 FUTURE DIRECTIONS

Finally it should be noted that further research is necessary on the following topics:

To prevent the formation of bubbles in the interface during injection

One of the main limiting factors is bubble formation due to electrolysis and Joule heating. Electrolysis bubbles appeared around the cylindrical electrode after longer injection times. The smaller bubbles start aggregating and formed a bigger bubble that obstructed the entire diameter of the interface. This posed a limitation to the injection time that could be used to preconcentrate sample ions from the flowing sample stream.

One possible solution to prevent bubble formation around the electrode could simply be to choose the total applied voltage, interface and capillary dimensions accordingly so that the current is decreased to a level where bubble formation is negligible within the used injection timeframe. Certainly this would limit the maximum depletion flow rate.

Another way to prevent bubble formation without compromising the depletion flow rate would be to place the ring electrode outside the interface. This would require a setup where the electrode is a few mm's away from the interface outlet. The interface outlet would have to be immersed in a container that contains sample liquid. The electrical connection from the electrode to the separation capillary entrance in the interface could be made by the sample liquid.

To find a background electrolyte that allows stable injection conditions with sample in the interface as a starting condition.

It has been shown in chapter 3 that the approach of replacing the BGE in the interface with sample during injection caused a delay in reaching stable stacking conditions. This led to bubble formation due to electrolysis before stable injection conditions could be reached. The solution would be to further optimize the BGE composition. This could allow reaching stable injection conditions when the sample is placed in the interface at the beginning of the injection. Having stable injection conditions from the beginning of the injection could prevent bubble formation due to long injection times.

Bubble formation due to Joule heating appears in the space between the electrode in the interface and the separation capillary entrance as well as inside the separation capillary. Since Joule heating bubble formation does not only appear around the electrode a different electrode position cannot solve this issue.

One obvious solution is to reduce the current. This would mean either a reduction in the total applied voltage, a reduction in capillary inner diameter or an increase in capillary length. All of these alterations would cause less depletion flow rate. A better solution would be to decrease the conductivities of both the sample solution and the BGE in the capillary while still maintaining a high conductivity ratio. This approach might face limitations since the conductivities of sample and BGE might be dictated by the stacking approach chosen and the sample that needs to be analysed. Another way to reduce the current would be to reduce the interface diameter which might compensate the depletion flow rate maximum. The last resort would be that at higher depletion flow rates the heat can be transported off more efficiently. This might reduce the

bubble formation at high depletion flow rates. Another more promising approach would be to use a glass interface and a cooling system when injecting at higher currents.

Increasing the depletion flow rate further

The aim was to inject from a big sample volume in a relatively short time. Within the presented work the maximum depletion flow rate in chapter 2 was 30 uL/min for the Tee interface and around 5 uL/min for the interface developed in chapter 3. The simulation model shows that a bigger interface diameter should lead to a higher depletion flow rate since the injection does not follow Kohlrausch's regulating function. The influence of different interface i.d.'s on the depletion flow rate needs to be examined experimentally and should allow high volumes of sample being quantitatively injected within a short time frame.

Utilizing the continuous flow interface to selectively inject sample ions below a certain mobility.

One of the key findings was that at a given injection voltage and flow only ions that are above certain mobilities can be injected. Any sample ions with lower mobilities will not be injected and get transported to the waste. This would allow to scan through a given sample mixture and inject selectively ions only up to a certain mobility.

Application of the continuous flow interface for real samples

We anticipate that the presented continuous flow interface can be used to detect ng/L levels of pharmaceuticals and personal care products (PPCP) in water samples. This could be achieved by using a powerful stacking method in combination with a continuous flow interface at optimum interface i.d, voltage and flow rate. When analyzing real water samples the ion concentration and

conductivity in the sample would cause a decreased conductivity difference to the BGE. The simulations predict that even without a conductivity difference preconcentration is possible as long as there is a flow of liquid into the capillary. This would ultimately mean that the continuous flow interface could be applied to real sample without being limited to stacking approaches that require a conductivity difference between sample and BGE.